DOT-TSC-FRA-80-29

FATIGUE CRACK GROWTH PROPERTIES OF RAIL STEELS

D. Broek
R.C. Rice

BATTELLE
Columbus Laboratories
505 King Avenue
Columbus OH 43201

FINAL REPORT

Prepared for

U.S. DEPARTMENT OF TRANSPORTATION
FEDERAL RAILROAD ADMINISTRATION
Office of Research and Development
Washington DC 20590

NOTICE

This document is disseminated under the sponsorship of the Department of Transportation in the interest of information exchange. The United States Government assumes no liability for the contents or use thereof.

NOTICE

The United States Government does not endorse products or manufacturers. Trade of manufacturers' names appear herein solely because they are considered essential to the object of this report.

Technical Report Documentation Page

1. Report No.	2. Government Accession No.	3. Recipient's Catalog No.
DOT-TSC-FRA-80-29		

4. Title and Subtitle	5. Report Date
FATIGUE CRACK GROWTH PROPERTIES OF RAIL STEELS	6. Performing Organization Code
	8. Performing Organization Report No.
7. Author(s) D. Broek, R.C. Rice	
9. Performing Organization Name and Address Battele Columbus Laboratories 505 King Avenue Columbus, OH 43201	10. Work Unit No. (TRAIS) RR119/R1322 11. Contract or Grant No. DOT-TSC-1076
12. Sponsoring Agency Name and Address Department of Transportation Federal Railroad Administration Washington DC 20590	13. Type of Report and Period Covered Final Report July 75 - July 77 14. Sponsoring Agency Code

15. Supplementary Notes

Under Contract to: Department of Transportation
Transportation Systems Center
Cambridge, MA 02142

16. Abstract

Fatigue crack propagation properties of rail steels were determined experimentally. The investigation covered 66 rail steels. The effects of the following parameters were studies: stress ratio (ratio of minimum to maximum stress in a cycle), frequency, temperature and orientation. The results were presented on the basis of the stress intensity factor. The threshold value of the stress intensity was determined. An equation correlating the crack growth rate and the stress intensity factor was established.

A limited number of mixed mode crack growth tests was conducted. Also the behavior of surface flaws was studied.

The results serve as a data base for a failure model presented in DOT-TSC-FRA-80-20

17. Key Words	18. Distribution Statement
Rail, Cracks, Fatigue Crack Propagation, Chemical Composition, Mechanical Properties, Mixed Mode Loading, Surface Flaws	DOCUMENT IS AVAILABLE TO THE PUBLIC THROUGH THE NATIONAL TECHNICAL INFORMATION SERVICE, SPRINGFIELD, VIRGINIA 22161

19. Security Classif. (of this report)	20. Security Classif. (of this page)	21. No. of Pages	22. Price
Unclassified	Unclassified		

Form DOT F 1700.7 (8-72) Reproduction of completed page authorized

PREFACE

This report presents the results of the second phase of a program on Rail Material Failure Characterization. It has been prepared by Battelle's Columbus Laboratories (BCL) under Contract DOT-TSC-1076 for the Transportation Systems Center (TSC) of the Department of Transportation. The work was conducted under the technical direction of Mr. Roger Steele of TSC.

The results of this phase of the program are the basis for the computational rail failure model described in part II of the final report. This model, in conjunction with the results of ongoing studies on Engineering Stress Analysis of Rails and on Wheel-Rail-Loads when incorporated into a reliability analyses will enable establishment of safe inspection schedules.

The cooperation of the American Association of Railroads (AAR) and the various railroads (Boston & Maine Railroad Company, Chessie System, Denver and Rio Grande Western Railroad Company, Penn Central Railroad Company, Southern Pacific Transportation Company, and Union Pacific Railroad Company) in acquiring rail samples is gratefully acknowledged. The cooperation and assistance of Mr. Roger Steele of TSC was of great value to the program.

METRIC CONVERSION FACTORS

Approximate Conversions to Metric Measures

Symbol	When You Know	Multiply by	To Find	Symbol
	LENGTH			
in	inches	*2.5	centimeters	cm
ft	feet	30	centimeters	cm
yd	yards	0.9	meters	m
mi	miles	1.6	kilometers	km
	AREA			
in^2	square inches	6.5	square centimeters	cm^2
ft^2	square feet	0.09	square meters	m^2
yd^2	square yards	0.8	square meters	m^2
mi^2	square miles	2.6	square kilometers	km^2
	acres	0.4	hectares	ha
	MASS (weight)			
oz	ounces	28	grams	g
lb	pounds	0.45	kilograms	kg
	short tons (2000 lb)	0.9	tonnes	t
	VOLUME			
tsp	teaspoons	5	milliliters	ml
Tbsp	tablespoons	15	milliliters	ml
fl oz	fluid ounces	30	milliliters	ml
c	cups	0.24	liters	l
pt	pints	0.47	liters	l
qt	quarts	0.95	liters	l
gal	gallons	3.8	liters	l
ft^3	cubic feet	0.03	cubic meters	m^3
yd^3	cubic yards	0.76	cubic meters	m^3
	TEMPERATURE (exact)			
°F	Fahrenheit temperature	5/9 (after subtracting 32)	Celsius temperature	°C

*1 in = 2.54 (exactly). For other exact conversions and more detailed tables, see NBS Misc. Publ. 286, Units of Weights and Measures, Price $2.25, SD Catalog No. C13.10:286.

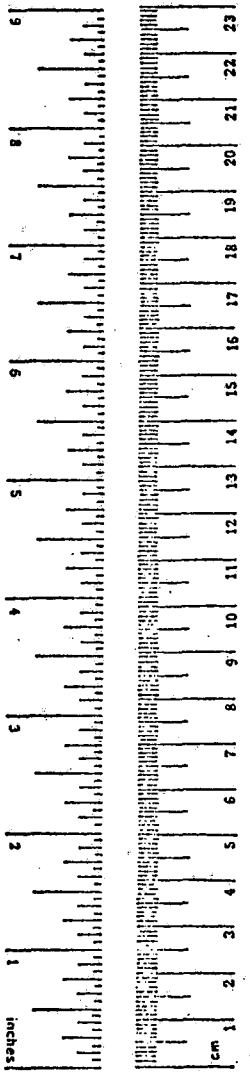

Approximate Conversions from Metric Measures

Symbol	When You Know	Multiply by	To Find	Symbol
	LENGTH			
mm	millimeters	0.04	inches	in
cm	centimeters	0.4	inches	in
m	meters	3.3	feet	ft
m	meters	1.1	yards	yd
km	kilometers	0.6	miles	mi
	AREA			
cm^2	square centimeters	0.16	square inches	in^2
m^2	square meters	1.2	square yards	yd^2
km^2	square kilometers	0.4	square miles	mi^2
ha	hectares (10,000 m^2)	2.5	acres	
	MASS (weight)			
g	grams	0.035	ounces	oz
kg	kilograms	2.2	pounds	lb
t	tonnes (1000 kg)	1.1	short tons	
	VOLUME			
ml	milliliters	0.03	fluid ounces	fl oz
l	liters	2.1	pints	pt
l	liters	1.06	quarts	qt
l	liters	0.26	gallons	gal
m^3	cubic meters	35	cubic feet	ft^3
m^3	cubic meters	1.3	cubic yards	yd^3
	TEMPERATURE (exact)			
°C	Celsius temperature	9/5 (then add 32)	Fahrenheit temperature	°F

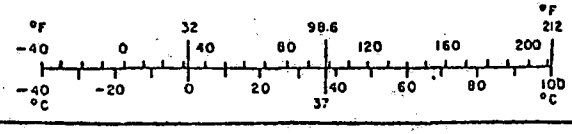

TABLE OF CONTENTS

TABLE OF CONTENTS (Continued)

LIST OF ILLUSTRATIONS

LIST OF ILLUSTRATIONS (Continued)

LIST OF ILLUSTRATIONS (Continued)

LIST OF ILLUSTRATIONS (Continued)

LIST OF TABLES

EXECUTIVE SUMMARY

This report presents part of the results of a study on rail material failure properties to better define fatigue crack growth mechanisms in rail steel. This work was conducted as part of the Improved Track Structures Research Program sponsored by the Federal Railroad Administration. The results are presented in five volumes entitled:

Fatigue Crack Propagation In Rail Steels - Interim Report No. FRA/ORD-77-14.

Fatigue Crack Growth Properties of Rail Steels - Final Report - DOT-TSC-FRA-80-29

Prediction of Fatigue Crack Growth in Rail Steels - Final Report - DOT-TSC-FRA-80-30

Cyclic Inelastic Deformation and Fatigue Resistance of a Rail Steel: Experimental Results and Mathematical Models - Interim Report DOT-TSC-FRA-80-28

Fracture and Crack Growth Behavior of Rail steels Under Mixed Mode Loadings - Interim Report (in preparation)

The objective of the work described in this report was to obtain the experimental data to be used as input to the development of a predictive rail failure model. Results of a total of 119 experiments are reported. Three categories of rail steel, which exhibited high, medium and low crack growth rates, were evaluated for the effect of:

- Stress Ratio R (ratio of minimum to maximum stress in a loading cycle).
- Cycling frequency
- Specimen temperature
- Specimen orientation
- Elliptical surface cracks
- Crack growth threshold value
- Mixed mode loading (combined tension and shear)

Test specimens were horizontal and vertical sections cut from the head of the rails and were representative of transverse fissures in rail, horizontal split heads and vertical split heads. Crack propagation lives up to 300 x 10^3 cycles were classified as Category I, high growth rates, lives of 300 - 700 x 10^3 cycles were classified as Category II, medium growth rates, and lives greater than 700 x 10^3 cycles were classified as Category III, low growth rates.

The effects of stress ratio R were determined in a series of constant amplitude fatigue crack growth experiments at 30 Hz on single-edge notch specimens for R = -10.0, 0.0, and 0.5, and on compact tension specimens at 2 Hz for R = 0.0. The potential effect of cyclic frequency was evaluated on compact tension specimens cycled at 2 Hz and R = 0.0. This rate of cycling was more than an order of magnitude lower than the other tests which were cycled at 30 - 50 Hz. Temperature effects were determined under constant amplitude loading at 40 Hz, at R = 0.0 and 0.5 at - 40°F, 68°F. Crack growth in the longitudinal and transverse directions was evaluated at 40 Hz, at 68°F for R = 0.0 and R = 0.5. Threshold experiments were conducted at three stress ratios (R = -1.0, 0.0 and 0.5) to develop estimates of threshold stress intensity levels, below which crack growth rates would asympototically approach zero. Surface flaw crack-propagation experiments were performed to evaluate the complex 2-dimensional cracking behavior typical of many in-service embedded flaws. A series of mixed mode (Mode I-tension, Mode II-shear) experiments were performed at ratio of K_{II}/K_I = 0, 0.34, 0.73 and 00.

Based on the data obtained, the following observations were made.

1) The stress ratio R has a significant effect on crack growth and ΔK_{th}.
2) Temperature (through the range of rail service temperatures) has a pronounced effect on crack growth. Generally, the effects of increased temperature appear to reduce the slope of the da/dN vs. ΔK curve and to increase the critical stress intensity limit at high crack growth rates.
3) The short transverse loaded specimens with the crack growing in the longitudinal direction, representative of a vertical split head, grew faster than the orientations for transverse fissure and horizontal split head samples for flaws subjected to equal crack tip stress intensities.

4) The effect of frequency appeared to be insignificant in view of the large inherent scatter in crack-growth properties.

5) In the surface flaw experiments, crack growth rates sidewise across the rail head through the width were higher than those through the thickness or down through the head toward the web.

6) The threshold asymptote, under the test conditions described in this report, was reached at crack growth rates of 10^{-8} in/cycle.

7) Mixed mode (I/II) crack growth could not be sustained under the experimental conditions used since the crack turned immediately to a plane of pure mode I. Analytical models for mixed mode loading are presented. These models show that the effect of model II loading is likely to be small for the mode I/II ratios expected during service.

These data were generated in view of a computational crack-growth prediction model for crack growth under rail service loading to be developed later in this program. The results of this effort provided the data base to develop the prediction model which is described in DOT-TSC-FRA-80-29 Prediction of Fatigue Crack Growth Properties In Rail Steels.

1. INTRODUCTION

Prevention of failures of railroad rails relies on timely detection of fatigue cracks. In order to establish safe inspection intervals, information is required on the rate of growth of fatigue cracks in service. The growth of cracks under service circumstances can be obtained from a predictive model, which in turn has to be based on fatigue crack growth data obtained in the laboratory.

One portion of the Federal Railroad Administration's (FRA) Track Performance Improvement Program is the development of a predictive rail failure model that enables a determination of optimal inspection periods through a calculation of fatigue-crack-propagation behavior. The research reported here concerns the second phase of a program to develop the rail failure model.

The laboratory fatigue-crack-growth data used as an input to the predictive model should be obtained from a sufficiently large sample of rails in order to manifest the statistical variability. In the first phase of the program, data were generated for 66 rail samples of various ages, suppliers, and weights. The samples were taken from existing track from all sections of the United States. Fatigue crack growth tests were performed under constant amplitude loading with zero minimum load (R=0); R is the ratio of minimum to maximum stress in a cycle). These results were reported in an Interim Report, Reference 1. A summary of the Phase L data is presented in Appendix B of this report and also in Reference 2.

Actual cracks in rails develop under more complex conditions than constant amplitude tension loading at R=0. They are subjected to stress histories with varying amplitudes of combined tension and shear (mixed mode), covering a wide range of R ratios. Cracks can initiate in different sections of the rail and have different orientations; they are internal flaws of predominantly quasi-elliptical shape. Moreover, the rail experiences varying temperatures, which may affect the behavior of cracks. A predictive failure model should be cognizant of these complex circumstances. Therefore, data are required on the influence of the various parameters on crack growth. Such data were generated during the second phase of the program, and they are compiled in the present report.

Since it was prohibitive to perform all the experimentation on all 66 rail materials of the first phase, three categories were selected for further characterization[1], consisting of materials that exhibited high, medium and low growth rates in the intial baseline crack growth experiments. These three categories were evaluated for the effect of

- Stress ratio (R)
- Cycling frequency
- Temperature
- Specimen orientation in the rail
- Mixed mode loading
- Low stress cycling in the regime of the threshold for crack growth
- Crack front curvature (elliptical cracks).

Results of a total of 119 experiments are reported here.

In the third phase of the program the predictive failure model will be developed. For this purpose, experiments will be performed under service-simulation loading. On the basis of those experiments, a crack growth integration model will be established that accounts for the variability of crack growth as observed in the first and second phase of the program.

2. RAIL MATERIALS

A detailed description of the sample sources is presented in Appendix B and Reference 1. The 66 samples were identified by numbers 001 through 066. A summary will be presented here of the information relevant to this phase of the program. The same rail sample identification as in Reference 1 will be used throughout this report, to facilitate access to the more detailed information in Reference 1.

All rail samples used for the present experiments are listed in

Table 1 in ascending order of crack propagation life as determined in Phase 1. The crack propagation life is defined as the number of cycles required to extend a crack in a compact tension specimen from 1-inch to failure. The crack propagation life was the basis for the categorization of the samples: lives up to 300×10^3 cycles were classified as Category I, (high growth rates), lives of $300 - 700 \times 10^3$ were classified as Category II (medium growth rates), and lives above 700×10^3 were classified as Category III (low growth rates). It should be noted that the selection of categories was arbitrary and that the classification was based on only one test result per sample.

The top three groups of samples in Table 1 for Categories I, II, and III were the samples used for the main body of experiments. The fourth group lists some samples of each category that were used for additional experiments in a further attempt to evaluate the effect of other properties on the variability of fatigue crack growth. The reasons for their selection is given in the column, "Remarks". The experiments performed on these materials were simply a duplication of Phase I experiments on these samples for two orientations of cracking.

Table 1 presents the most important details for all samples. First are given the weight and the year of production. Then follows the Carbon, Manganese, Sulfur and Oxygen content. Also, the primary processing variables are indicated, i.e., Control Cooled (CC) and Vacuum Degassed (Vac. Deg.). Finally, the most important mechanical properties are given, via Tensile Ultimate Strength (TUS), Tensile Yield Strength (TYS), and the elongation for a 1-inch gage length.

3. EXPERIMENTAL DETAILS

3.1 Specimens

The majority of the specimens were of the Compact Tension (CT) type. Their dimensions are shown in Figure 1. The specimens were provided with a 1.650-inch deep chevron notch (0.900 inch from the load line). These specimens were precracked in a Krause fatigue machine until a crack of about 0.1 inch had formed. At this point the specimens contained a simulated fatigue crack of about 1 inch (as measured from the load line, see Figure 1).

TABLE 1. CHARACTERISTICS OF RAIL SAMPLES USED FOR PRESENT EXPERIMENTS

Sample	Crack growth life 1-inch to failure	Category	Weight	Year	Chemical Composition				Processing		Mechanical Processing			Remarks
					C	Mn	S	O	CC	Vac. Deg.	TUS	TYS	Elonga-tion	
	10^3 cycles		lbs/yd		wt %	wt %	wt %	ppm	- no + yes	- no + yes	ksi	ksi	% in 1-inch	
016	150	I	133	1957	.81	.93	.044	41	+	-	138.6	75.6	9.5	
025	153	I	133	1966	.80	.91	.016	28	+	-	141.1	75.7	9.5	
023	155	I	133	1957	.79	.92	.040	40	+	-	135.1	77.3	10.5	
030	197	I	119	1958	.80	.90	.028	53	-	-	-	76.8	-	
013	216	I	127	1954	.74	.89	.028	49	-	-	129.3	72.8	12.5	
002	270	I	85	1911	.74	.61	.154	47	-	-	134.4	74.7	12.0	
009	381	II	130	1929	.61	1.46	.039	57	-	-	139.8	81.8	14.0	
018	384	II	133	1953	.75	.89	.046	44	+	-	133.2	70.6	11.0	
032	404	II	133	1953	.80	.94	.035	62	+	-	139.5	80.0	12.0	
021	419	II	133	1955	.79	.90	.024	43	+	-	132.3	77.2	12.0	
019	435	II	133	1965	.74	.88	.038	37	+	-	131.2	73.4	12.0	
006	490	II	115	1974	.72	.97	.028	24	-	+	135.0	71.2	11.0	
024	495	II	133	1956	.81	.83	.030	27	+	-	136.7	74.6	10.0	
031	596	II	133	1956	.79	.76	.022	51	-	-	133.4	75.6	11.0	
001	736	III	130	1929	.63	1.48	.022	98	-	-	136.4	76.5	13.5	
007	796	III	115	1974	.73	.93	.037	25	-	+	135.8	70.0	12.0	
022	803	III	133	1956	.78	.87	.028	47	+	-	130.7	76.0	13.0	
056	1150	III	132	1949	.80	.90	.039	45	-	-	136.0	72.6	9.5	
035	1218	III	115	1955	.76	.80	.028	27	+	-	128.1	69.3	12.5	
029	1256	III	119	1958	.72	.89	.046	44	+	-	125.5	61.7	12.0	
036	1269	III	112	1939	.75	.81	.016	56	-	-	132.1	74.6	12.0	
020	1302	III	119	1957	.75	.83	.033	33	-	-	131.4	72.0	11.0	
Additional Testing														
026	233	I	133	1957	.78	.94	.050	47	+	-	135.0	74.4	11.0	High S
060	247	I	124	1975	.80	.90	.013	48	+	-	135.3	74.2	12.0	Low S
005	271	I	130	1929	.63	1.36	.033	53	-	-	134.8	76.4	13.5	Low C, High Mn
017	288	I	133	1957	.79	.85	.048	44	+	-	137.1	74.4	10.0	High S
040	323	II	100	1928	.58	.64	.030	37	-	-	138.8	83.3	9.5	99% pearlite, Low C, Mn
028	536	II	133	1953	.71	.90	.022	68	+	-	129.1	70.5	11.5	95% pearlite, Low S
037	617	II	115	1943	.72	193	.017	71	+	-	127.7	68.6	16.0	97% pearlite, Low S
027	890	III	133	1956	.78	.87	.022	45	-	-	136.4	69.4	10.0	Low Ratio TYS/TUS
045	1019	III	110	1930	.65	.65	.027	330	-	-	-	66.0	-	85% pearlite, Low S

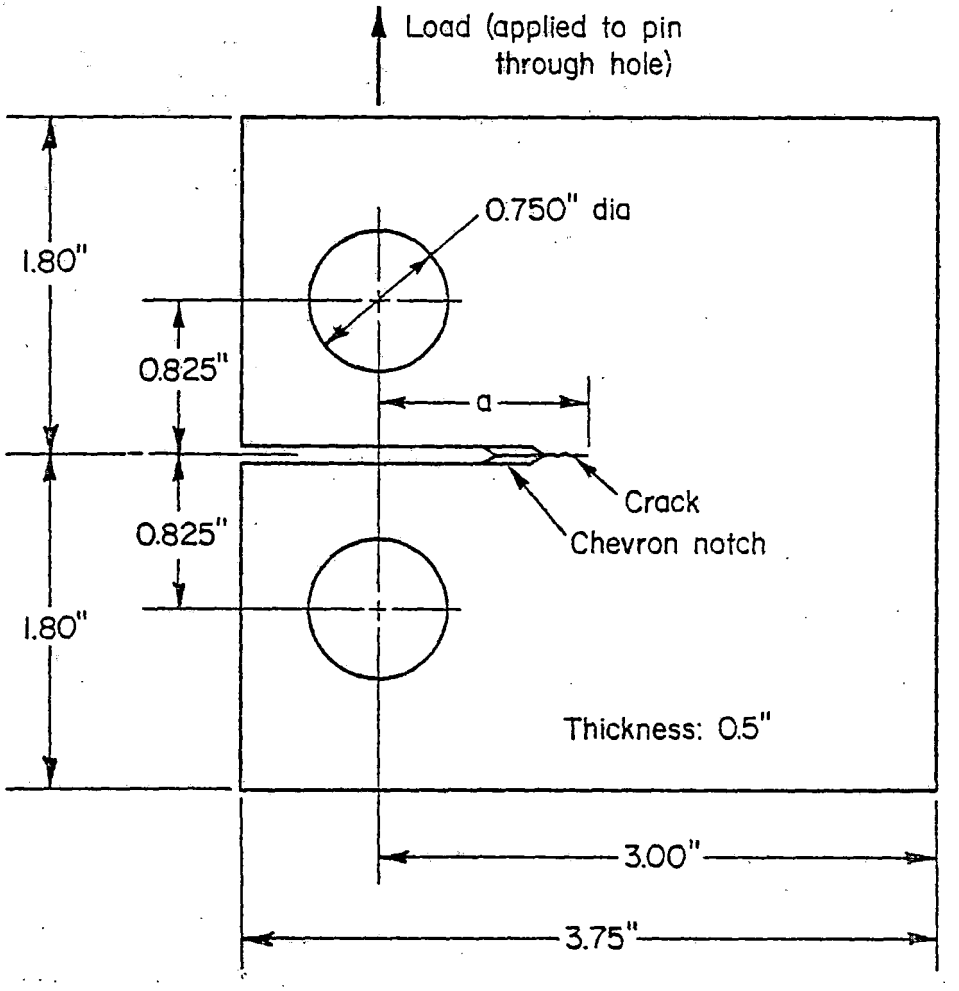

FIGURE 1. COMPACT TENSION FATIGUE CRACK GROWTH SPECIMEN

CT specimens are not suitable for experiments with negative R-ratios, (i.e., in cases where the minimum load in a cycle is compressive), since the stress distribution in a CT specimen in compression bears no straightforward relation to compressive stress distributions in rail. Therefore, the experiments with negative R ratios were performed on Single Edge Notch (SEN) specimens, illustrated in Figure 2. In order to establish a basis of comparison between SEN specimens and CT specimens, a few experiments with zero R-ratio were also run with SEN specimens. The SEN specimens were precracked in the same fatigue machine they were subsequently tested in.

Figure 3 shows the Surface Flaw (SF) specimen. The starter notch in these specimens was a semi-elliptical slot cut by means of Electric Discharge Machining (EDM). The SF specimens were also precracked in the same fatigue machine they were tested in.

Specimens for Mixed-Mode (MM) loading were of the type shown in Figure 4. The location of the crack was varied in order to achieve different combinations of tension and shear. Figure 5 shows the MM specimen in the fatigue machine. Precracking was done prior to testing in the same machine.

The orientations of the various specimen types within the rail are shown in Figure 6. Three orientations were used for the CT specimens, namely, LT, TL and SL. The first letter in these designations gives the direction of loading with respect to the rail, i.e., Longitudinal (L), Transverse (T) and Short Transverse (S). The second letter is the direction of crack growth, also with respect to the rail. (Note that crack growth in LT specimens is representative of a transverse fissure in a rail, crack growth in TL specimens is representative of a horizontal split head crack growth, whereas the SL specimens represent crack growth for a vertical split head). The orientation of the SEN and MM specimens was LT, the orientation of the SF specimen was LS, as shown in Figure 6.

A matrix of all specimens tested is presented in Table 2. Rail sample numbers are also indicated. Different specimens cut from one rail sample are designated by sequential numbers after the sample identification, i.e., Specimens 032-1, 032-2, 032-3 are three specimens from Sample 032. Table 2 lists a total number of 99 experiments. Not included in Table 2 are the additional tests on the last group of samples listed in Table 1. Those samples were all tested in both LT and TL direction at R=0, which accounts

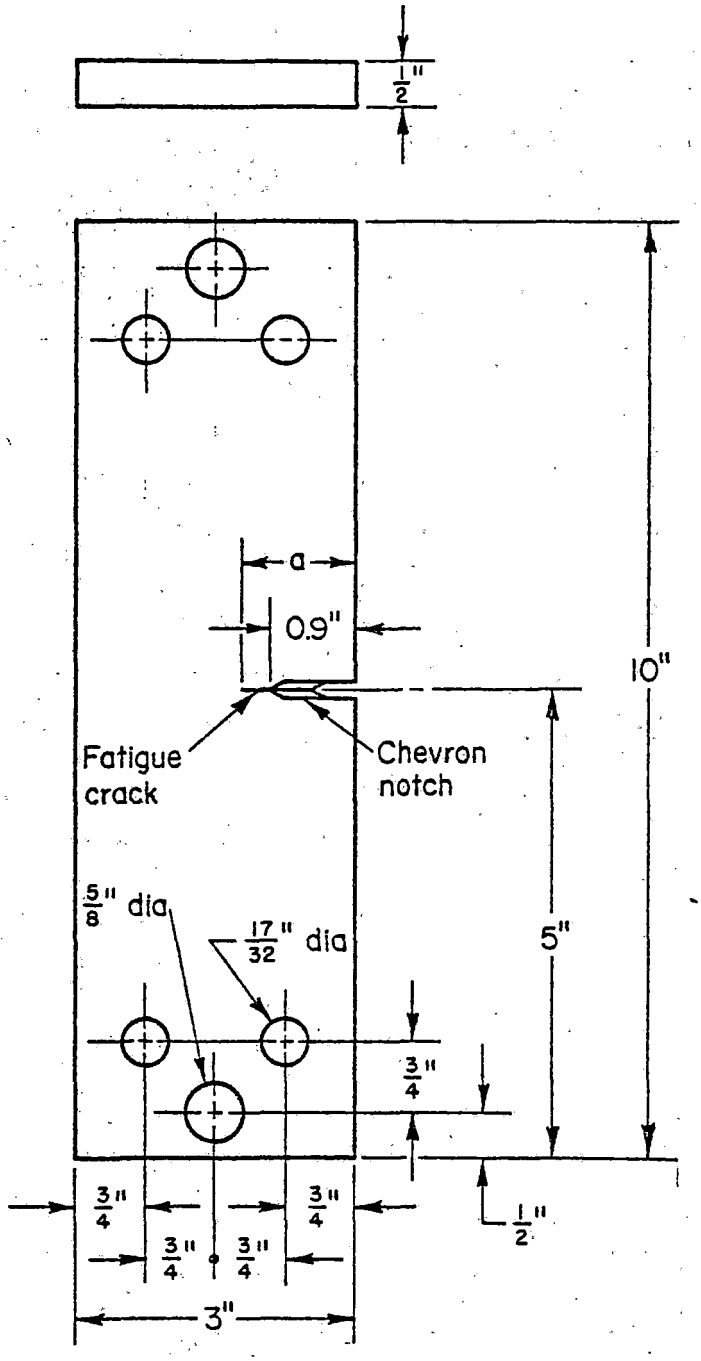

FIGURE 2. SINGLE-EDGE NOTCH CRACK GROWTH SPECIMEN

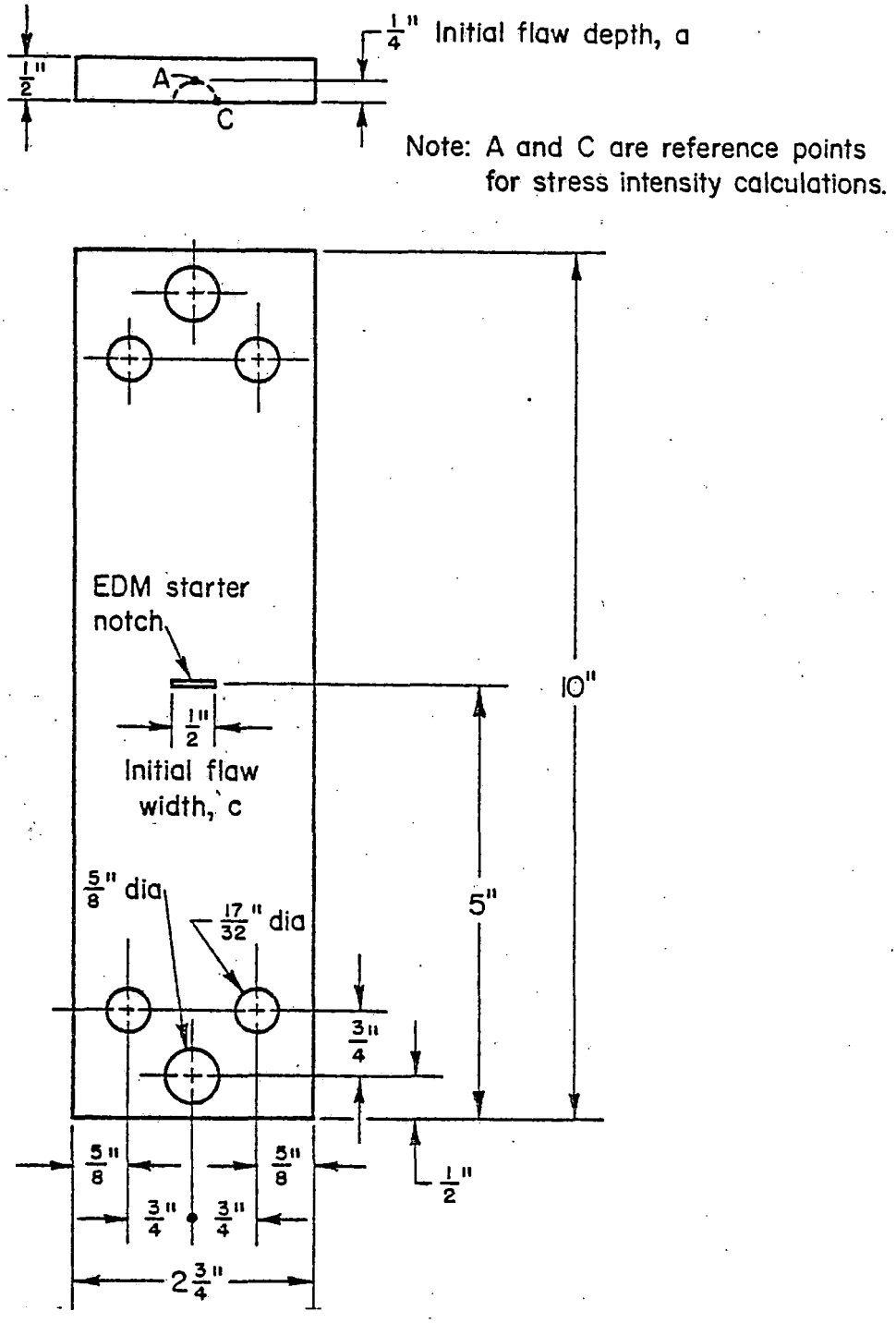

FIGURE 3. SURFACE-FLAW CRACK GROWTH SPECIMEN

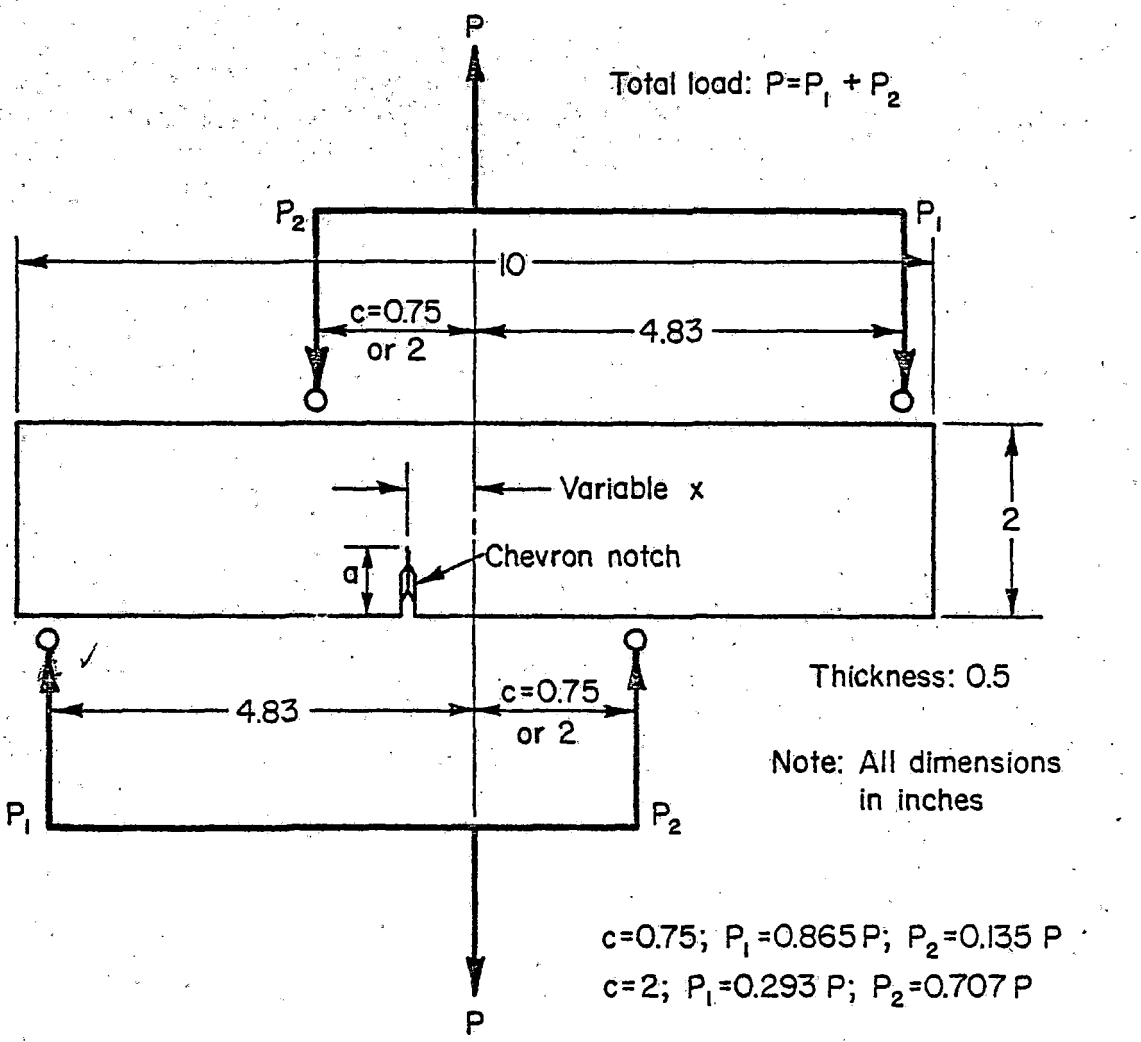

FIGURE 4. MIXED MODE SPECIMEN

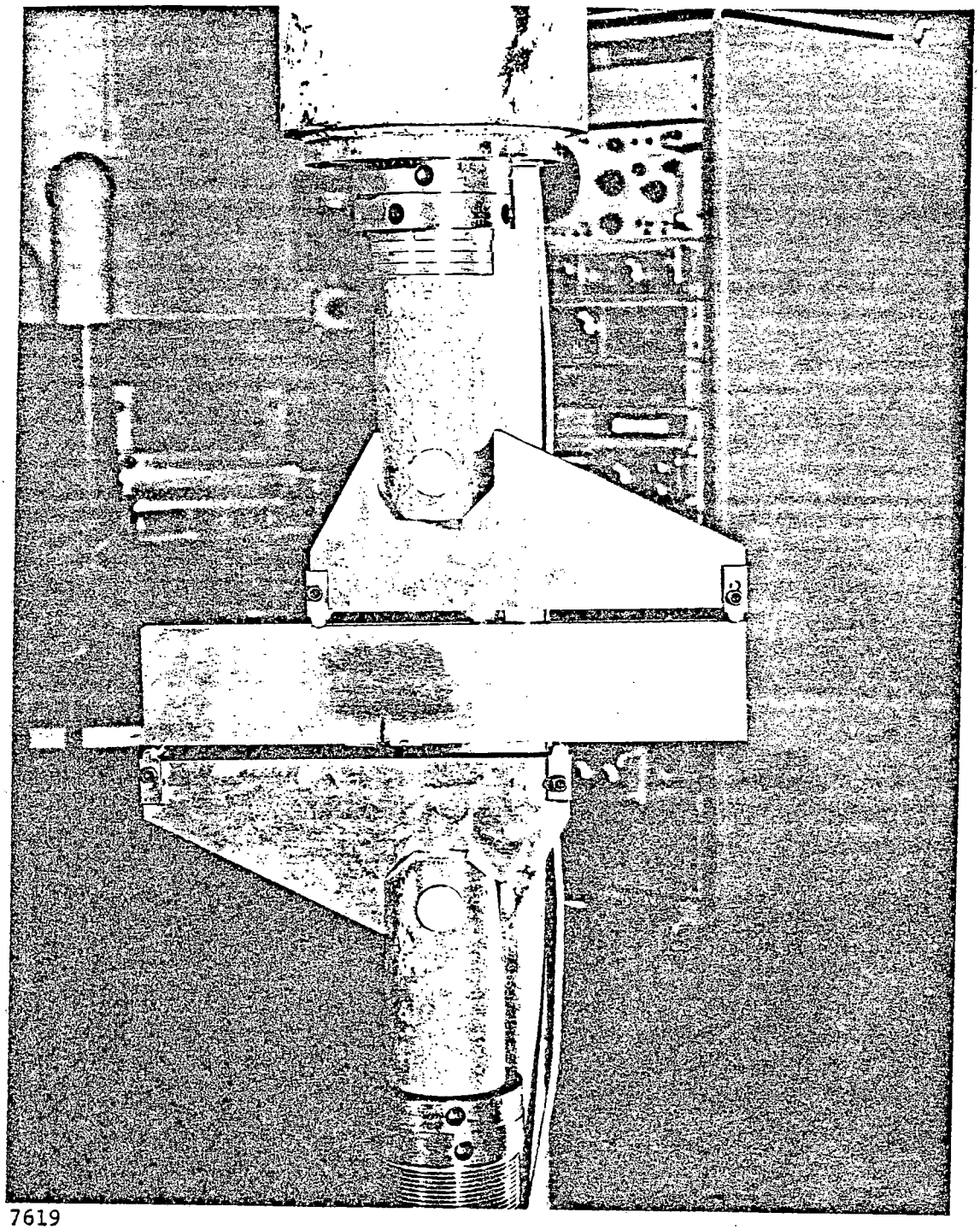

7619

FIGURE 5. MIXED MODE TEST SETUP

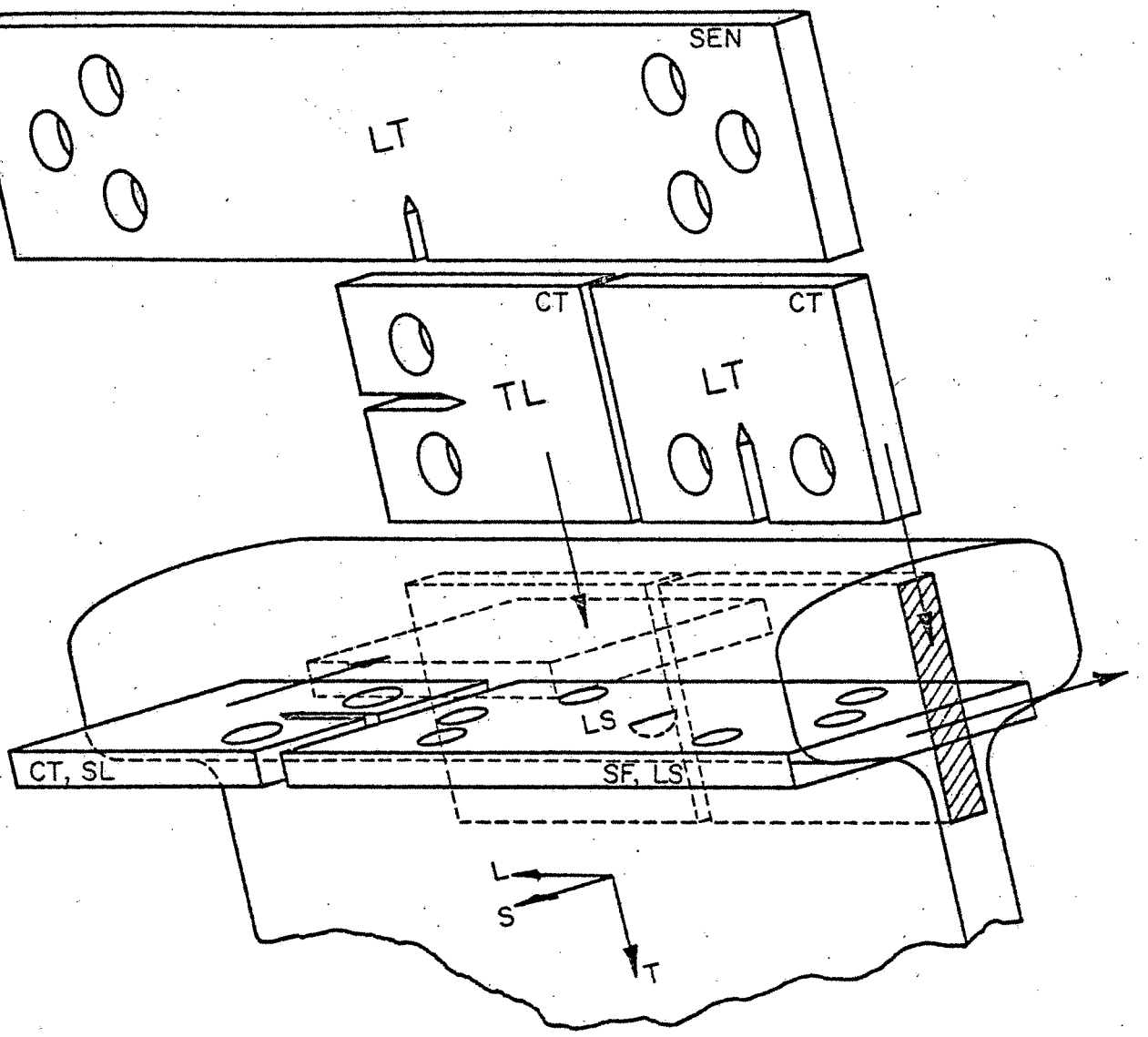

FIGURE 6. ORIENTATION OF SPECIMENS

TABLE 2. TEST MATRIX (SPECIMEN NUMBERS)

Type of Experiment Or Orientation	Temp. (°F)	Freq. (H_z) Hz	Specimen Type	Category I			Category II			Category III		
				R = -1	R = 0	R = 0.5	R = -1	R = 0	R = 0.5	R = -1	R = 0	R = 0.5
TL	-40	40	CT		016-1	016-2		019-2 024-3	024-2		029-2	022-2
	68	40	CT		023-2	023-1 002-1		009-1	006-1 009-2		007-1	001-1 007-2
	+140	40	CT		013-1	002-2		019-1	024-1		020-2	022-1
SL	68	40	CT		016						029 022	
LT	-40	2	CT		002-2			031-1			029-2	
		40	CT		013-2 030-2	023-2		006-2	009-2 019-1		001-2 007-2	
	68	2	CT		002-1						035-1 036-1	
		4-30	SEN	016 030	013-1 023-1	013-2 016-1	009 031 024	019 006		035	029 020	036 020-1 022 007
	140	2	CT		030-1			031-2			029-1	020-1
		40	CT		013-1	023-3		006-1			001-1	022-2
Threshold TL	68	30-50	CT		030-1	030-1		031-1	031-1		029-1	029-1
LT		30-50			016	016		009	009		022	022
LT	68	30-50	SEN	013-1			018 024					
Surface Flaw	68	20-30	SF		025-5 025-6			021-5 021-6			056-1 056-2	
Mixed Mode												
$K_{II}/K_I = 0$	68	9	MM		013-1			018-1 024-1				
$K_{II}/K_I = 0.34$					016-1			018-2			001-1	
$K_{II}/K_I = 0.72$					013-2			018-3			029-1	
$K_{II}/K_I = \infty$					013-3			018-4 009-1				

for 20 experiments. This brings the grand total of experiments in Phase II to 119 experiments.

3.2 Testing Procedures

Crack growth experiments on CT specimens were conducted in a 25-kip capacity electrohydraulic servocontrolled fatigue machine. The tests were performed under constant amplitude cyclic loading. The maximum load for the experiments was 2500 pounds for all R-values. Cycling frequency was as indicated in Table 2.

All tests at room temperature were conducted in laboratory air kept at 68 F and 50 percent relative humidity. For the tests conducted at 140 F, the specimen was surrounded by a closed chamber through which hot air was circulated. For the tests at -40 F cold air (cooled by dry ice) was circulated through the chamber. The nonambient temperatures were automatically controlled to within $\pm$ 3 F. The environmental chamber was provided with a glass window to enable observation of the specimen and the crack.

SEN and SF specimens were tested in a 25-kip electrohydraulic fatigue machine. The maximum load during constant amplitude cycling was 9000 pounds for all R-ratios.

Threshold tests were performed in the same machine. Starting at crack growth rates of about 10^{-6} inches per cycle, the load was reduced in steps until growth rates had decreased to approximately 10^{-9} inches per cycle. Subsequently, the load was increased stepwise to accelerate crack growth to 10^{-6} inches per cycle. This procedure was repeated several times. The number and sizes of the load steps will be given in the section on tests results.

Mixed mode experiments were conducted in a 25-kip fatigue machine of the same type as described above. The loading principle is shown in Figures 4 and 5.

Two methods of crack-length measurement were used. For about half of the experiments, crack growth was measured visually, using a 30 power traveling microscope. The cracks were allowed to grow in increments of approximately 0.05 inch after which the test was stopped for an accurate crack size measurement. Crack size was recorded as a function of the number of load cycles.

In the other experiments crack size was recorded automatically by means of a crack growth gage. The gage consisted of 20 parallel strands of copper foil, adhesively bonded to the specimen, as illustrated in Figure 7. The strands ran perpendicular to the crack at a spacing of 0.05-inch. When the crack tip reached a strand, failure of the strand occurred, so that the successive breakage of strands was a measure for crack growth.

Electric current through the gage was affected by the failure of a strand. This was detected by an electronic decoder and stored in the process computer in line with the fatigue machines. At the end of the test, the growth data could be retrieved from the computer for processing and analysis. On several occasions the automatic crack growth records were compared with visual crack size measurements and found satisfactory. Use of the crack gage permitted continuation of experiments during off-work hours.

4. DATA PROCESSING AND DATA PRESENTATION

4.1 Crack Growth Rates

The crack growth records of CT and SEN specimens are not directly comparable, nor are they directly applicable to the case of a crack in a rail. The correlation between cracks of different types can only be made if crack growth data can be expressed in a unique way, independent of the crack size, the geometry and loading system. This can be done on the basis of the stress-intensity factor, K.[3]

The stresses at the tip of a crack can always be described as

$$\sigma_{ij} = \frac{K}{\sqrt{2\pi r}} f_{ij}(\theta) \qquad (4.1)$$

where σ_{ij} (i = x,y,z; j = x,y,z) represents the stress in any direction, r and θ are polar coordinates originating at the crack tip. The functions $f_{ij}(\theta)$ are known functions. Thus, Equation (4.1) shows that the stress field at the tip is completely described by the stress intensity factor, K.

As shown in Figure 8, a crack can be subjected to three different loading cases (modes). Tension loading is denoted as Mode I, in-plane shear is Mode II, and out of plane shear is Mode III. Equation (4.1) is valid for

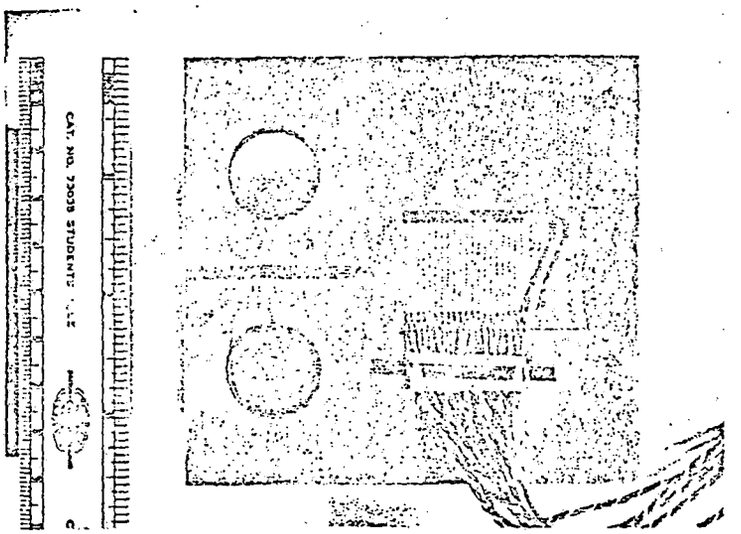

FIGURE 7. CRACK PROPAGATION GAUGE MOUNTED ON CT SPECIMEN

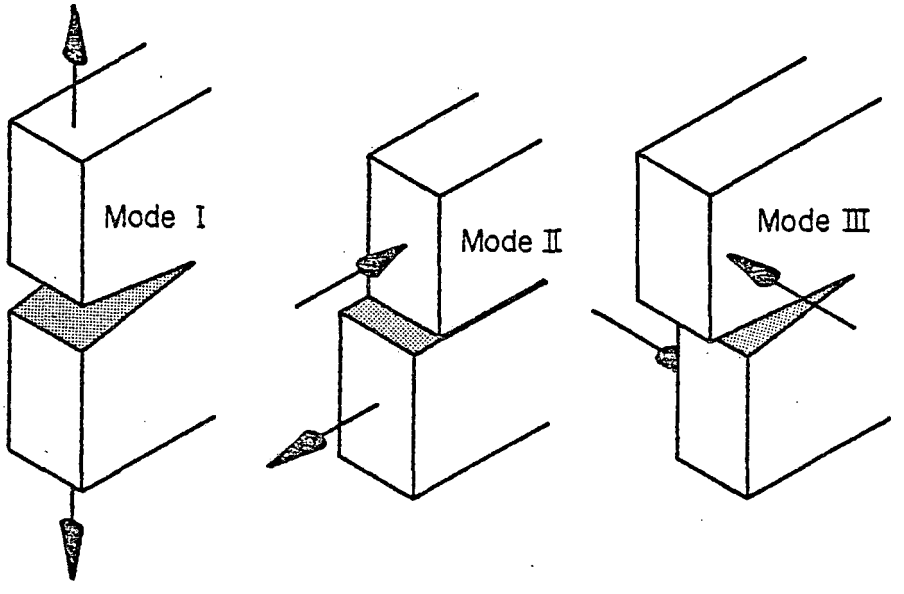

FIGURE 8. THREE MODES OF LOADING

all three modes, except that the functions $f_{ij}(\theta)$ are different for each mode, but apart from that they are independent of geometry. Naturally, the stress intensity factors for the three modes are different, yielding

$$\sigma_{ij} = \frac{K_I}{\sqrt{2\pi r}} f_{ij\ I}(\theta),\ \sigma_{ij} = \frac{K_{II}}{\sqrt{2\pi r}} f_{ij\ II}(\theta),\ \sigma_{ij} = \frac{K_{III}}{\sqrt{2\pi r}} f_{ij\ III}(\theta) \qquad (4.2)$$

The general loading case is a combination of Modes I, II, and III; the stresses can simply be added. Mode I is technically the most important. For this reason the subscript I is usually omitted for applications to fatigue crack propagation. Thus, K without subscript is always referring to Mode I loading.

Stress intensity factors can be calculated for various types of cracks. The general form for the expression of K is

$$K = \beta\sigma\sqrt{\pi a} \qquad (4.3)$$

where a is the crack size, σ is the remote stress, and β is a geometry function.

Since the stress intensity factor describes the whole stress field by Equation (4.1), the stress distribution at the tips of two different cracks will be equal if the stress intensities have the same value. For example, for a case where $\beta = 1$, two cracks differing by a factor of 4 in size would have the same stress intensity if the remote stress for the large crack was half the remote stress intensity of the small crack, and the two crack tips would carry equal stress fields. This suggests that the cracks would also behave in the same way, i.e., show the same rate of growth. As a consequence fatigue crack growth rates associated with different geometries can be compared on the basis of the stress intensity factor; equal K means equal growth rates, within the range of variability of crack growth rates of a given material.

The rate of crack growth per cycle is denoted by the derivative da/dN, which is related to K by

$$\frac{da}{dN} = f(\Delta K) \qquad . \qquad (4.4)$$

In this equation ΔK is the range of the stress intensity factor, obtained by substituting $\Delta\sigma$ in Equation (4.3). In turn, $\Delta\sigma$ is the range over which the

remote stress varies during a load cycle.

If da/dN data are plotted as a function of ΔK on a double-logarithmic graph paper the result is often a straight line. This suggests that

$$\frac{da}{dN} = C\ \Delta K^n \quad , \tag{4.5}$$

a commonly used expression in which C and n are constants. Figure 9 presents an illustration of this equation, using the data of 66 rail steel samples tested at R = 0 in the first phase of this program[12].

It is generally recognized that da/dN is dependent not only on the range of stress, but also on the maximum stress in a cycle or the stress ratio R (which is equivalent). Also, there is generally an upswing of the rate of crack growth towards the end of the test, because the failure conditions are approached. Failure occurs when the stress intensity factor approaches a critical value, K_{Ic}. This is reflected in the following equation:

$$\frac{da}{dN} = C\ \frac{\Delta K^n}{(1-R)K_{Ic}-\Delta K} \quad . \tag{4.6}$$

Equation (4.6) accounts for the effect of R-ratio, and it shows that da/dN becomes infinite when the stress intensity at maximum load becomes equal to K_{Ic}. It does not yet reflect the fact that crack growth rates approach zero when the stress intensity is below a certain threshold level ΔK_{th}. An equation that accounts for the threshold can be written[4] as:

$$\frac{da}{dN} = C(\Delta K^2-\Delta K_{th}^2)\left\{1+\frac{(1-R)\Delta K}{(1-R)K_{Ic}-\Delta K}\right\} \quad . \tag{4.7}$$

According to Equation (4.7) the relation da/dN-ΔK has two asymptotes, one at $\Delta K = \Delta K_{th}$, the other at $\Delta K/(1-R) = K_{Ic}$, as shown schematically in Figure 10.

In the following sections crack propagation data will be presented as da/dN = f(ΔK). The applicability of Equations (4.5) - (4.7) will be discussed. As for mixed mode crack propagation a generally accepted correlation equation does not yet exist. This problem will be discussed in more detail in a later section.

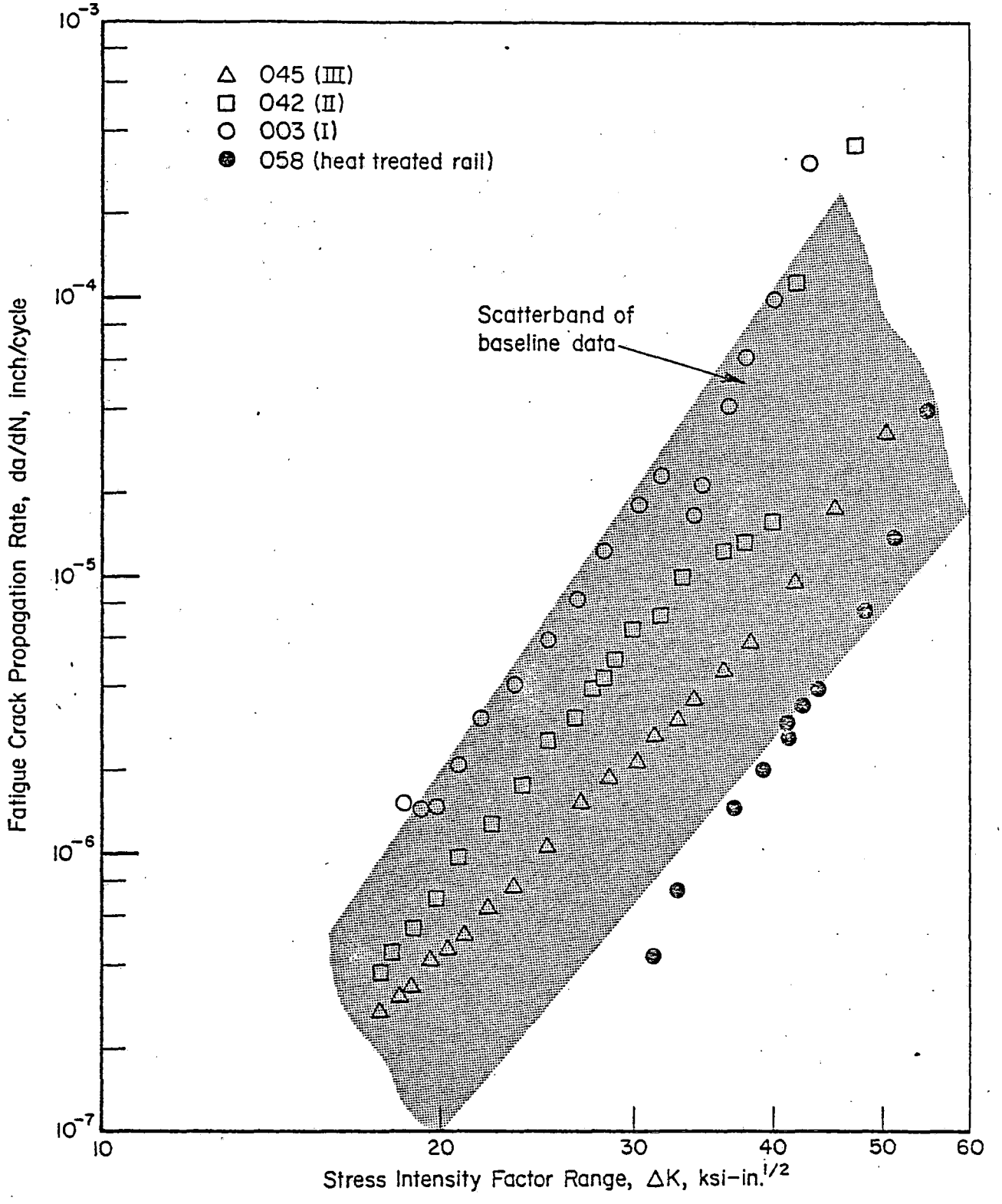

FIGURE 9. FATIGUE CRACK PROPAGATION RATE BEHAVIOR OF 66 RAIL SAMPLES TESTED AT R = 0 IN THE FIRST PHASE OF THE PRESENT PROGRAM[1,2]

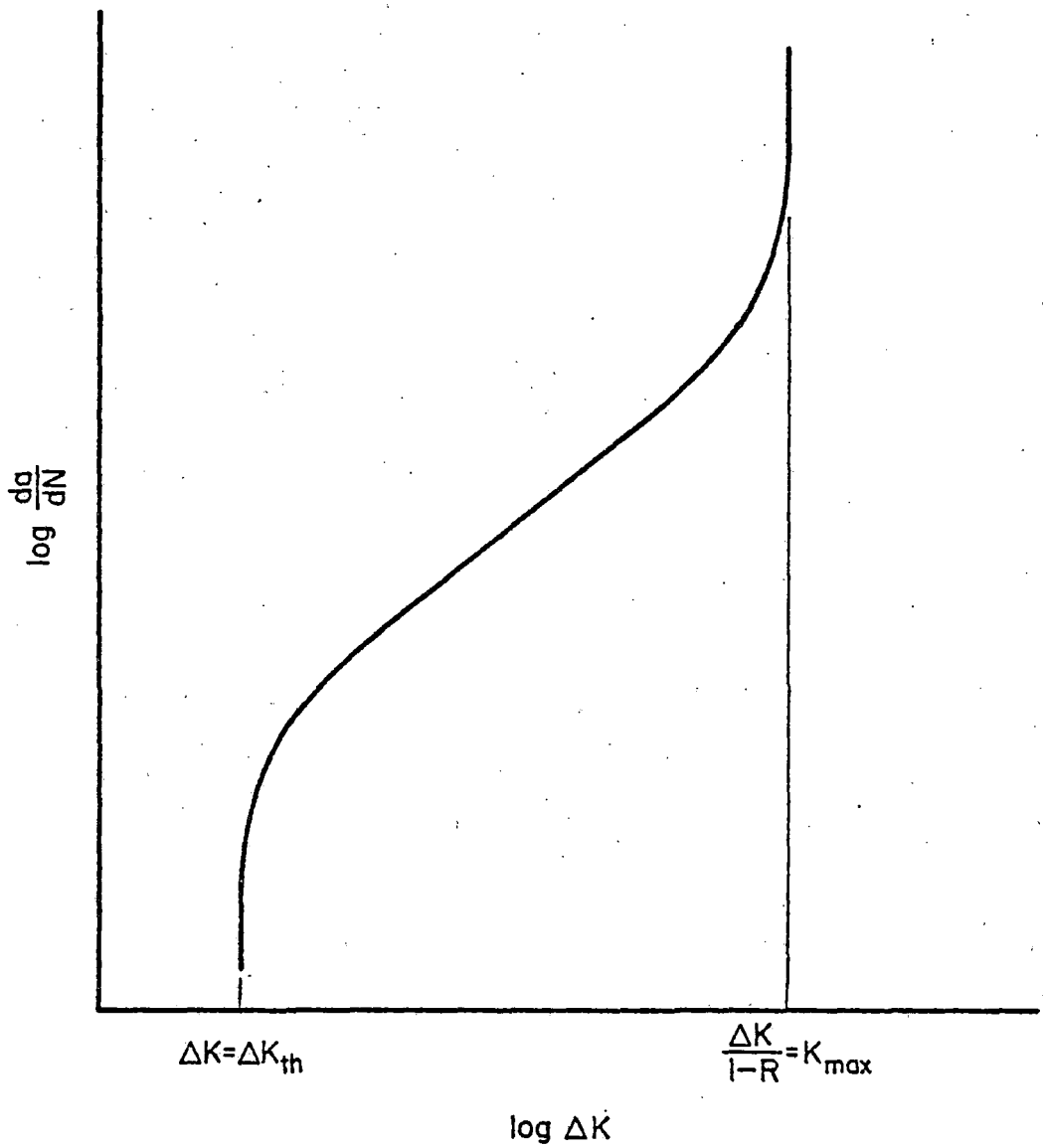

FIGURE 10. SCHEMATIC REPRESENTATION OF da/dN - ΔK

4.2 Stress Intensity Factors

The stress intensity factor for the CT specimen used in this investigation is given as:

$$K = \frac{P}{2BW^{1/2}} \left(1 + \frac{a}{W}\right) \left(1 - \frac{a}{W}\right)^{-\frac{3}{2}} \left\{7.000 - 7.050 \frac{a}{W} + 4.275 \left(\frac{a}{W}\right)^2\right\} \qquad (4.8)$$

in which P is the applied load, and a, B and W are as defined in Figure 1.

It is not immediately clear that Equation (4.8) has the character of Equation (4.3). This is more evident in the stress intensity factor for the SEN specimen, which is given as:

$$K = \frac{P}{BW} \sqrt{a} \left\{1.99 - 0.41 \frac{a}{W} + 18.7 \left(\frac{a}{W}\right)^2 - 38.48 \left(\frac{a}{W}\right)^3 + 53.85 \left(\frac{a}{W}\right)^4\right\} \qquad (4.9)$$

with a, B and W as defined in Figure 2. Obviously P/BW is the remote stress.

The stress intensity factor for an elliptical surface flaw varies along the crack front. If the semi-major axes of the ellipse is c, and the semi-minor axis is a (see Figure 3), the stress intensity factor for the SF specimen is:

$$\text{Point A (Figure 3)} \quad K = 1.12 \frac{M_k}{\phi} \frac{P}{BW} \sqrt{\pi a}$$

$$\text{Point C (Figure 3)} \quad K = 1.12 \frac{M_k}{\phi} \frac{P}{BW} \sqrt{\pi a^2/c}$$

$$\text{with} \quad \phi = \int_0^{\pi/2} \left[1 - \frac{c^2 - a^2}{c^2} \sin^2\psi\right] d\psi \quad .$$

In these equations ϕ is a completely defined elliptical integral of the second kind, values for which can be found in mathematical tables, M_k is a factor depending upon a/B and a/c derived by Kobayashi et al.[5,6] and also to be found in textbooks[3]. Since the stress intensity is higher at Point A than at Point C, the surface flaw will have a tendency to grow faster in depth than in length.

The bending moment and shear force distribution in the MM specimen are shown in Figure 11. The relative magnitude of bending moment and shear force depends upon the location. Thus, the ratio between K_I (due to bending moment) and K_{II} (due to shear) can be varied by varying the location of the crack. Stress intensity solutions for this specimen did not exist. Therefore, a finite element model was made of the specimen with a crack and stress intensity factors were calculated numerically*. The specimen dimensions and crack locations were taken in such a way that the ratio K_{II}/K_I covered the desired range. The stress intensity factors for the four cases considered are given in Figure 11. The change of the stress intensity factors as a function of crack size will be discussed later.

* This work was done by E. F. Rybicki

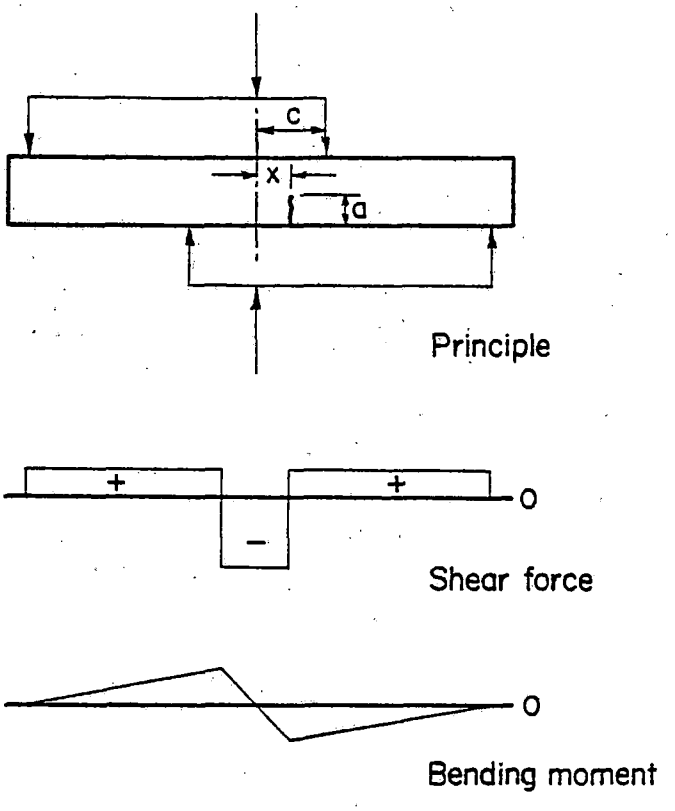

a, in.	c, in.	x, in.	K_I/P, ksi$\sqrt{\text{in.}}$ per lb of Load P	K_{II}/P, ksi$\sqrt{\text{in.}}$ per lb of Load P	K_{II}/K_I
0.5	2	2	3.5×10^{-3}	0	0
0.5	2	1	1.74×10^{-3}	0.6×10^{-3}	0.34
0.5	0.75	0.25	0.78×10^{-3}	0.57×10^{-3}	0.72
0.5	0.75	0	0	1.16×10^{-3}	∞

FIGURE 11. BENDING MOMENT AND SHEAR FORCE DISTRIBUTION IN MM SPECIMENS

5. TEST RESULTS

5.1 Introduction

The results of the fatigue-crack growth experiments to determine the effect of stress ratio, cycling frequency, test temperature, and specimen orientation are presented in this section. The threshold and surface flaw results are also presented and discussed; however, the mixed-mode results will be presented in Section 6. Actual tabulated crack length-cycle readings for the various specimens are reported in Appendix A. The specific test conditions for each specimen are cited in Table 2. Experimental procedures were as discussed in Section 2.

5.2. Effects of Stress Ratio

To evaluate the effects of stress ratio on the crack-growth behavior of rail-steels in the LT orientation, a series of constant amplitude fatigue-crack growth experiments at R = 0.0, -1.0, and 0.50 were performed on 18 SEN-type specimens. In addition, to verify that specimen geometry did not influence test results, three experiments at R = 0.0 were performed on the CT-type specimen.

The results of these experiments are displayed in Figures 12 through 14 for R = 0.0, -1.0, and 0.50, respectively. Individual specimens are identified by a unique symbol so that the crack-growth behavior of a specific sample (or heat or category) can be compared and contrasted with other data. The rate data displayed are based on 3-point divided difference calculations of crack growth rate. To facilitate illustration, only alternate points for a given specimen are shown where there are more than 10 crack growth readings on a specimen.

Several observations can be made regarding the R = 0.0 data in Figure 12. First the effect of specimen geometry on crack-growth behavior appears to be negligible, with SEN and CT specimens displaying nearly identical crack-growth trends. Second the behavior of specimens from different crack-growth rate categories (as specified in Table 1) are really indistinguishable. In fact, specimen 023-1 which displayed particularly low crack-

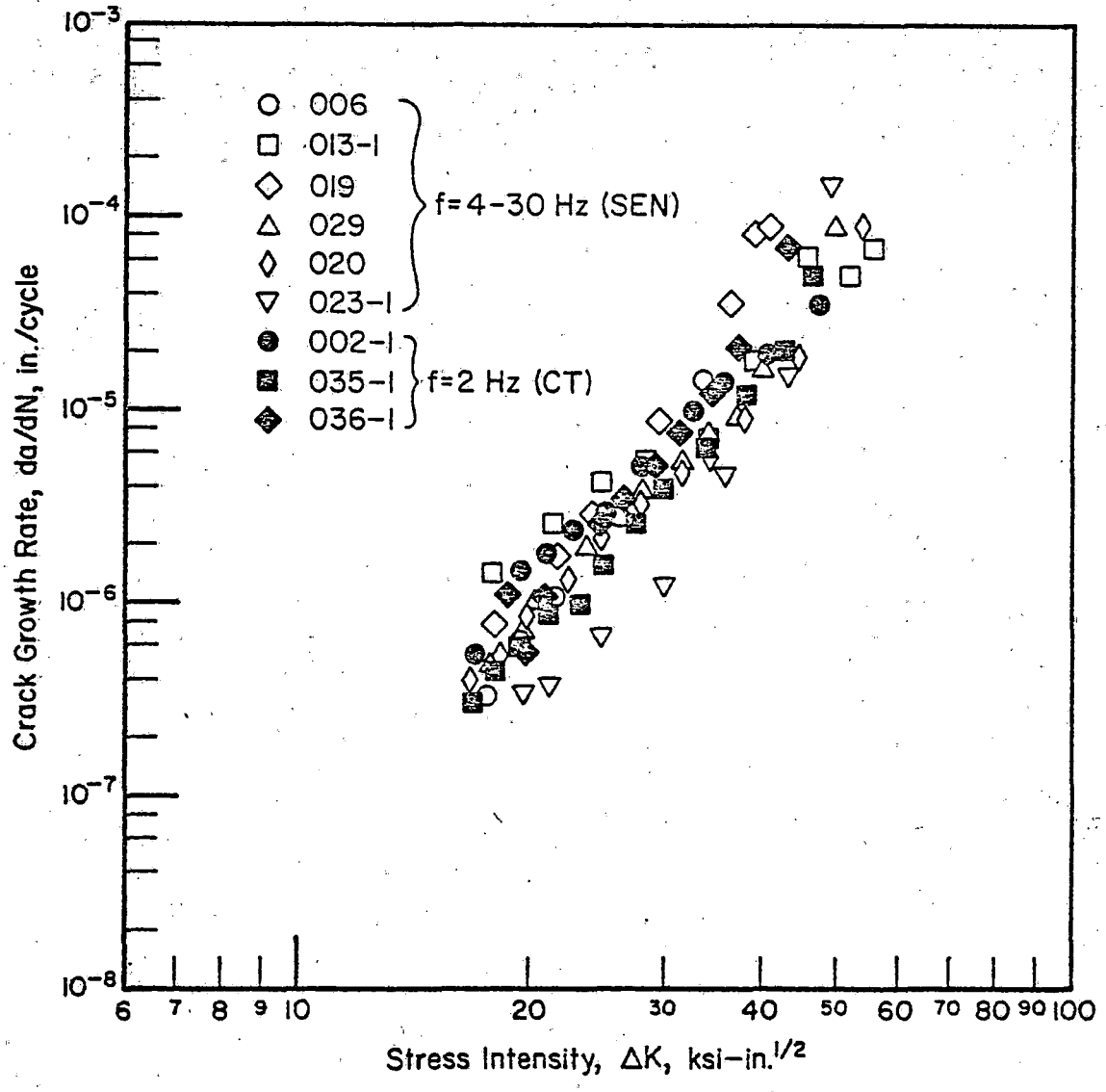

FIGURE 12. CRACK GROWTH DATA AT ROOM TEMPERATURE, LT DIRECTION, R = 0, DIFFERENT FREQUENCIES

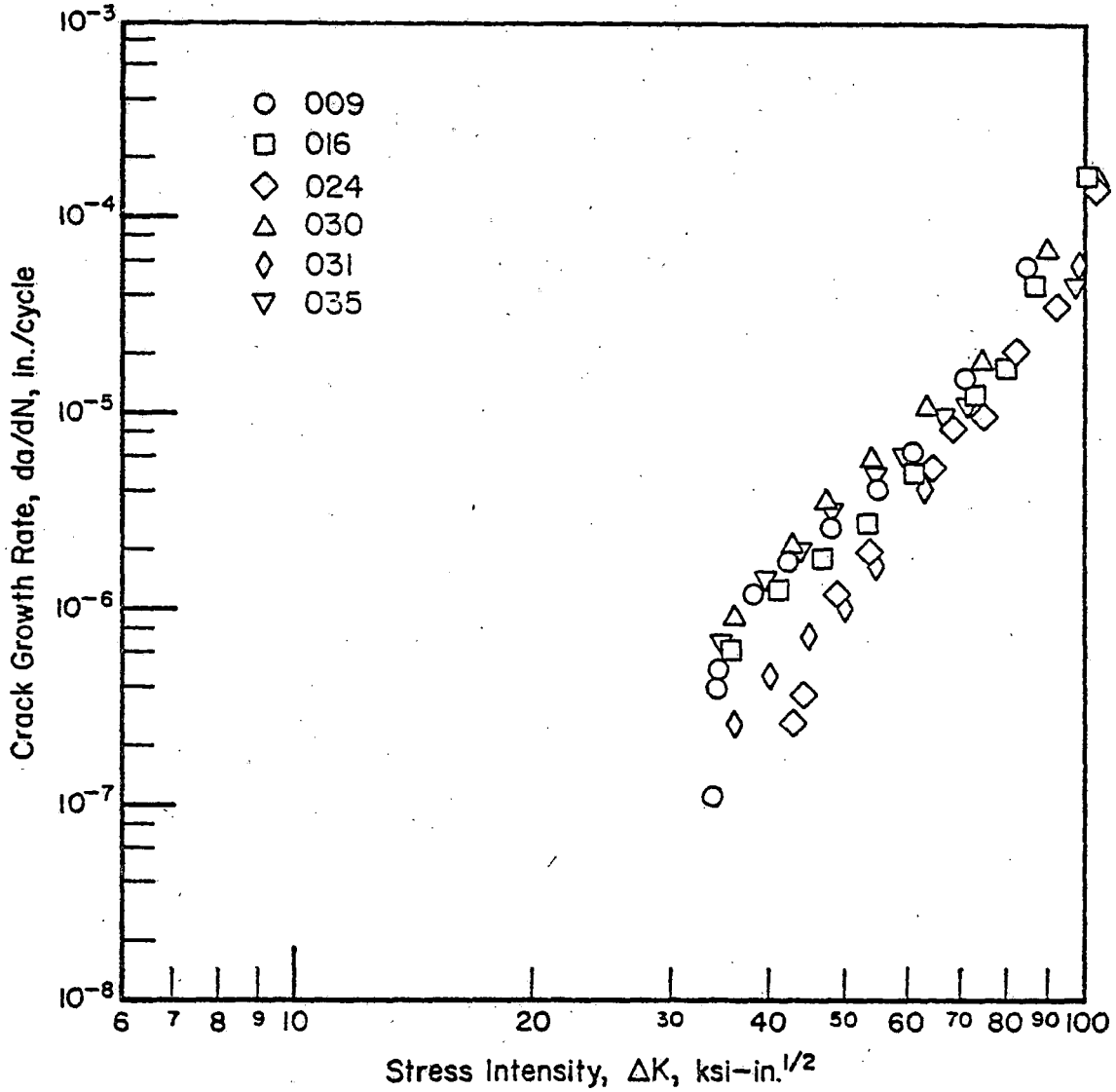

FIGURE 13. CRACK GROWTH DATA AT ROOM TEMPERATURE AND R = -1, SEN SPECIMENS IN LT DIRECTION, FREQUENCY OF 4 - 30 HZ

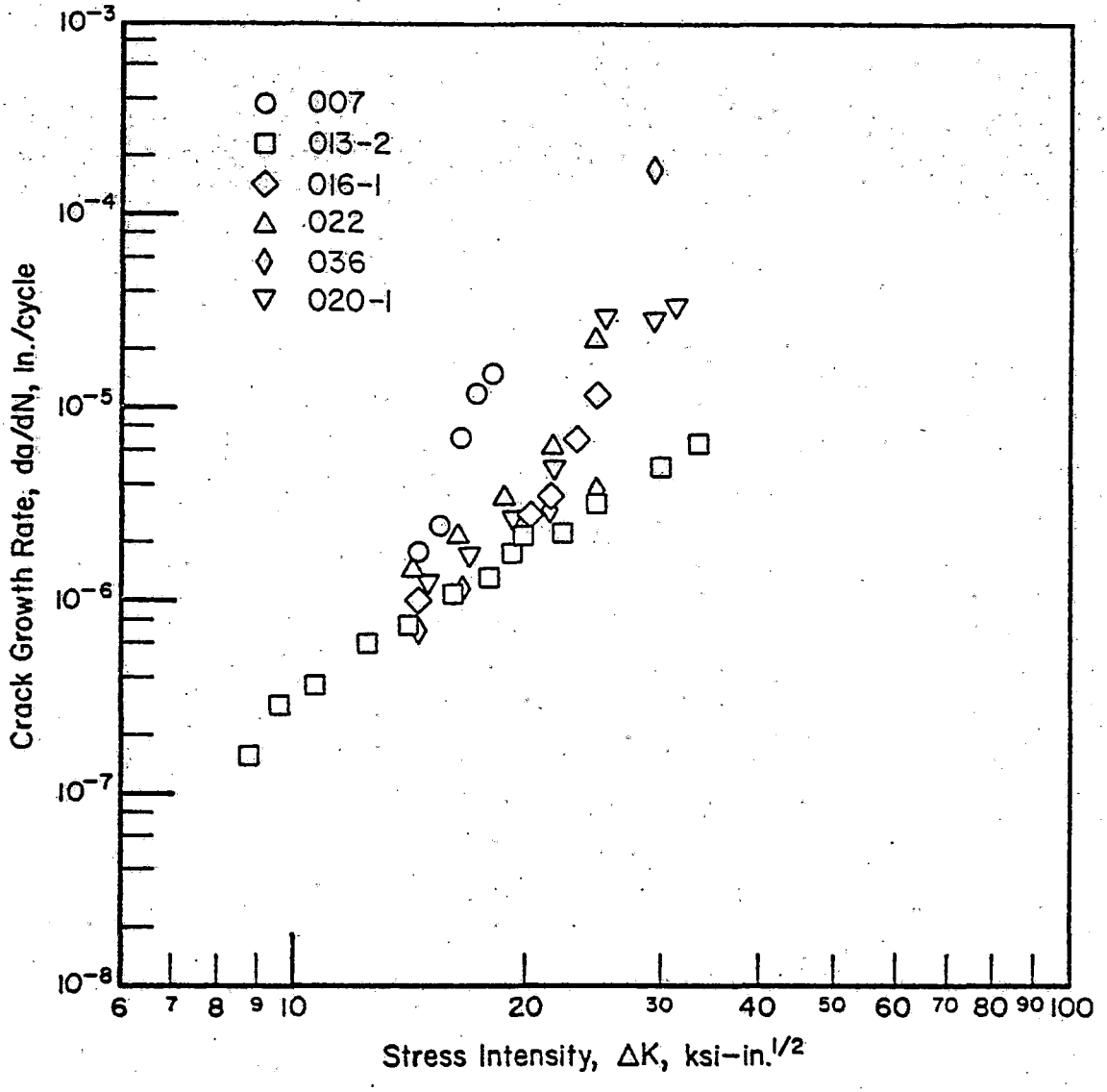

FIGURE 14. CRACK GROWTH DATA AT ROOM TEMPERATURE AND R = 0.5, SEN SPECIMENS IN LT DIRECTION, FREQUENCY OF 4 - 30 HZ

growth rates came from a rail that was identified as Category I (high rate). The reason for this disparity appears to be that the original rate categories were assigned on the basis of individual test results that could not be statistically analyzed for variability. Subsequent tests have shown that the crack-growth behavior of different test specimens from the same rail may vary nearly as much as specimens taken from totally different rails. This problem of data variability will be addressed in more detail in Section 8.

The R = -1.0 data shown in Figure 13 displayed a similar variability in rate behavior to the R = 0.0 experiments, while the R = 0.50 data shown in Figure 14 exhibited substantially greater scatter, especially at the highest crack-growth rates. The increased scatter for the latter case is not fully understood, but may be partially due to differences in fracture toughness of the rail samples.

The overall data trends for the room temperature crack-growth experiments on LT orientation specimens are shown in Figure 15. Three distinct bands are formed for each stress ratio when the data are plotted versus the stress intensity range, ΔK. Each band has an average slope of approximately 4 in the logarithmically-linear range of the data. This simply implies that a two-fold increase in stress intensity would result in a new average crack growth rate 16 times (2^4) that of the initial rate.

The effects of R-ratio displayed in Figure 15 are partially accounted for by simply considering crack-growth rate as a function of maximum stress intensity, K_{max} rather than ΔK. Figure 16 illustrates the result of that simple transformation. The R = 0.0 and -1.0 data bands nearly overlap for all values of K_{max}, which effectively means that negative loads are insignificant factors in the propagation of cracks in rail steels (at least for constant amplitude loading conditions). The R = 0.5 data band does not coincide with the lower R ratio bands, which indicates that some combination of K_{max} and ΔK is necessary to accurately represent the effects of positive R-ratios on crack-growth rates.

The analytical representation of observed R-ratio effects is given in Section 7 of this report.

5.3 Specimen Orientation Effects

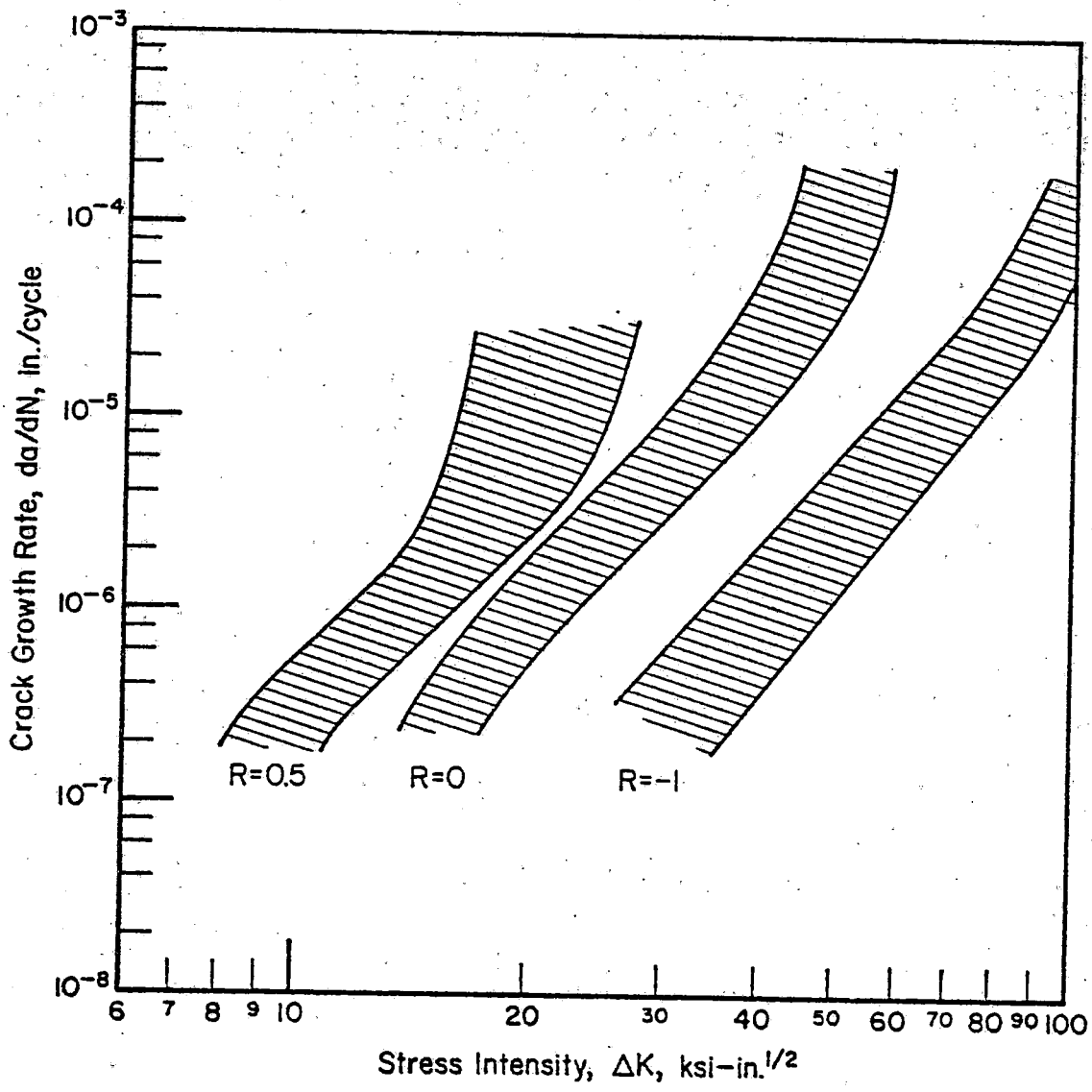

FIGURE 15. BANDS OF DATA VARIABILITY FOR LT ORIENTATION RAIL SAMPLES AT ROOM TEMPERATURE

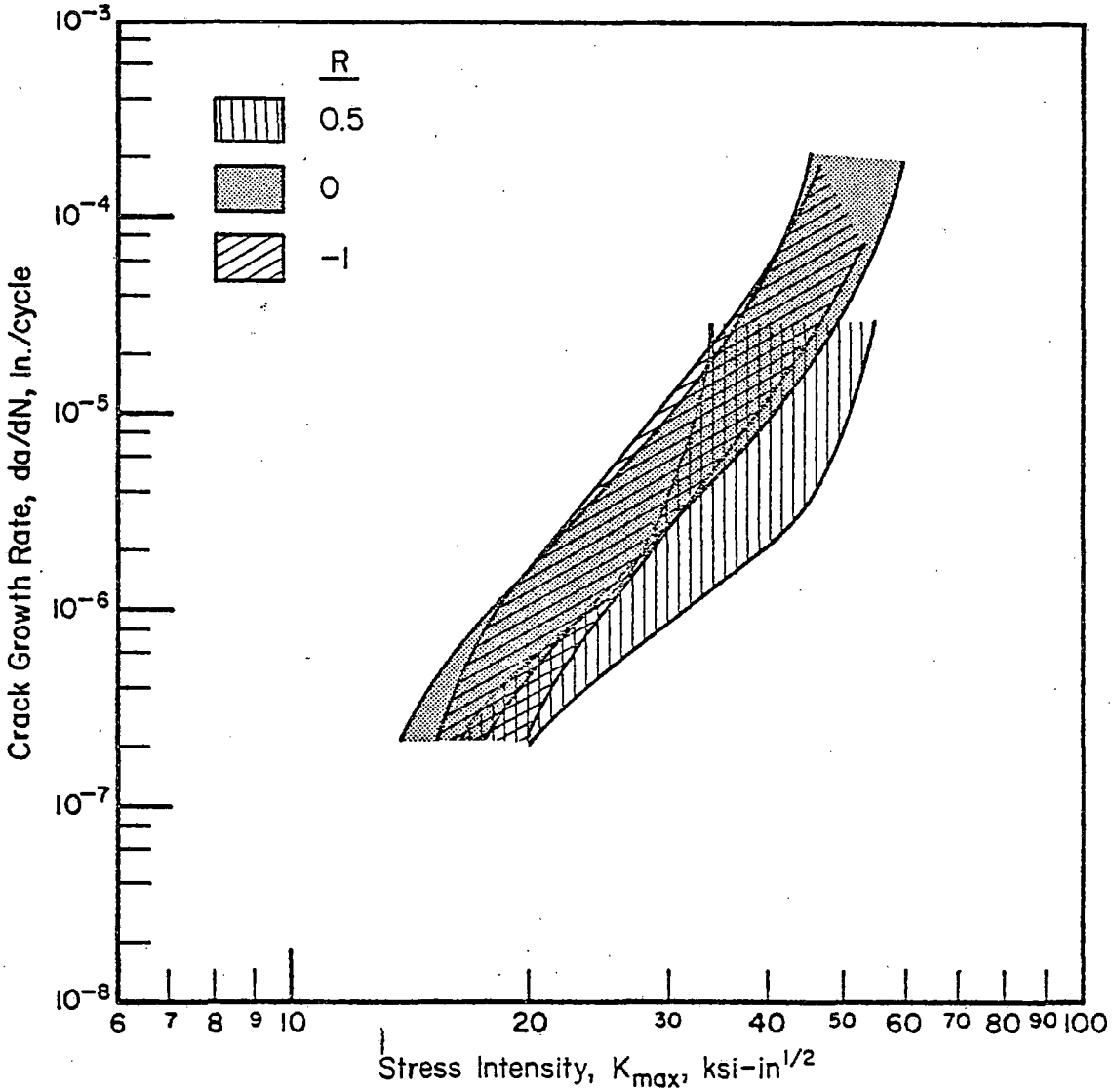

FIGURE 16. BANDS OF DATA VARIABILITY FOR LT ORIENTATION RAIL SAMPLES AT ROOM TEMPERATURE WHEN PLOTTED VERSUS MAXIMUM STRESS INTENSITY

Twelve CT specimens were tested at room temperature to evaluate the effect of crack orientation on Mode I crack-growth rates. Nine specimens were TL orientation samples, and three were SL orientation. Half of the experiments were completed at R = 0.50 (all TL orientation) and the other half were run at R = 0.0. The results of those experiments are shown in Figures 17 through 19 for the different R-ratio and orientations.

From Figures 17 and 18 it is evident that the crack-growth behavior of the TL orientation specimens was not grossly different from that of the LT orientation data shown in Figures 12 and 14. For purposes of comparison, the upper and lower limits of variability on the LT orientation specimens are shown with the basic TL orientation data. The TL data tend to fall to the high side of the LT data band at high crack-growth rates for R = 0.0, and at low crack-growth rates for R = 0.5. The differences are sufficiently small, however, that the TL orientation data could be used to represent a conservative (high-growth rate) LT orientation sample.

The same conclusion cannot be made for the SL orientation crack-growth data shown in Figure 19. For all stress intensities, the SL data fall above the LT orientation data bands. The definite indication is that SL-orientation flaws would grow faster than LT- or TL-orientation flaws subjected to equal crack tip stress intensities.

The comparative crack-growth trend lines for the three specimen orientations are shown in Figure 20.

5.4 Temperature Effects

A rather extensive series of crack-growth experiments was completed at high and low extremes in expected rail service temperatures to evaluate the effect of temperature on crack-growth rates. A total of 20 LT and 13 TL orientation specimens were fatigue cycled under constant-amplitude loading conditions at R = 0.0 and 0.50 and at temperatures of +140 F and -40 F.

The LT orientation crack-growth results at +140 F are shown in Figures 21 and 22 for R-ratios of 0.0 and 0.50, respectively, while the comparable data generated at -40 F are shown in Figures 23 and 24. Generally, the effects of increased temperature on crack-growth rates appears to be to reduce the slope of the da/dN-ΔK function and to increase the critical stress intensity limit

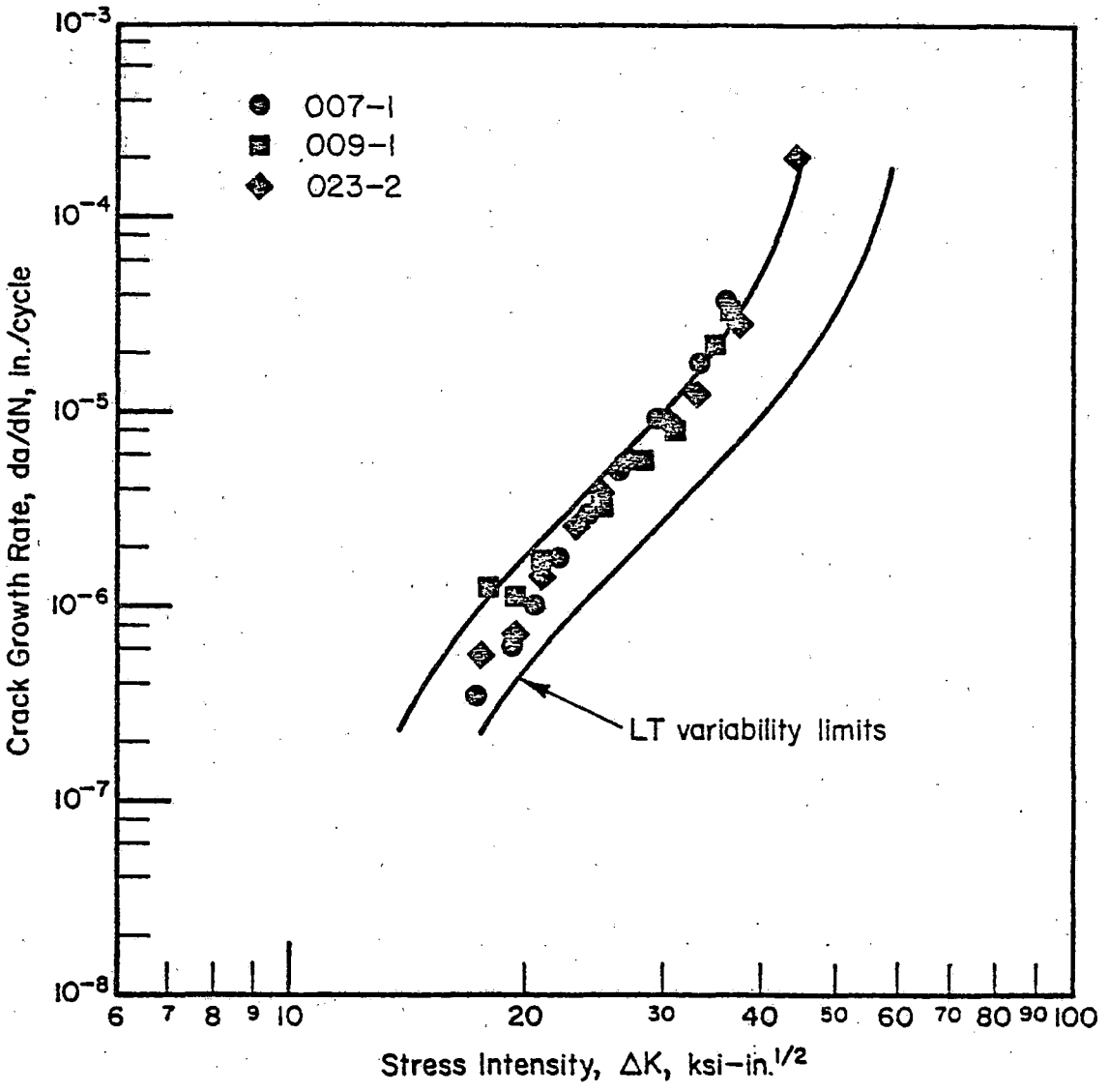

FIGURE 17. CRACK GROWTH DATA AT ROOM TEMPERATURE AND R = 0, CT SPECIMENS IN TL DIRECTION, FREQUENCY OF 40 HZ

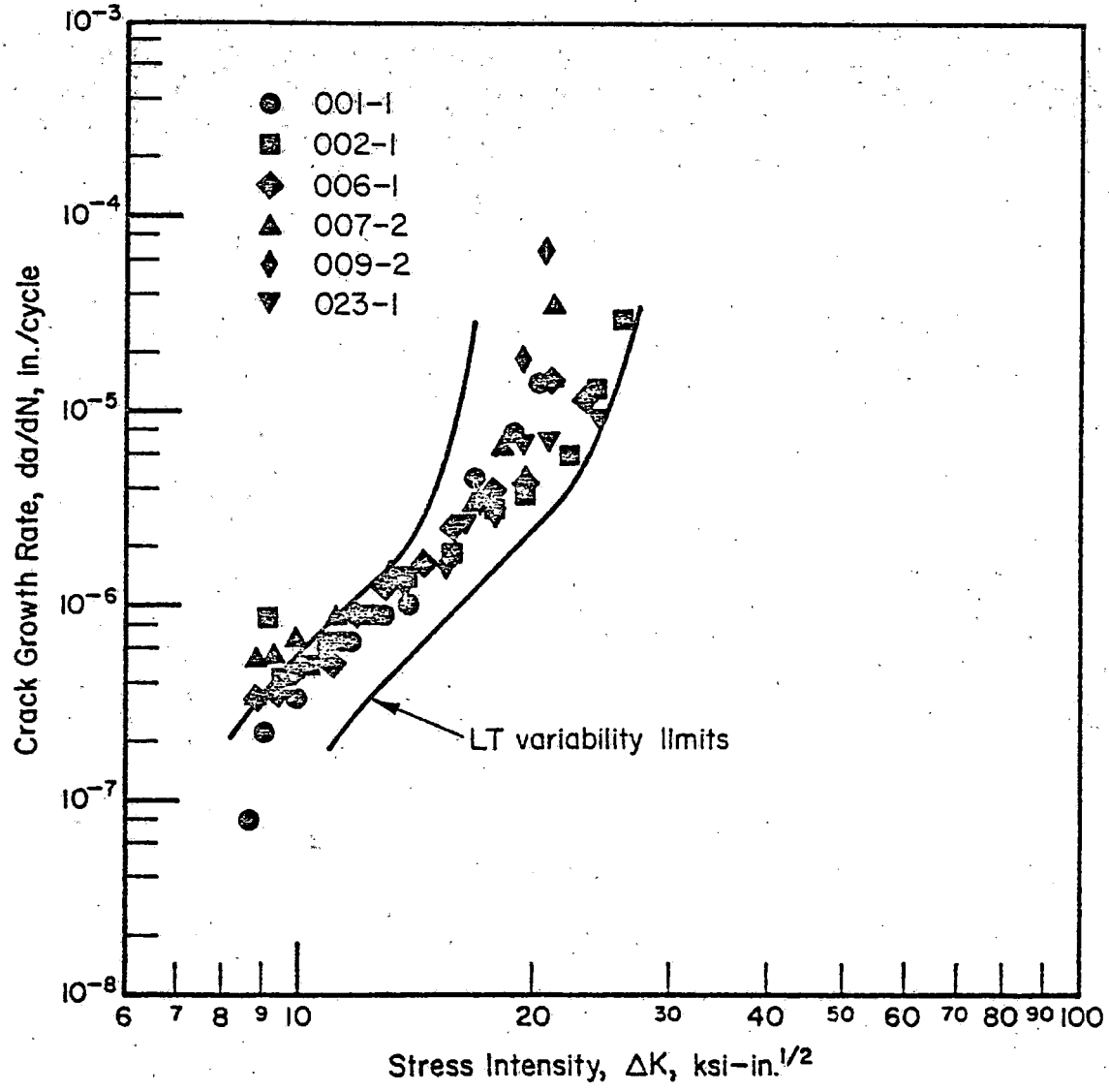

FIGURE 18. CRACK GROWTH DATA AT ROOM TEMPERATURE AND R = 0.5, CT SPECIMENS IN TL DIRECTION, FREQUENCY OF 40 HZ

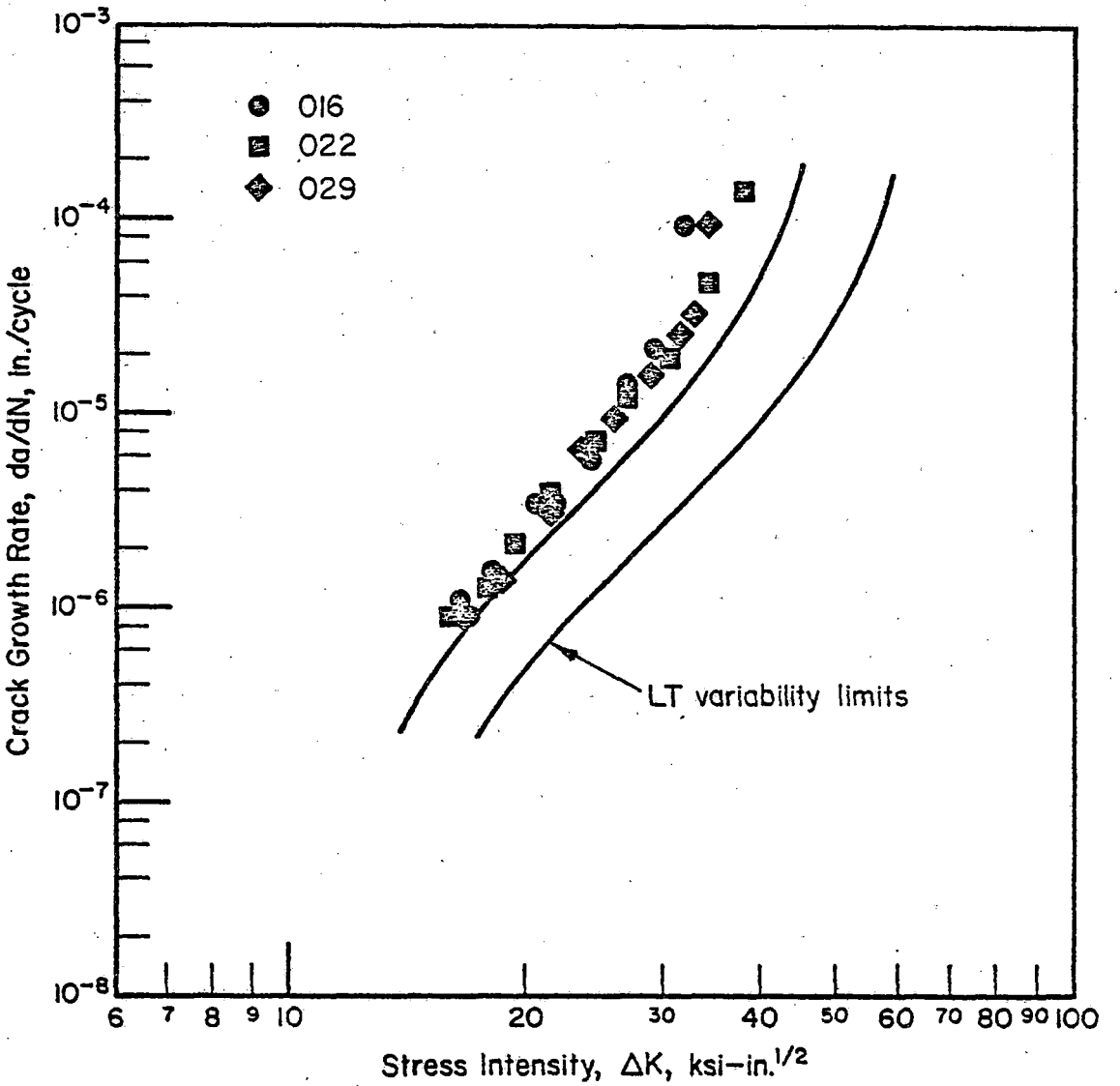

FIGURE 19. CRACK GROWTH DATA AT ROOM TEMPERATURE AND R = 0, CT SPECIMENS IN SL DIRECTION, FREQUENCY OF 40 HZ

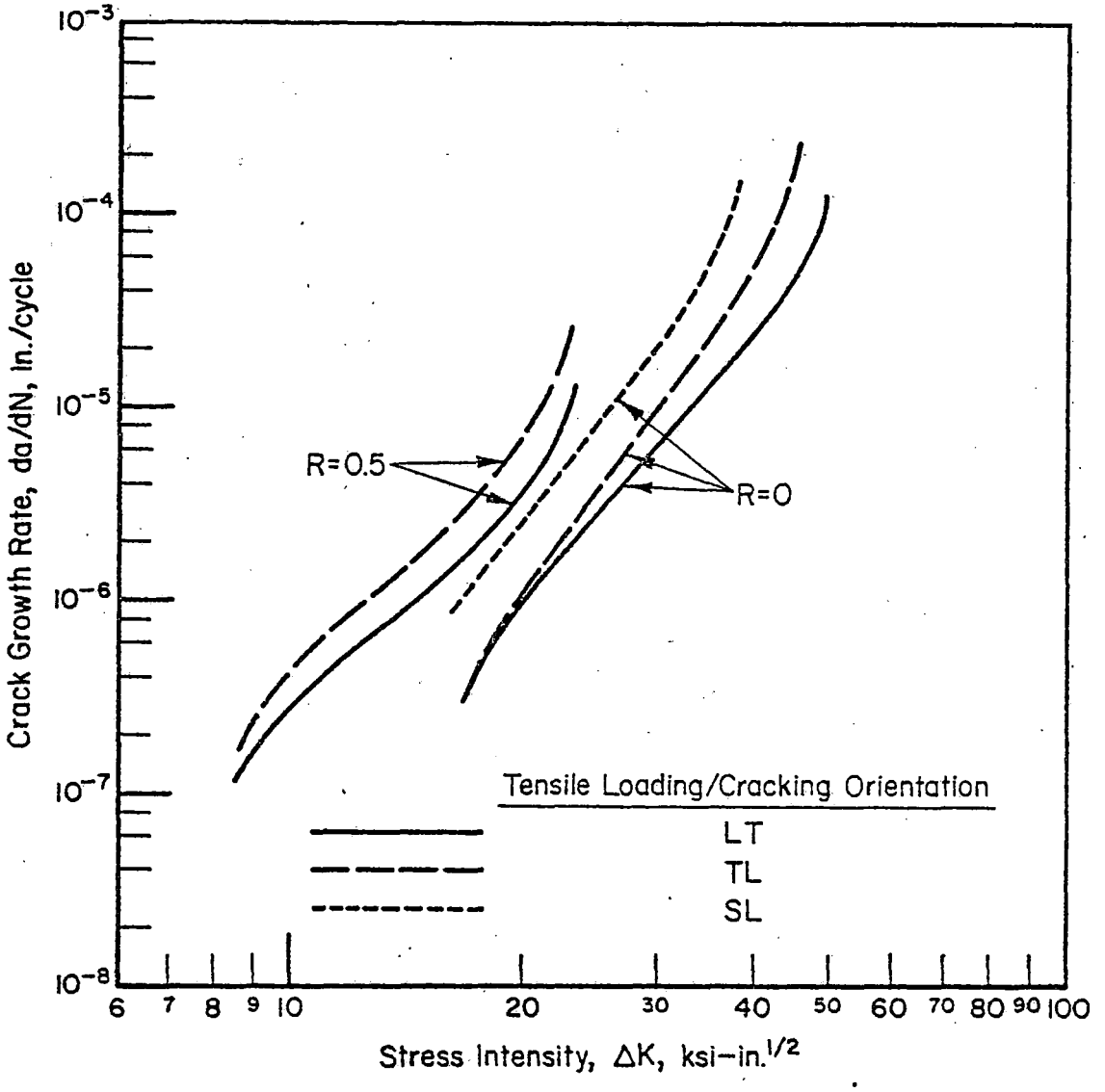

FIGURE 20. FCP TREND LINES FOR RAIL SAMPLES TESTED AT ROOM TEMPERATURE IN 3 DIFFERENT ORIENTATIONS

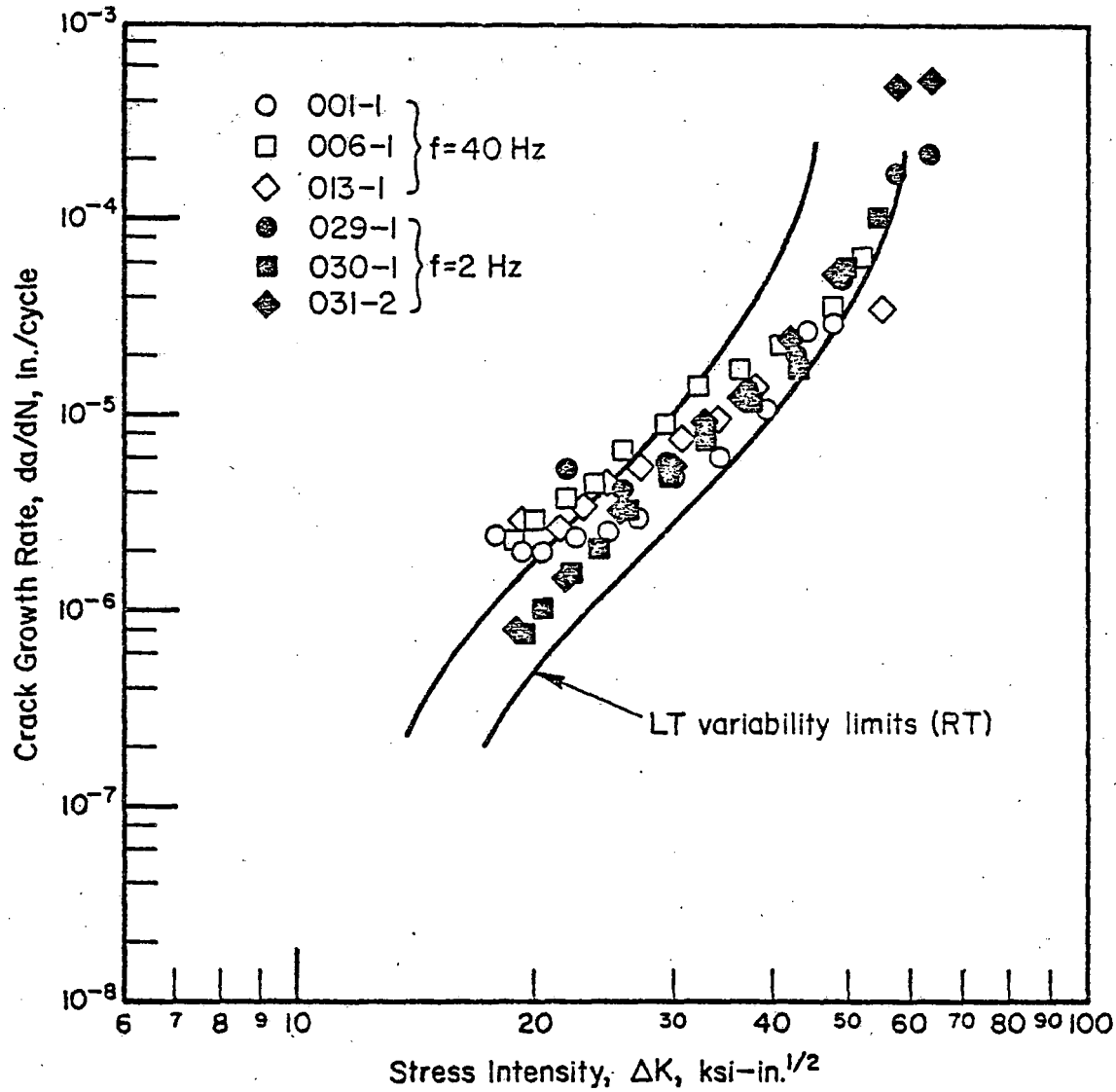

FIGURE 21. CRACK GROWTH DATA AT +140 F AND R = 0, CT SPECIMENS IN LT ORIENTATION

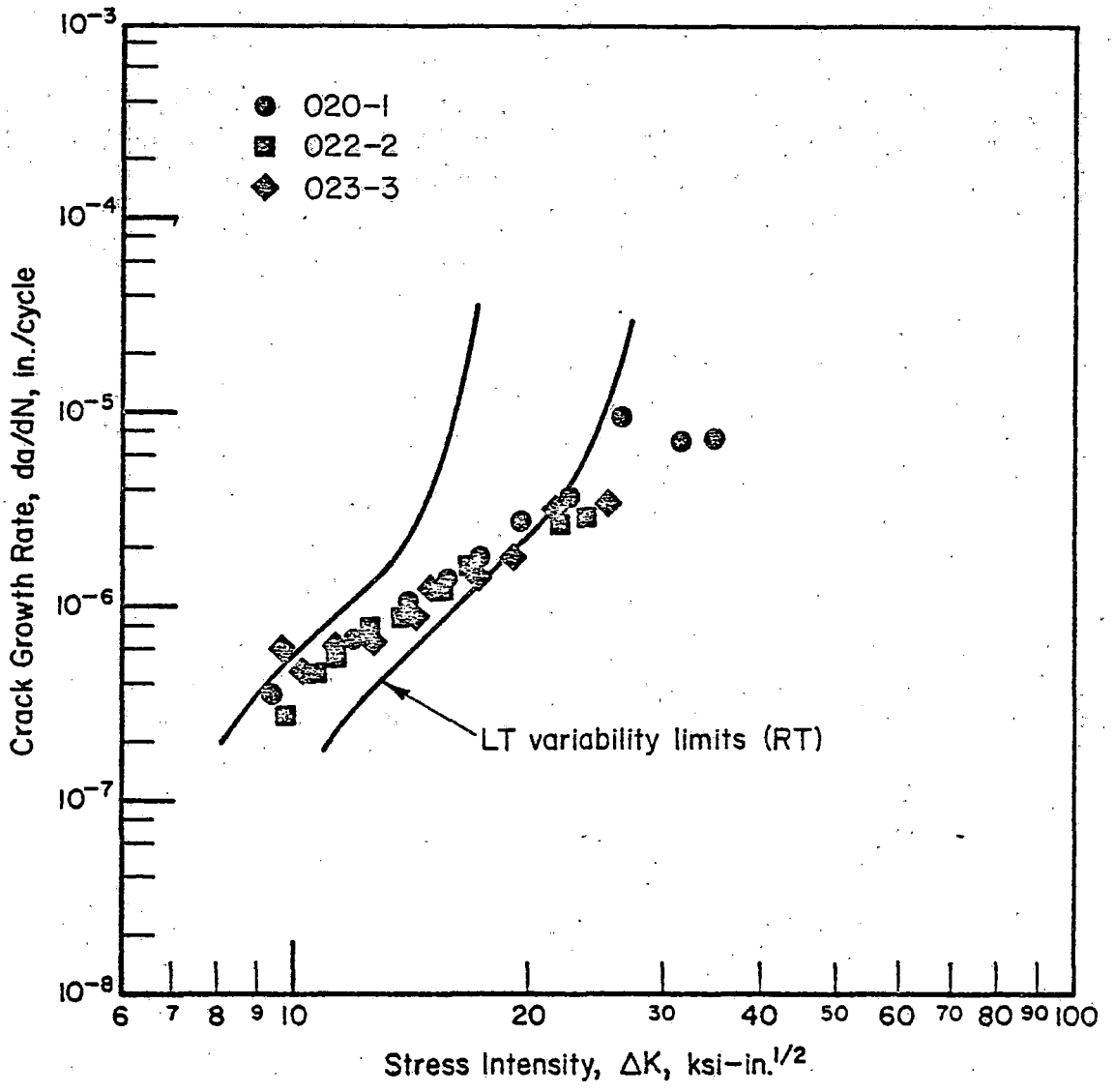

FIGURE 22. CRACK GROWTH DATA AT +140 F AND R = 0.5, CT SPECIMENS IN LT ORIENTATION

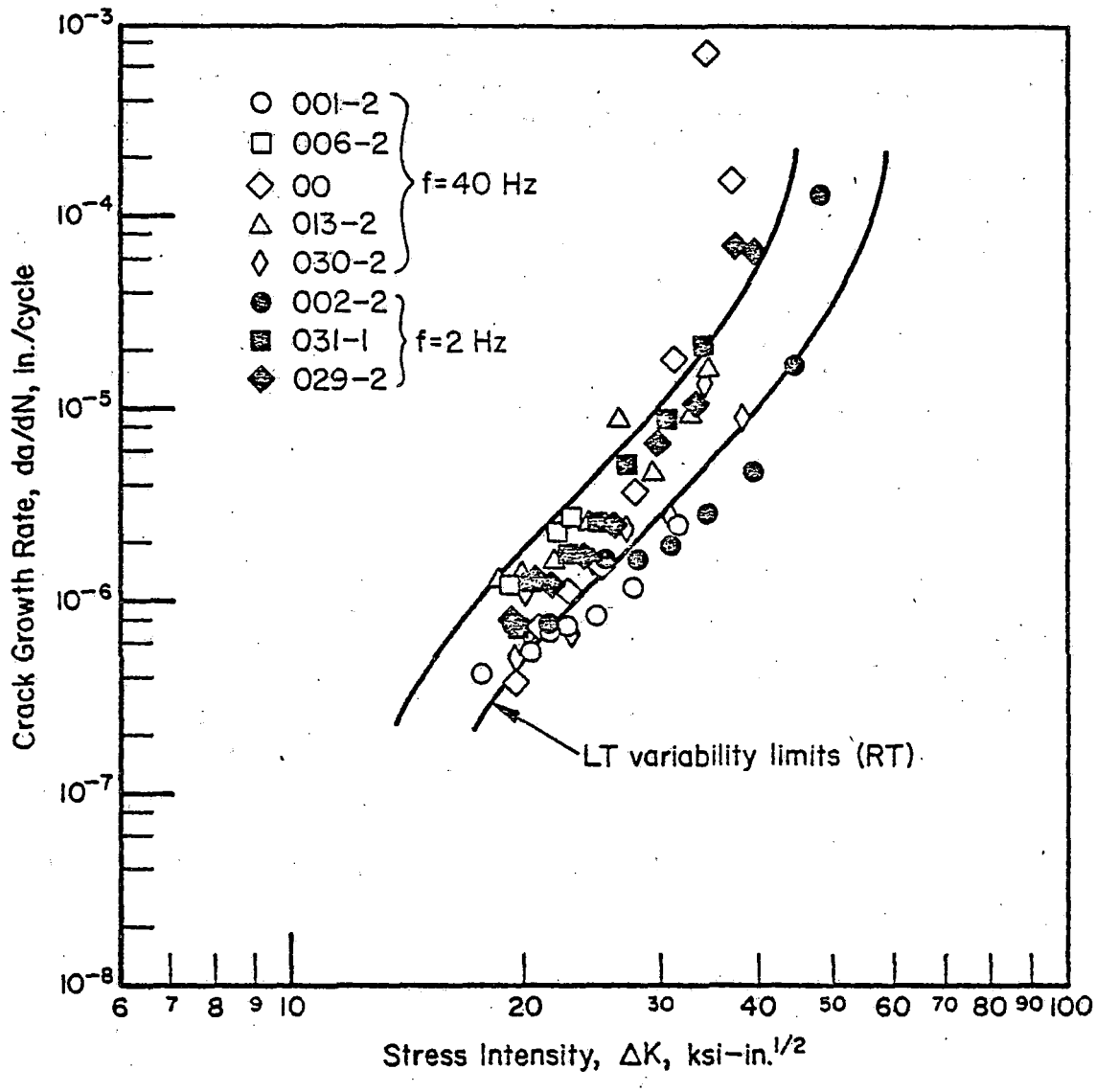

FIGURE 23. CRACK GROWTH DATA AT -40 F AND R = 0, CT SPECIMENS IN LT DIRECTION

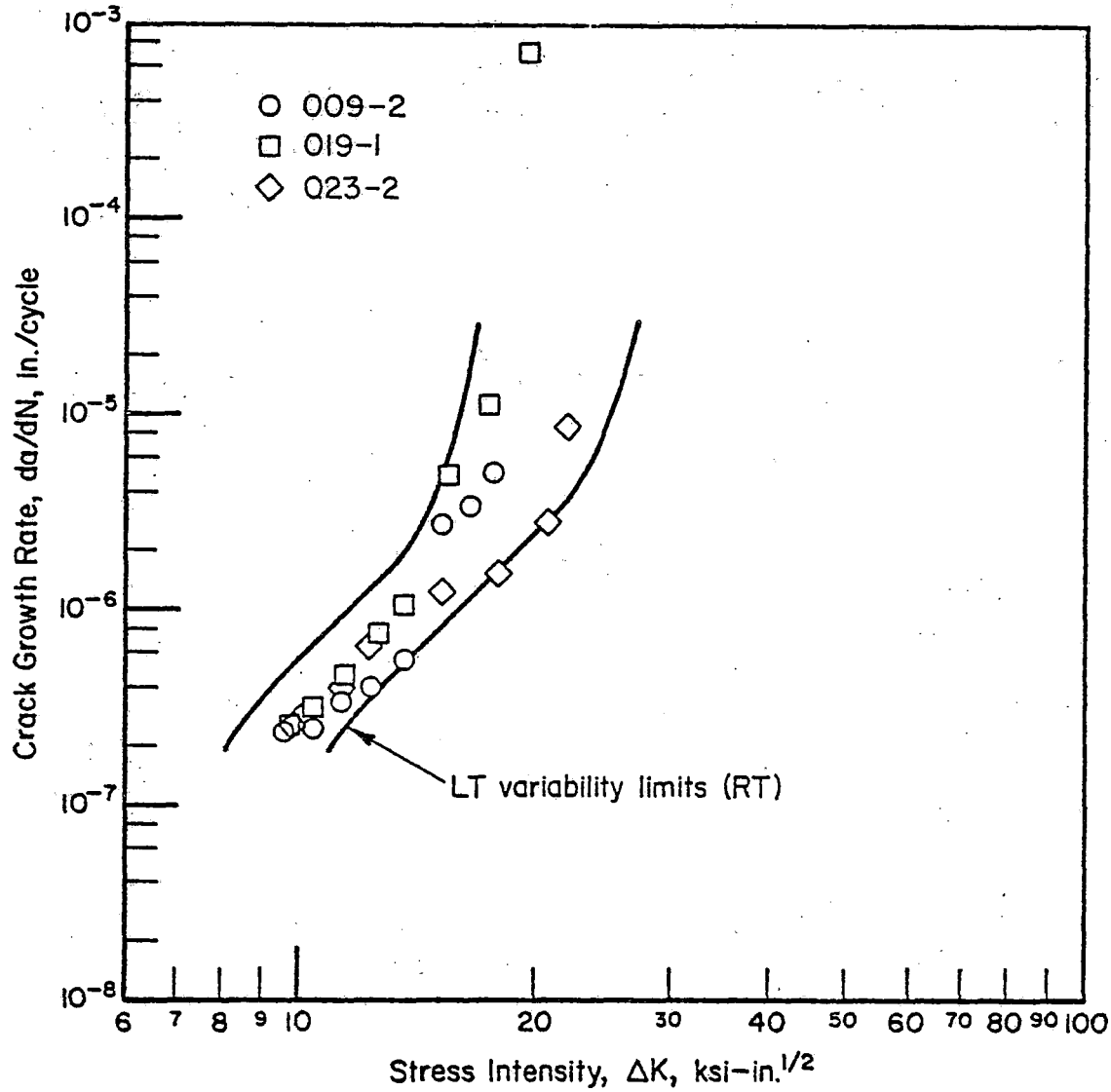

FIGURE 24. CRACK GROWTH DATA AT -40 F AND R = 0.5, CT SPECIMENS IN LT ORIENTATION

at high crack-growth rates. This trend is especially evident in Figure 22 for the R = 0.50 data. Conversely, the effects of decreased temperature on crack-growth rates appears to be to increase the slope of the da/dN-ΔK function and to decrease the critical stress intensity. These conclusions are most clearly illustrated in Figure 25 where the trend lines for LT orientation samples are shown for all test temperatures and stress ratios.

The same general effect of temperature on crack-growth rates was found for the TL orientation samples that were tested. These data are presented in Figures 26 and 27 for the +140 F experiments and in Figures 28 and 29 for the -40 F tests. The composite results of the TL orientation experiments are shown in Figure 30 for R = 0.0 and R = 0.50.

It is also important to note that the superior crack-growth characteristics of LT-orientation specimens are maintained at both high and low temperature, regardless of stress ratio. This trend is best observed through comparison of composite Figures 25 and 30.

5.5 Frequency Effects

The potential effect of cyclic frequency on crack-growth rates was evaluated through completion of nine CT-type specimen tests on LT orientation samples cycled at 2 cycles/second (Hz) and an R-ratio of zero. This rate of cycling was more than an order of magnitude slower than most of the tests completed under otherwise identical test conditions. Laboratory-air environmental conditions were maintained for these experiments, as they had been for all other crack-growth tests in this program.

The results of those experiments are included in Figures 12, 21, and 23 for test temperatures of +68 F, +140 F, and -40 F. As these plots illustrate, there was no discernable effect of the reduced cyclic frequency on crack-growth trends at any of the test temperatures.

5.6 Threshold Experiments

Experiments were completed at three stress ratios (R = -1.0, 0.0, and 0.50) to develop estimates of threshold stress intensity levels, below

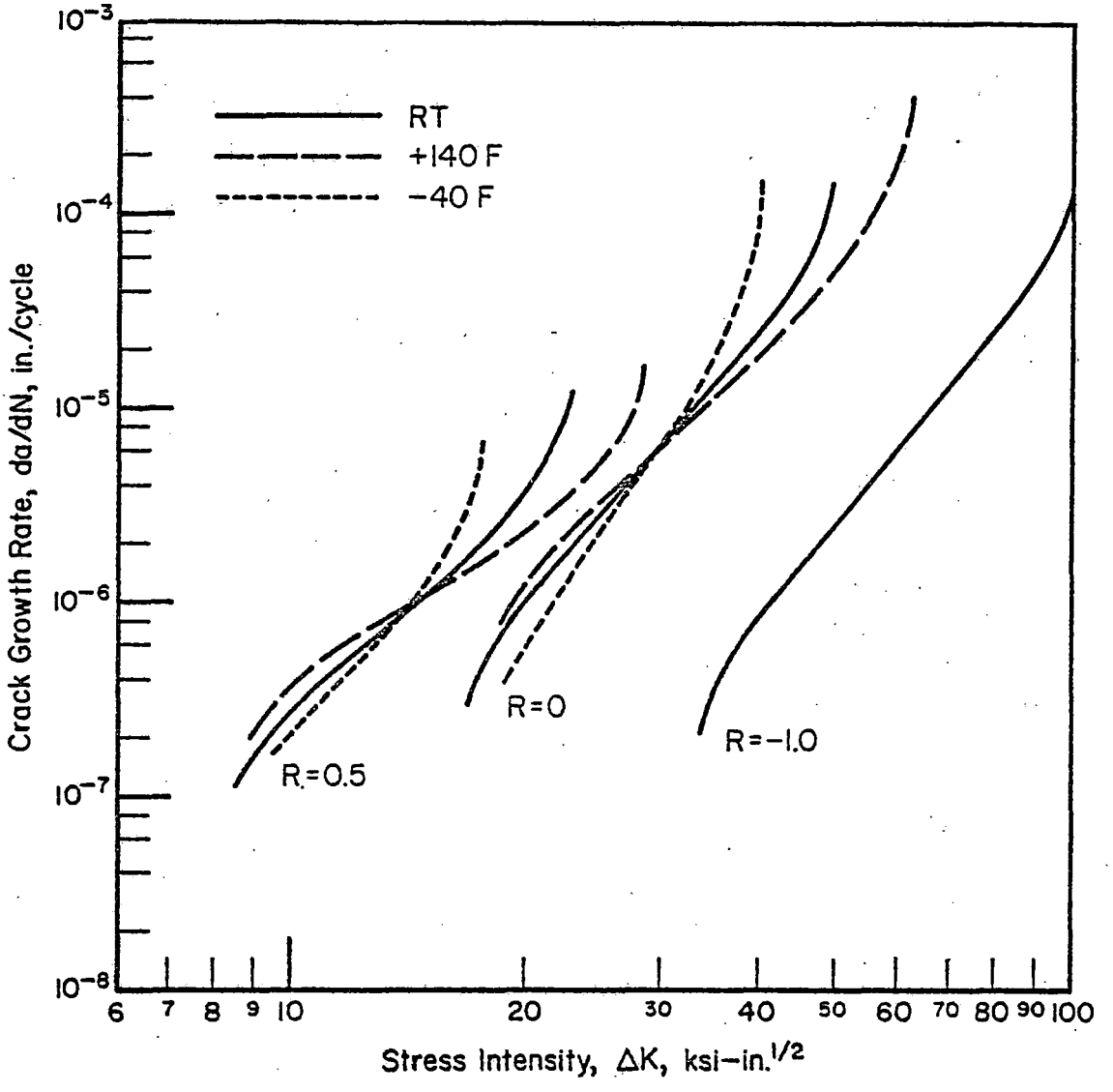

FIGURE 25. FCP TREND LINES FOR LT ORIENTATION RAIL SAMPLES AT 3 TEMPERATURES AND R RATIOS

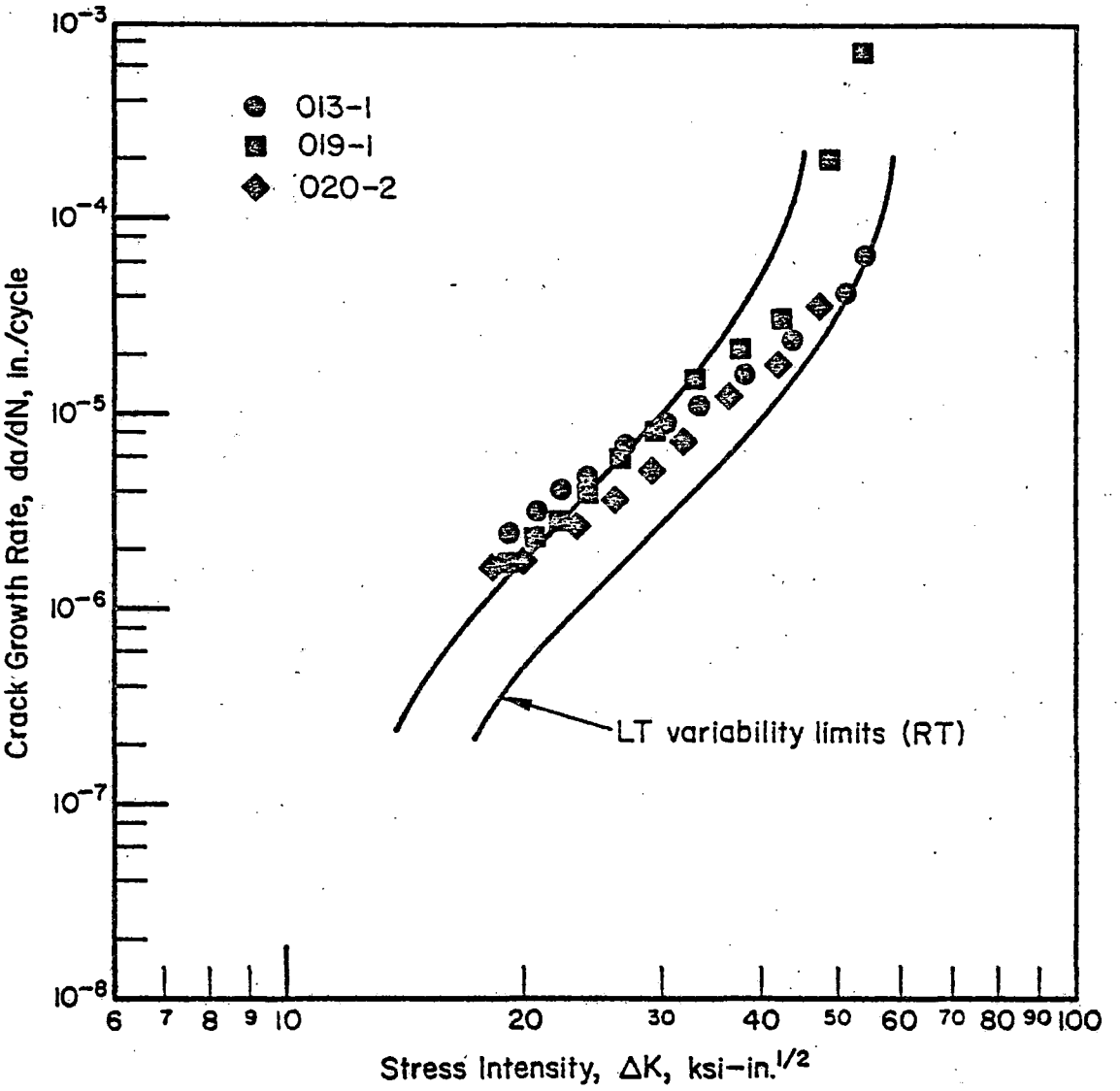

FIGURE 26. CRACK GROWTH DATA AT +140 F AND R = 0, CT SPECIMENS IN TL DIRECTION

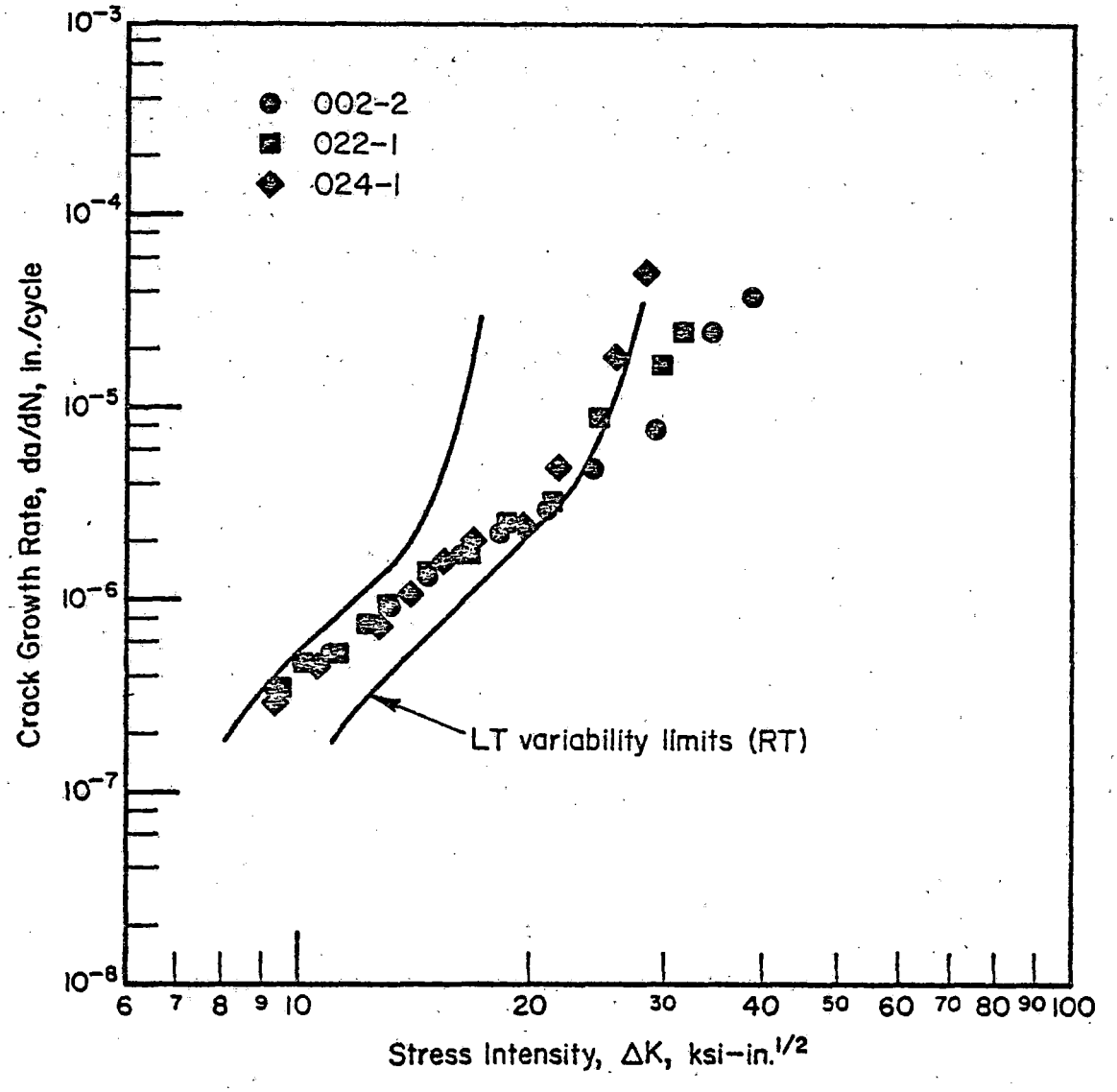

FIGURE 27. CRACK GROWTH DATA AT +140 F AND R = 0.5, CT SPECIMENS IN TL DIRECTION

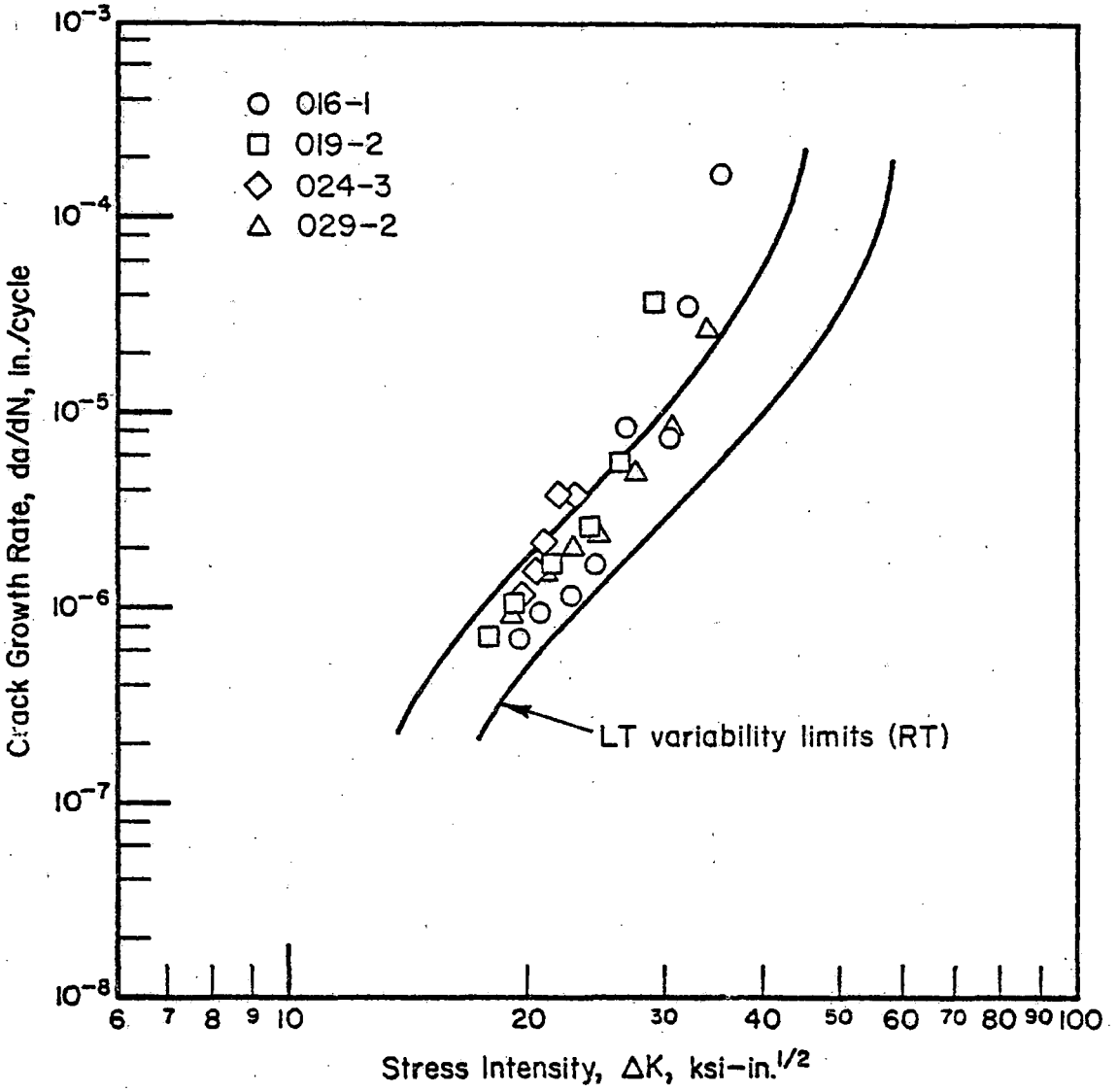

FIGURE 28. CRACK GROWTH DATA AT -40 F AND R = 0, CT SPECIMENS IN TL DIRECTION

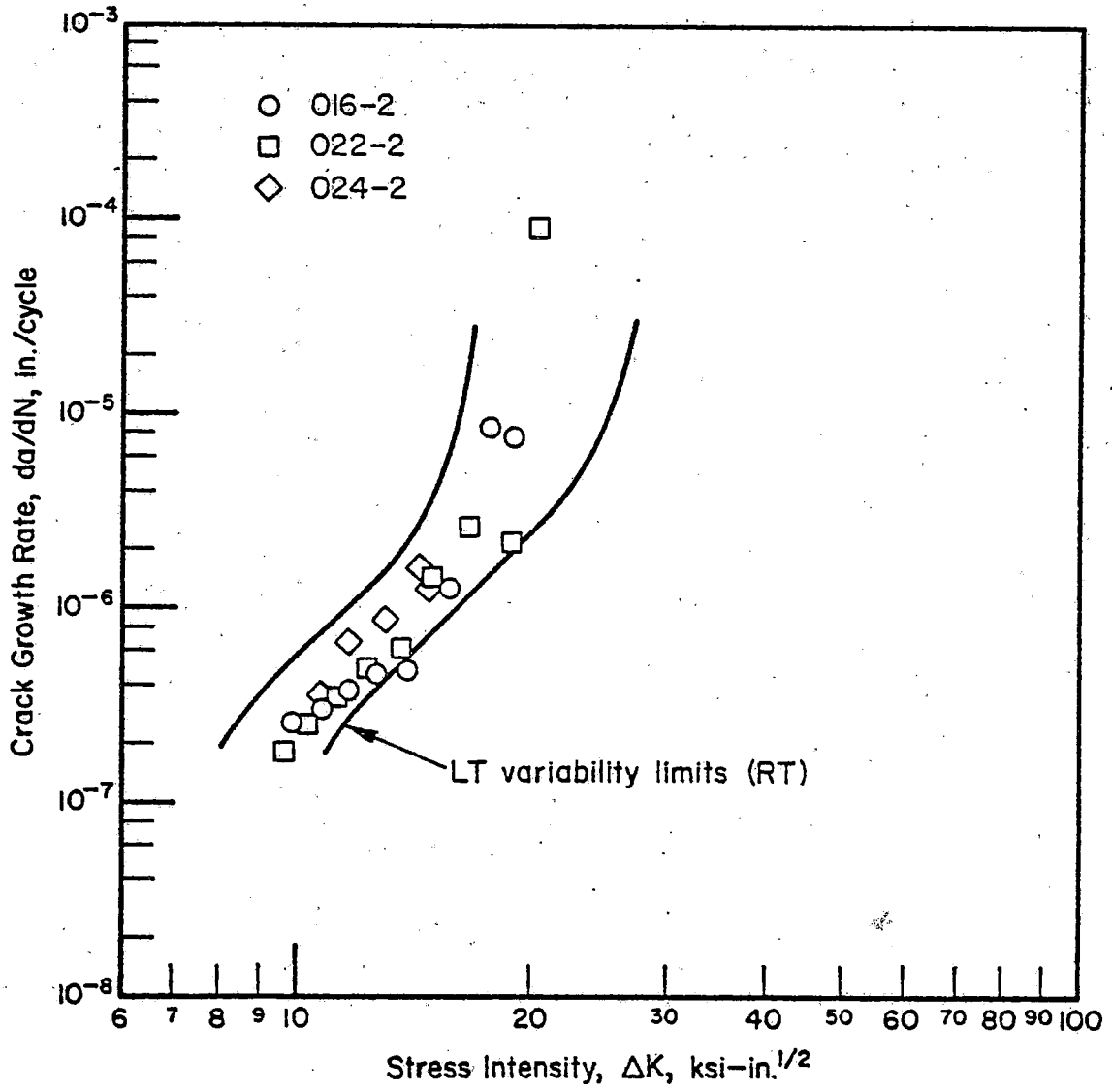

FIGURE 29. CRACK GROWTH DATA AT -40 F AND R = 0.5, CT SPECIMENS IN TL DIRECTION

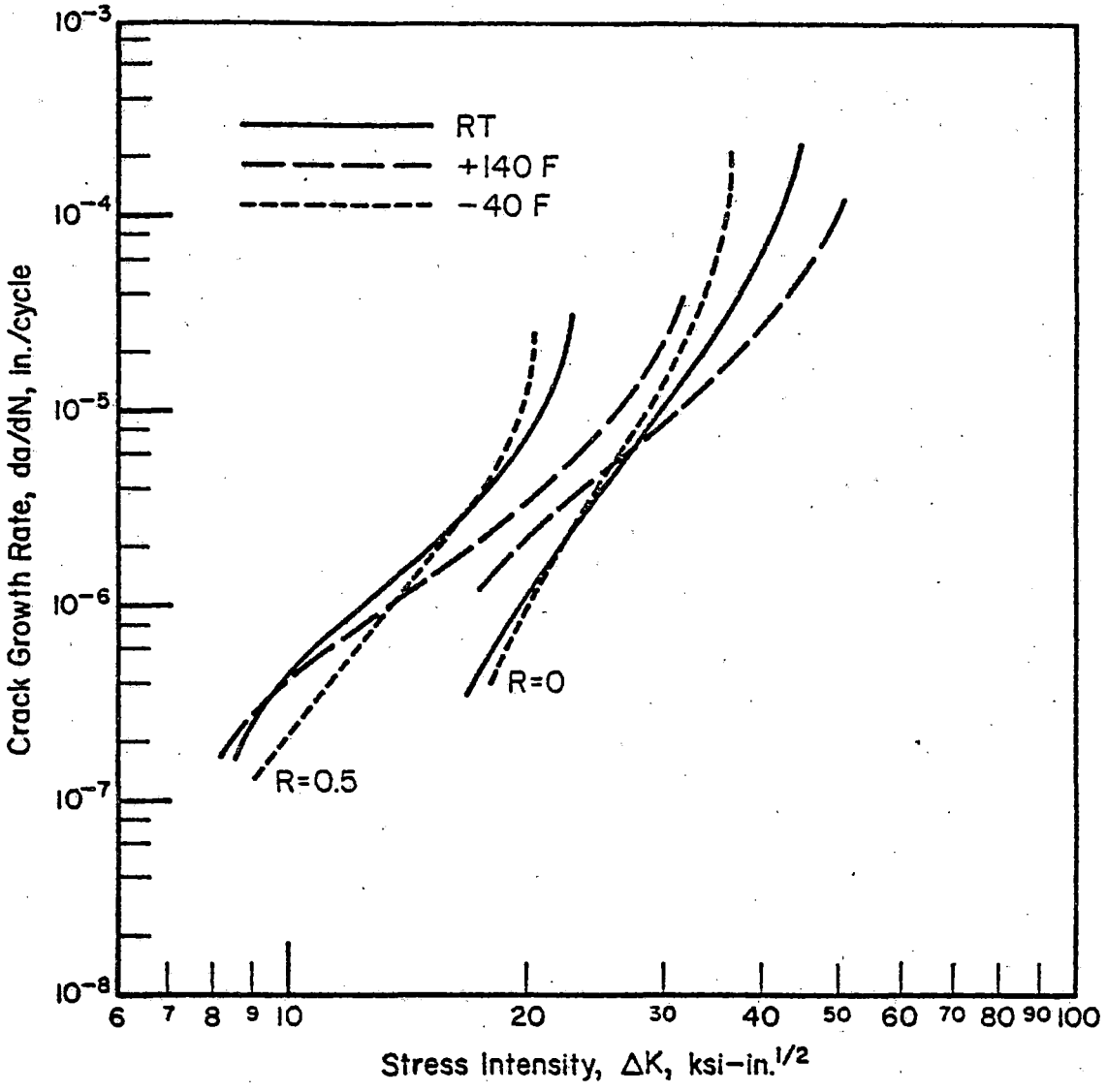

FIGURE 30. FCP TREND LINES FOR TL ORIENTATION RAIL SAMPLES AT 3 TEMPERATURES AND 2 R RATIOS

which crack-growth rates would asymptotically approach zero. The R = 0.0 and 0.50 stress ratios were evaluated using CT specimens; both LT and TL orientation samples were tested. The R = -1.0 stress ratio condition was evaluated using an LT orientation, SEN specimen.

Each experiment was started by choosing a cyclic load that would produce a stress intensity range that was expected to cause initial crack-growth rates of about 10^{-6} in./cycle. After crack growth had stabilized at this initial level (beyond the precrack) the load range was reduced by 5 to 10 percent of the preceding level, while maintaining the same stress ratio. Then after crack growth had again stabilized at this reduced load level (usually involving crack growth of 0.030 to 0.050 in.), the load range was again reduced by 5 to 10 percent of the previous level. After the crack-growth rates had been reduced to a minimum of about 10^{-9} in./cycle, the load range was again increased in steps of about 10 percent of the previous load range, allowing crack growth to stabilize at each level until a rate of approximately 10^{-6} in./cycle was again achieved. The total process usually involved 5 to 8 steps down in load range and 4 to 7 steps back up to the maximum load. As the crack grew longer for a particular specimen, the stress intensities increased so that the load range required to cause crack-growth rates of approximately 10^{-6} in./cycle decreased with each series of descending and ascending loads.

For most of the experiments three series of decreasing and increasing load levels were applied to each stress ratio, so that some replication of near-threshold crack-growth rates could be achieved. The repetition of this step-down-loading process also made it possible to check the consistency of crack-growth trends in this cracking regime.

A cyclic frequency of 30 to 50 Hz was employed for the threshold experiments. Most of the specimens received from 50 to 100 million cycles of loading during the course of a threshold experiment. An example of the sequential steps and the resulting crack growth rates is presented in Figure 31.

The results of all threshold experiments are shown in Figures 32, 33, and 34 for the various conditions tested. In Figure 32 the LT orientation specimen data are displayed and compared with the high rate crack-growth experiments that were completed in other phases of this program. Data below 10^{-8} in./cycle are not shown because they do not shift the actual threshold level from what is apparent at 10^{-8} in./cycle. In other words, the threshold asymptote is virtually reached (for the test conditions and materials considered) at crack growth rates of 10^{-8} in./cycle.

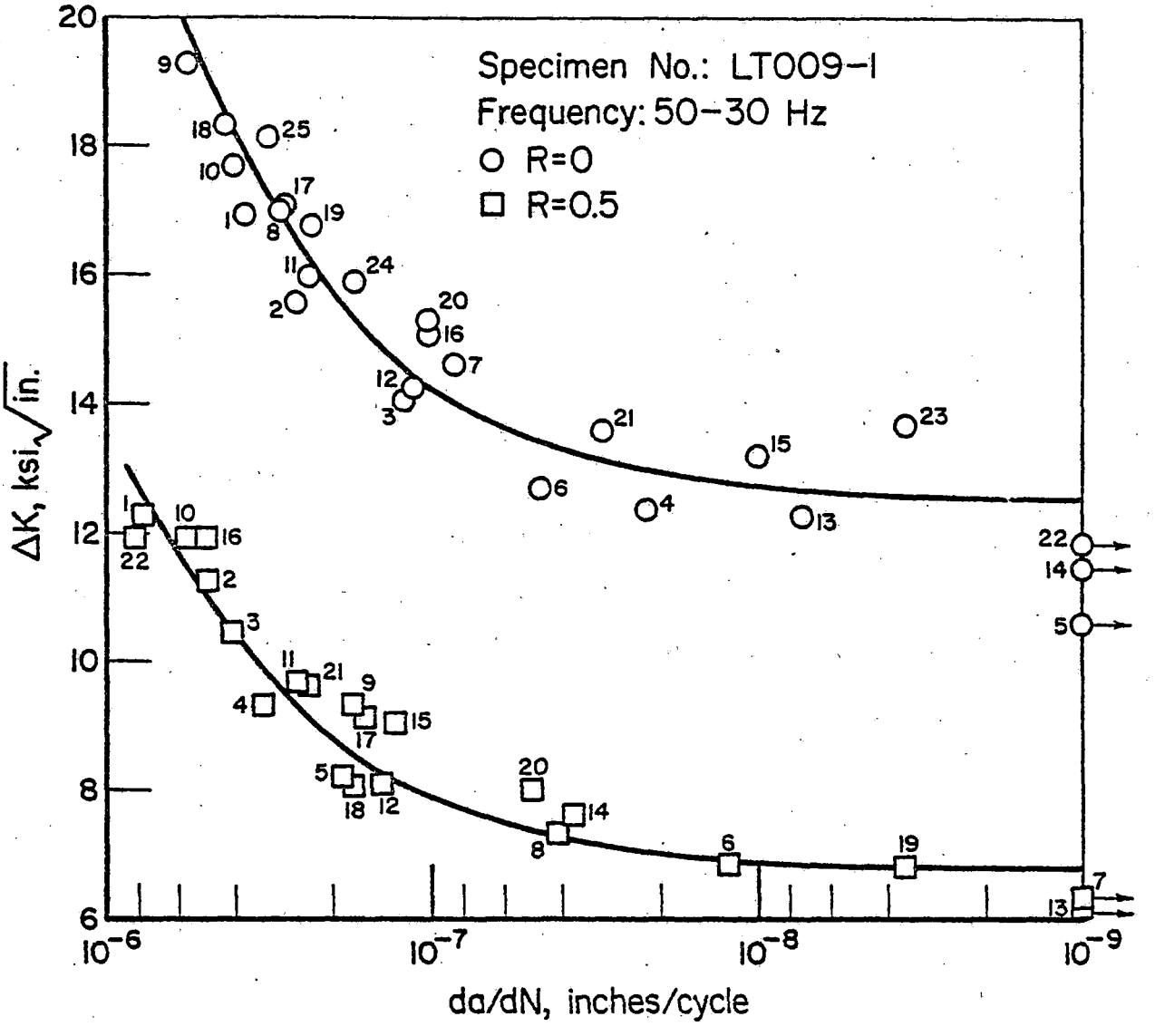

FIGURE 31. EXAMPLE OF THRESHOLD DATA WITH STEP-DOWN-STEP-UP PROCEDURE INDICATED BY A NUMERICAL SEQUENCE OF DATA POINTS

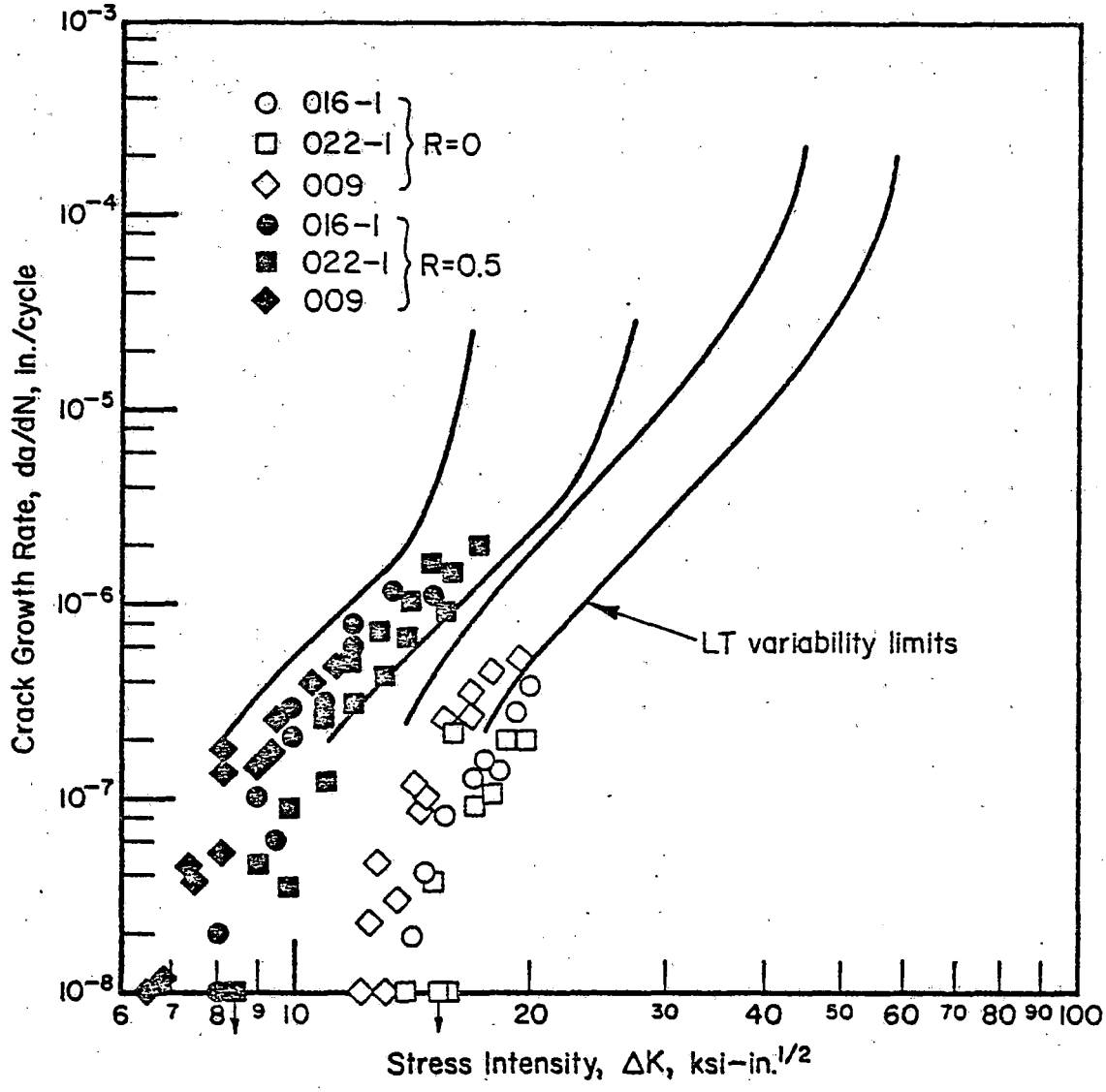

FIGURE 32. THRESHOLD DATA AT ROOM TEMPERATURE, R = 0 AND 0.5, LT DIRECTION

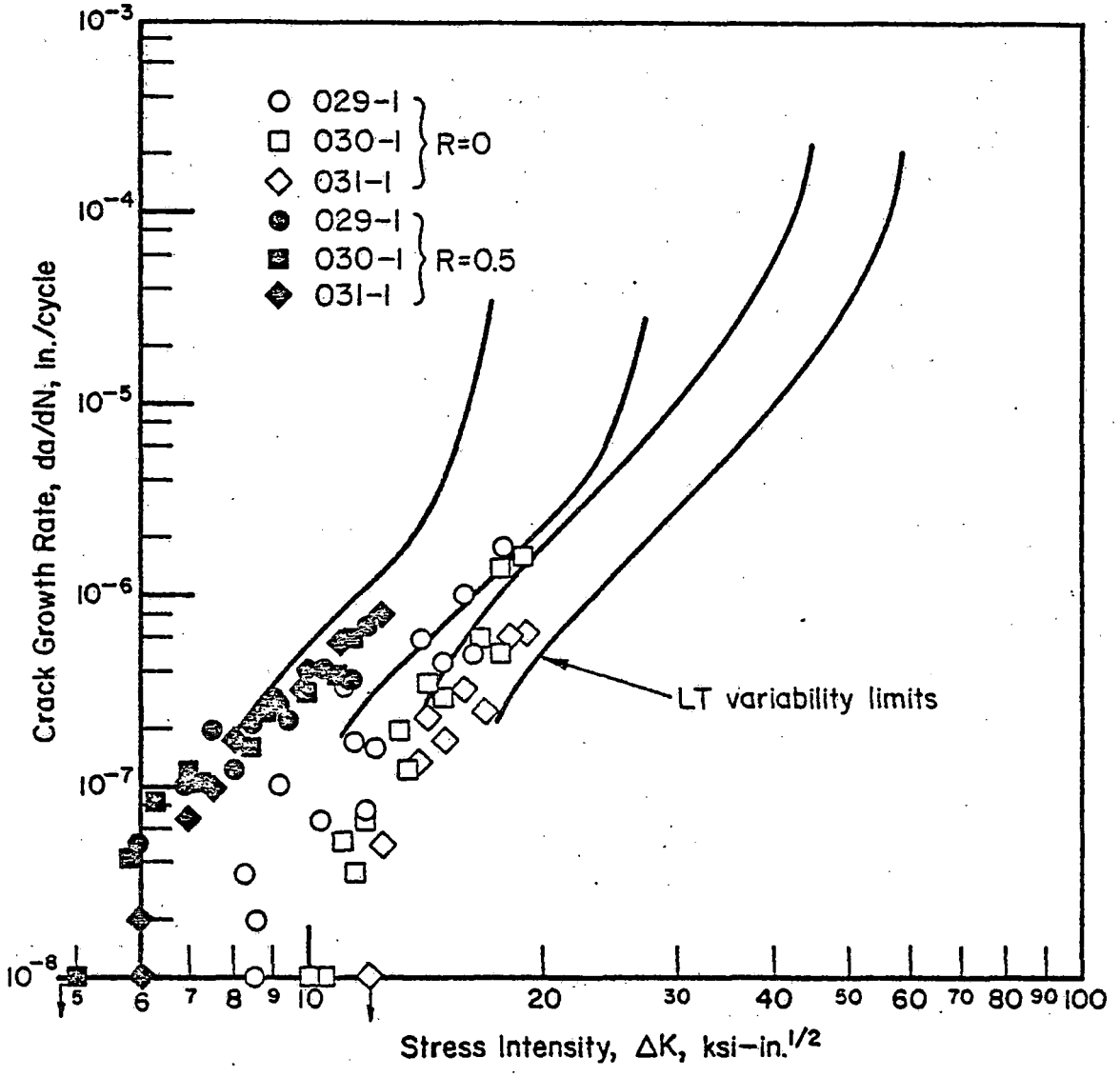

FIGURE 33. THRESHOLD DATA AT ROOM TEMPERATURE, R = 0 AND 0.5, TL DIRECTION

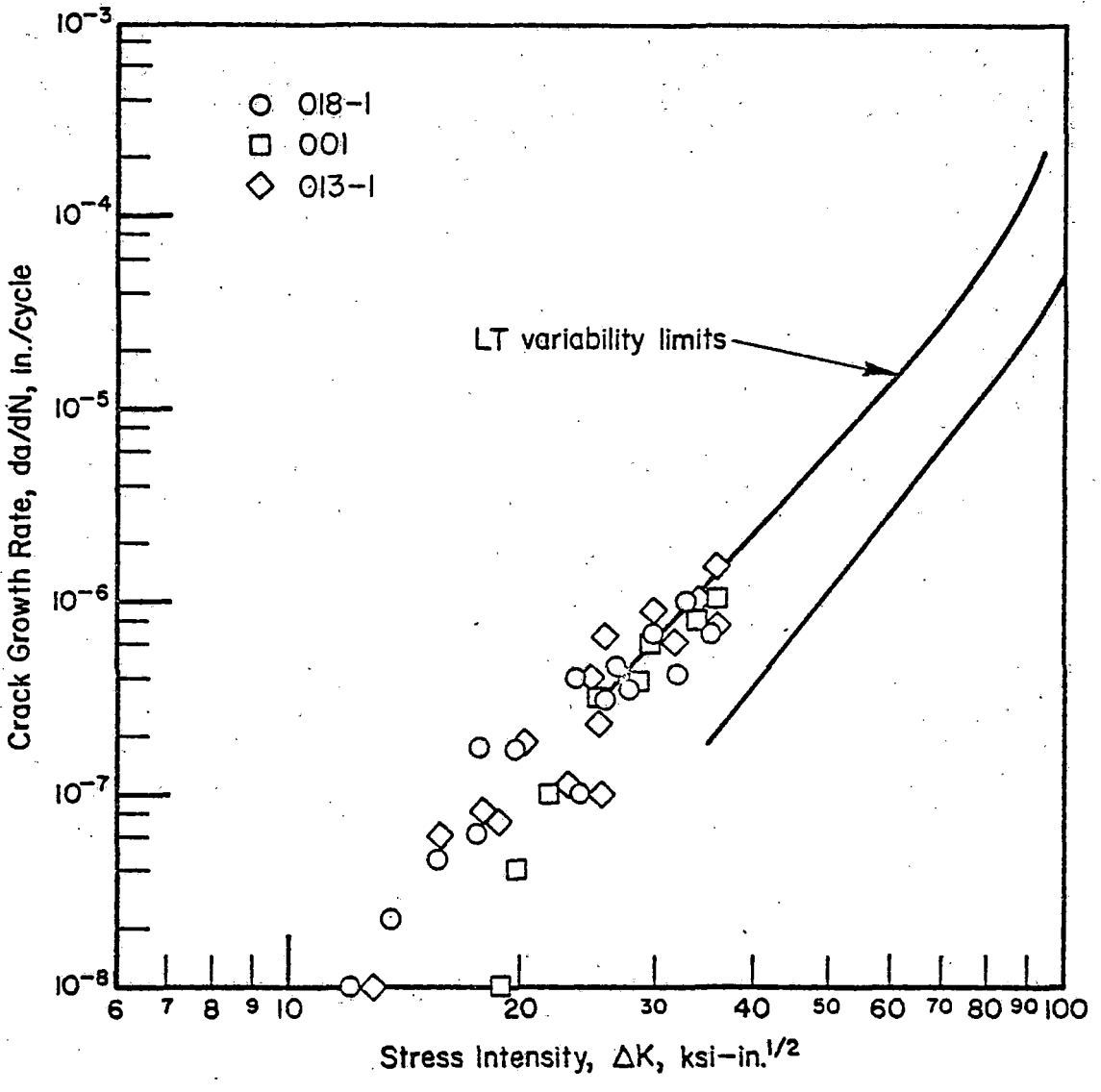

FIGURE 34. THRESHOLD DATA AT ROOM TEMPERATURE, R = -1, LT DIRECTION

Figure 33 displays the threshold data for the TL orientation specimens. Comparing the TL and LT orientation threshold data, it is apparent that for similar stress ratios the TL orientation results in slightly higher crack-growth rates and lower threshold stress intensities. For the LT orientation samples tested, threshold stress intensity ranges varied from 6.5 to 9 and 12 to 15 for R = 0.50 and 0.00, respectively; while the TL orientation samples exhibited threshold stress intensity ranges of 5 to 6 and 8 to 11 for the same stress ratios.

Figure 34 presents the threshold data generated on LT orientation, SEN-type specimens. These data do not correspond as well to the high-rate crack-growth experiments as might have been expected based on the LT orientation results presented in Figure 32 for R = 0.0 and 0.50. On the average, however, the data do match the high growth-rate side of the data-variability band generated earlier using SEN specimens tested at R = -1.00. Apparent threshold values for the R = -1.00 stress ratio condition vary from about 12 to 19.

5.7 Surface Flaw Experiments

In addition to the large number of SEN and CT type specimen tests performed in this program, six surface flaw crack-propagation experiments were also performed to evaluate the more complex 2-dimensional cracking behavior typical of many in-service embedded flaws.

The surface flaw specimens were machined from the rail head (Figure 6) so that a flaw machined in its side surface would propagate in a manner similar to a transverse fissure. The cracking orientation of this specimen is properly described as LT for through-the-thickness crack growth and LS for through-the-width crack extension. In reality, since the crack surface is curved, a combination of LT and LS material properties would be expected to control the surface flaw-cracking process.

An initial semicircular flaw, 0.50-in. long and approximately 0.010 in. wide was EDM machined in the side surface of each specimen as shown in Figure 3. This relatively large, 0.250-in. deep flaw was required to achieve initial stress intensities sufficiently high to reach specimen failure in 1 to 2 million cycles.

The results of the surface flaw experiments are shown in Figures 35 a and b. The first figure presents crack-growth trends in the LS orientation of the surface flaw and the second figure presents approximate crack-growth trends in the LT orientation. The method for computing LT growth rates is described later in this section. Two specimens were tested from each of the three crack-growth categories listed in Table 1. All of the experiments were conducted at a stress ratio of 0.0. As can be seen from the test results, the crack-growth behavior of all specimens were relatively consistent and the behavior of one crack-growth category compared to another was not significantly different.

An attempt was made in the course of these experiments to identify the curvature of the crack front as the crack extended by inserting "marker bands" (a series of low-load cycles that cause a small crack extension and may be visible on the fracture surface as dark conchoidol bands). These attempts were unsuccessful, however, so the crack aspect ratio (the ratio of crack depth to surface crack length) could only be determined at the point where each specimen failed or at the point where the surface flaw broke through the back surface of the specimen and became a through crack. The ratio of crack depth (specimen thickness) to surface crack length was known at these points and they served as approximations of the ratio of secondary and primary axes of each crack surface ellipse. From these measurements, it was concluded that the initially semi-circular shape of the surface flaw progressed toward an elliptical flaw whose depth stabilized from 0.30 to 0.34 of its surface length. This crack-aspect ratio of 0.30 to 0.34 was reached on most of the specimens at a surface crack length of about 1.30 inches. Assuming an exponentially decaying rate of change in crack aspect ratio from the initial ratio of 0.50 to the average final ratio of 0.32, it was calculated that the initial through-the-thickness crack growth rates (da/dN) were about 25 percent of the surface crack growth rates (dc/dN). As the surface crack became more elliptical, the surface crack tip stress intensity decreased relative to the internal crack tip stress intensity. This condition progressed until the poorer growth characteristics (dc/dN) in the LS orientation at the lower relative stress intensities matched the through-the-thickness crack growth rates at the higher internal stress intensities. This equilibrium crack-growth rate condition along the surface crack front was evidenced by the stabilized crack aspect ratio values. In the ideal case where edge effects

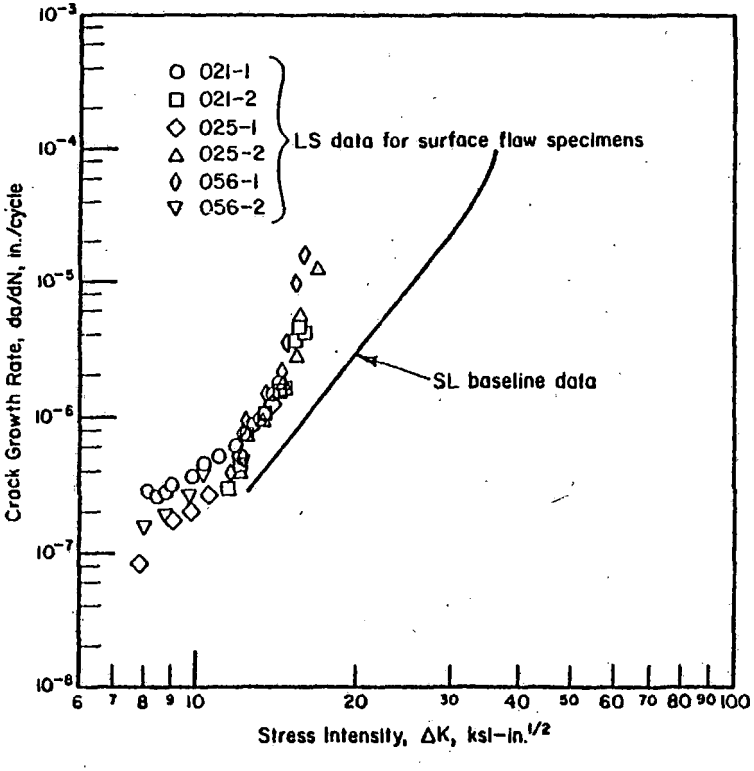

a. LS Orientation (sidewise across rail head)

FIGURE 35.

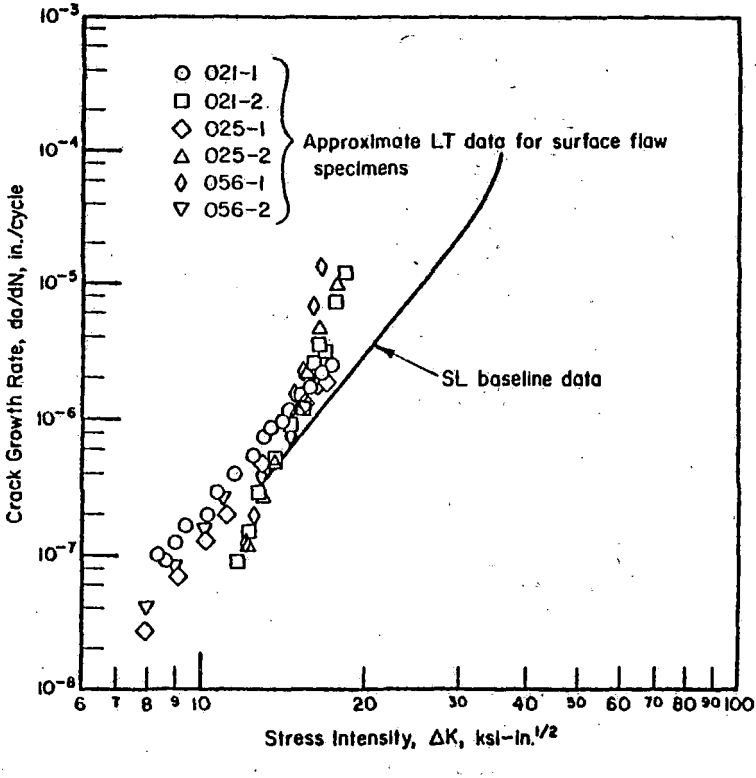

b. LT Orientation (down through the rail head toward web)

SF DATA

are negligible, Equation (4.10) predicts that an elliptical flaw with a crack aspect ratio of 0.32 has a stress intensity 10 percent lower at its major axis tip than it does at the minor axis tip. In this actual case, results indicate that crack tip stress intensities in the LS orientation need be only 90 percent of those in the LT orientation to cause equal crack growth rates. From this observation, it became apparent that through-the-width crack-growth rates (LS orientation) were higher than through-the-thickness crack-growth rates (LT orientation). This behavior was consistent with the previously observed effects of orientation on crack growth.

6. MIXED MODE

6.1 Test Results

The mixed mode specimens contained a chevron edge notch perpendicular to the specimen's length direction. The specimens were precracked in three-point bending, giving a straight crack, a $\approx$ 0.5-inch (see Figure 4). Under the loading conditions used, these straight initial cracks resulted in the stress-intensity factors for Modes I and II as given in Figure 11. While the specimens were tested under mixed mode loading according to the principle shown in Figure 11, the cracks extended by following a curved path. The crack paths were similar for different specimens tested under the same conditions, but different crack paths occurred when the testing conditions were changed. Thus, four basic crack types were observed for the four initial ratios of K_{II}/K_I, as illustrated in Figure 36.

Finite element analyses were run for the two cases with initial ratios K_{II}/K_I of 0.34 and 0.72. The cracks in the finite element models were extended in accordance with the curved crack paths observed in the experiments. Thus, the stress intensities K_I and K_{II} could be calculated as a function of crack size*. The results are presented in Figure 37. According to Figure 37 the value of K_{II} reduced to zero, almost immediately after the crack started to grow. This means that the crack turned into a direction that would reduce Mode II loading to zero, and subsequently followed a path for which $K_{II} = 0$. As a consequence, crack growth was basically under Mode I conditions only, apart from the very first crack increment.

Since the cracks were growing in Mode I, the test results were plotted as da/dN versus ΔK_I. (da/dN was based on the developed crack length, i.e., not on projected length.) The results are given in Figures 38, 39, and 40. Unprocessed test records are given in the appendix.

---

* This work was performed by E. F. Rybicki.

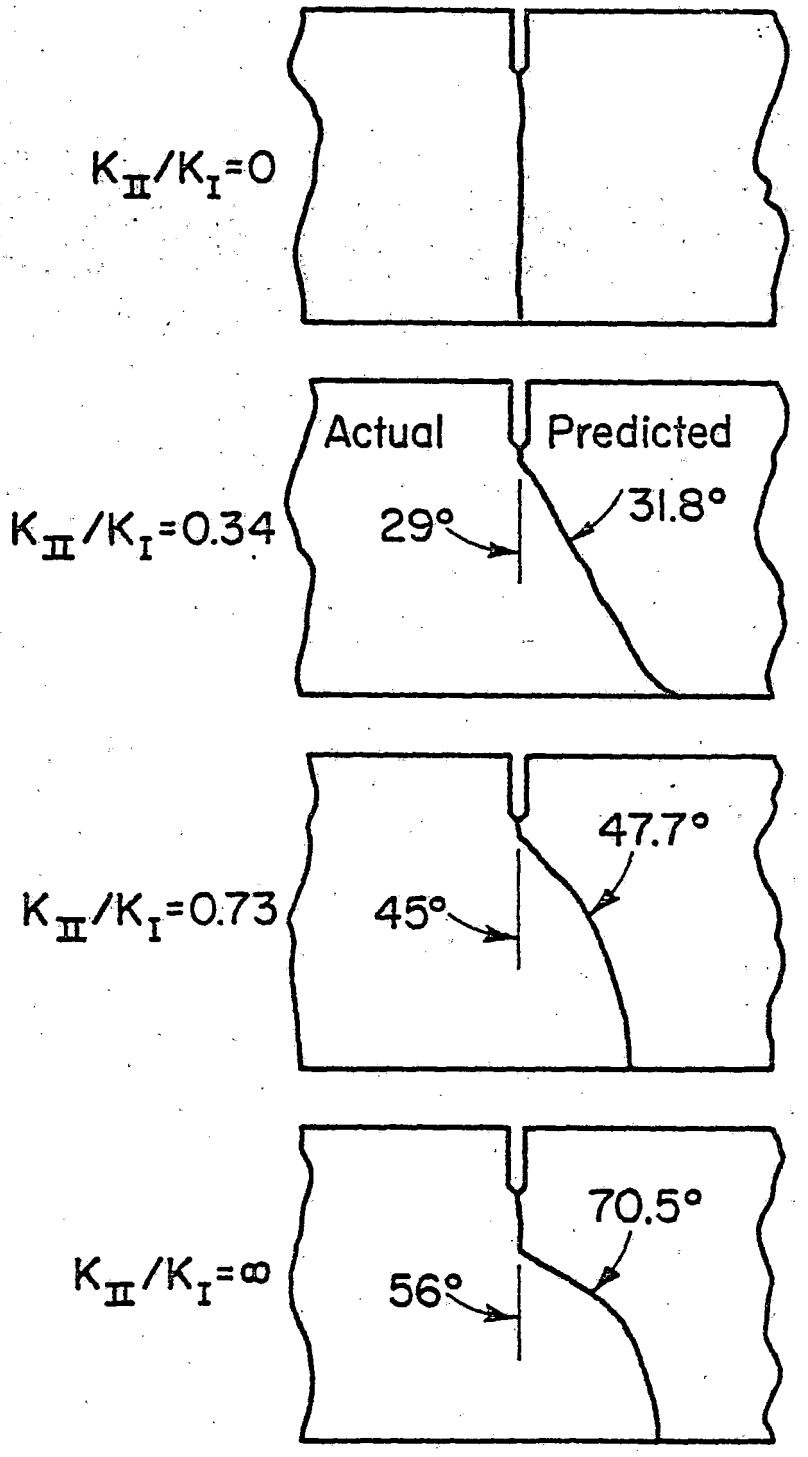

FIGURE 36. CRACK PATH FOR CASES OF DIFFERENT INITIAL K_{II}/K_I RATIOS

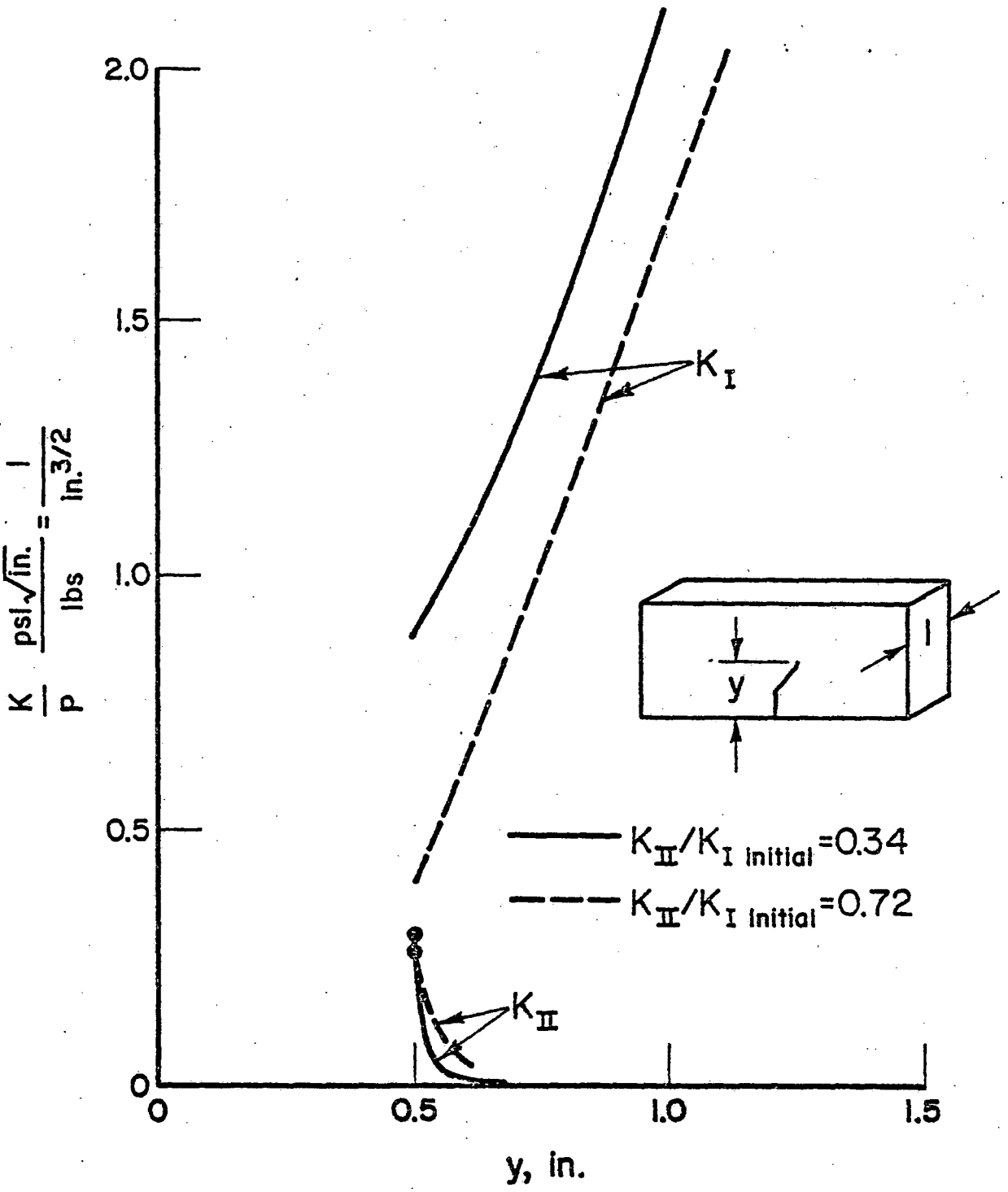

FIGURE 37. K_I AND K_{II} FOR ACTUAL CRACK CASES (SPECIMEN OF UNIT THICKNESS)

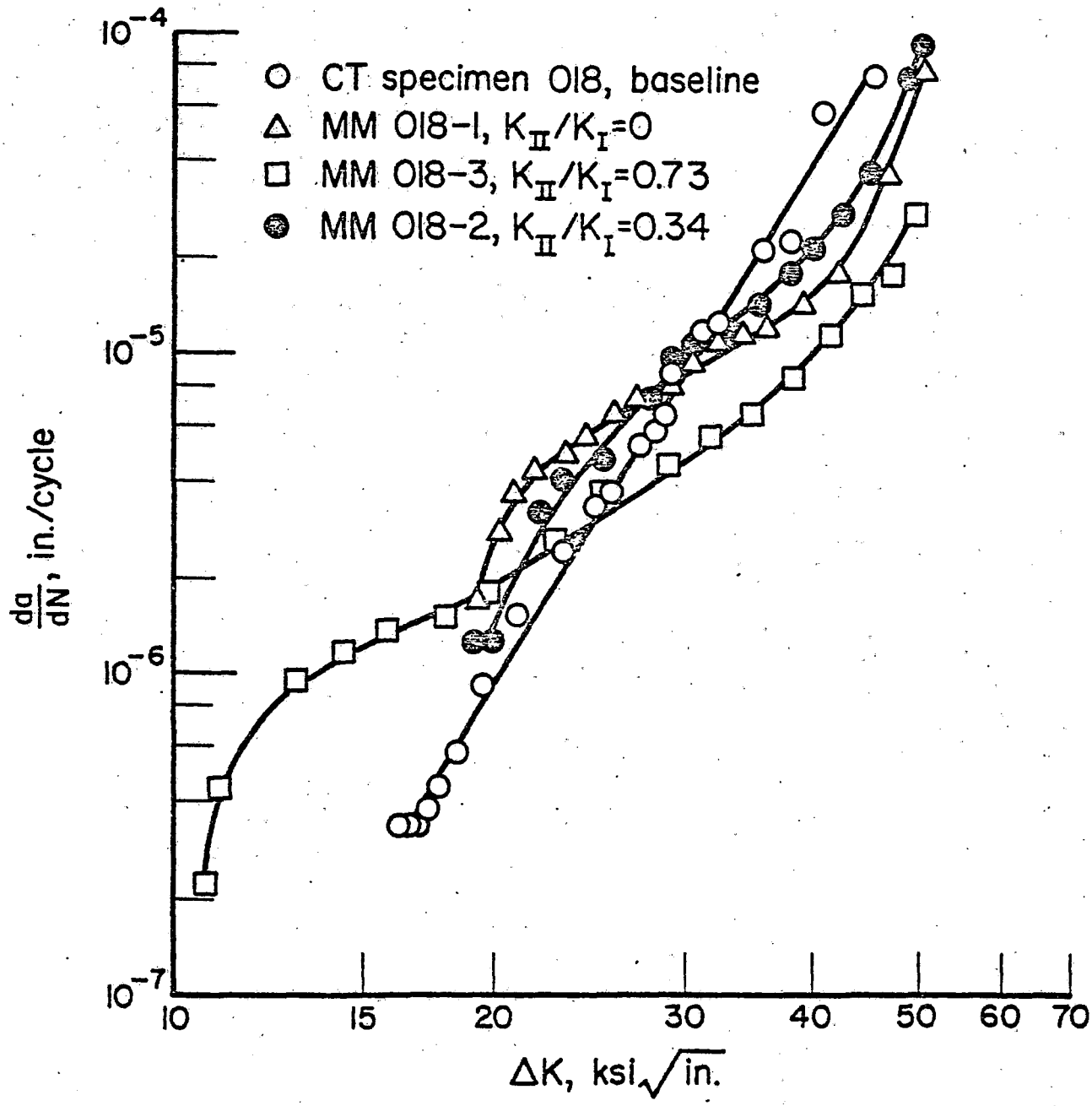

FIGURE 38. MIXED MODE TEST RESULTS; RAIL SAMPLE 018 (CATEGORY II)

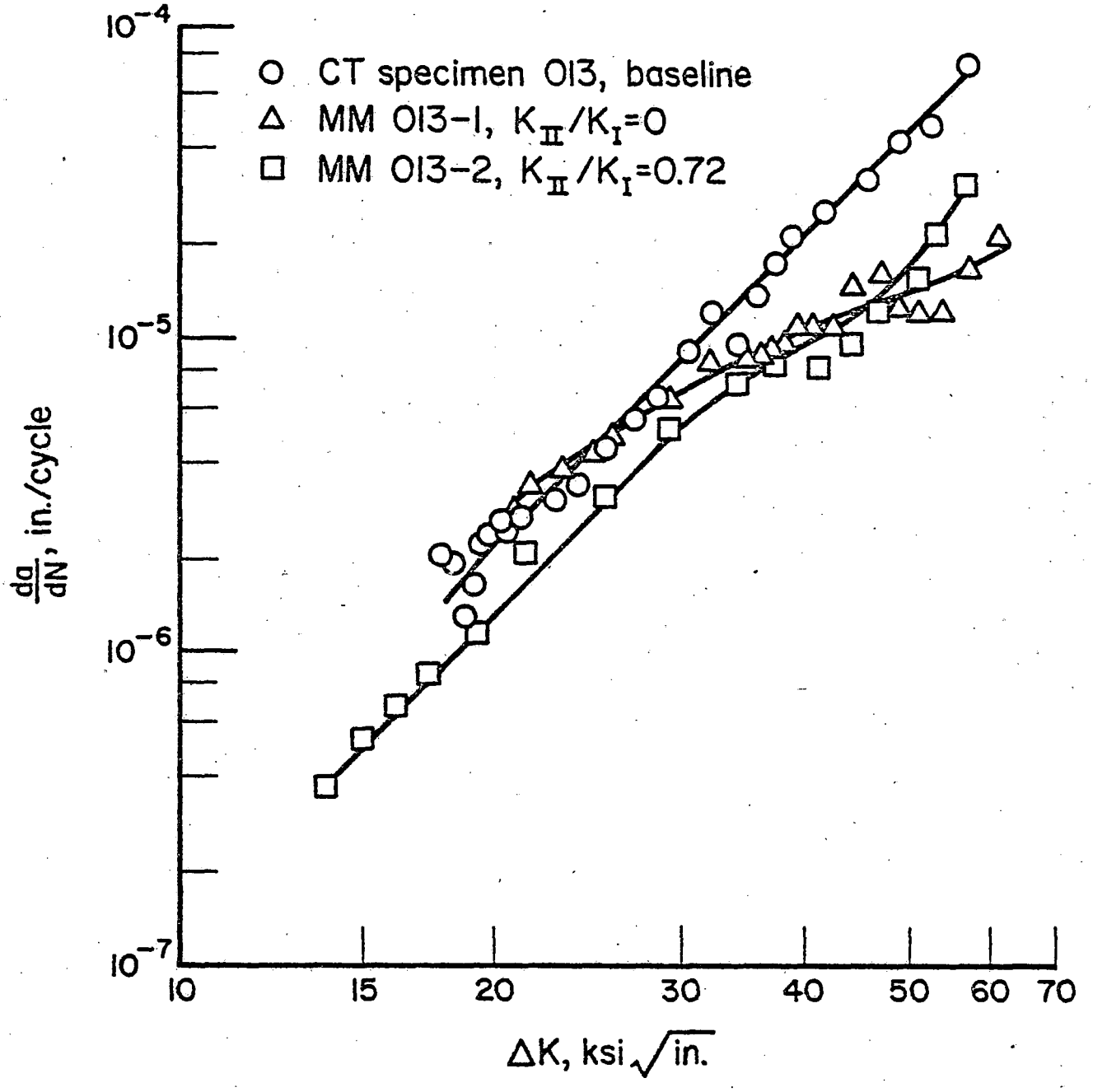

FIGURE 39. MIXED MODE TEST RESULTS; RAIL SAMPLE 013 (CATEGORY I)

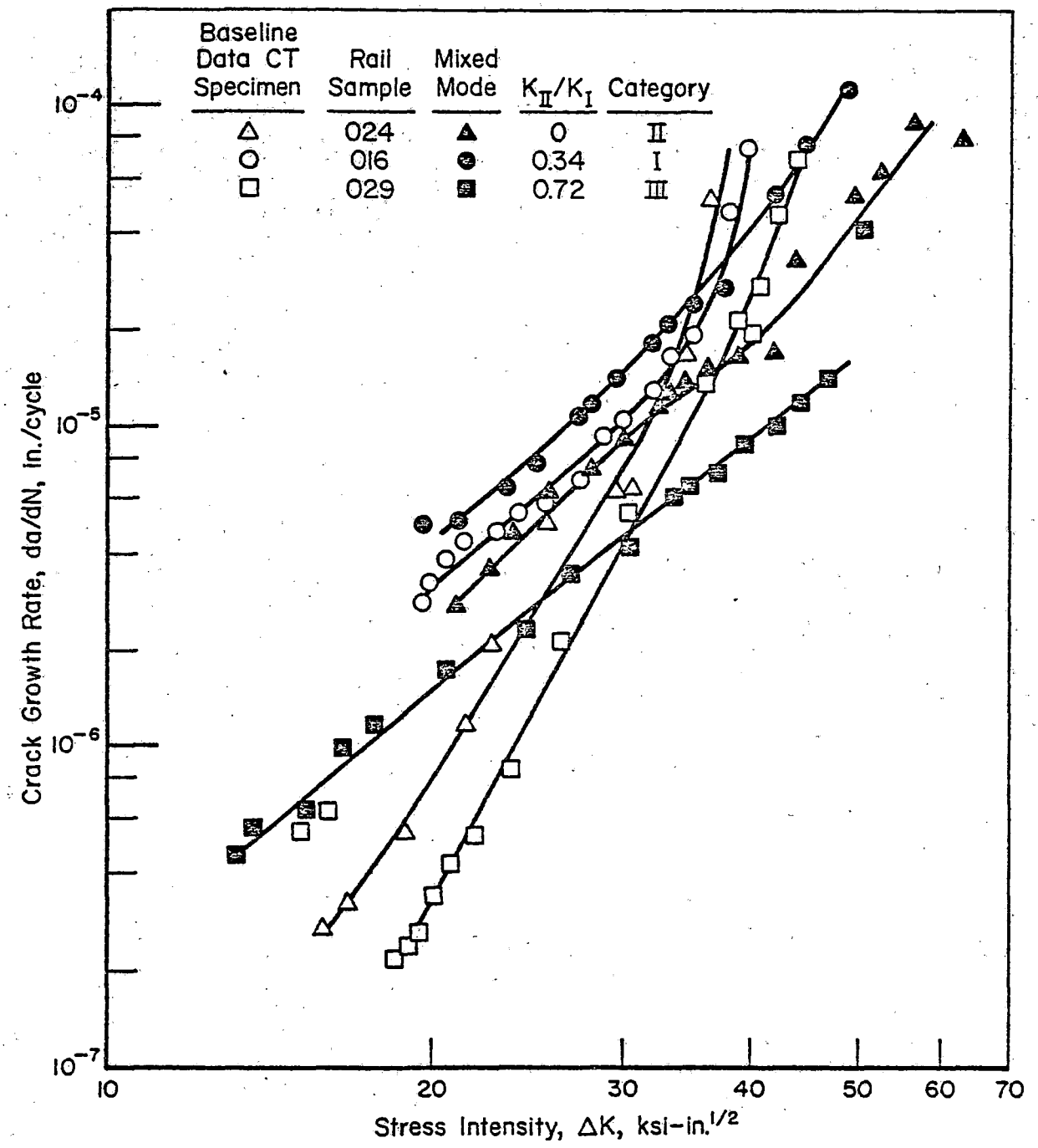

FIGURE 40. MIXED MODE TEST RESULTS; VARIOUS SAMPLES

6.2 The Principal Stress Criterion

According to Figure 37 the Mode II stress-intensity factor almost immediately dropped to zero after very little crack extension. Apparently, the crack followed a path that eliminates Mode II loading, i.e., it grows in a direction perpendicular to the maximum principal stress. This appears to confirm the criterion for mixed mode loading proposed by Erdogan and Sih[7], as shown below.

Consider a crack subjected to combined Mode I and II loading. Polar coordinates r and θ are taken with the crack tip as the origin. The stresses σ_θ and $\tau_{r\theta}$ can be written as:

$$\sigma_\theta = \frac{1}{\sqrt{2\pi r}} \cos\frac{\theta}{2}\left[K_I \cos^2\frac{\theta}{2} - \frac{3}{2} K_{II} \sin\theta\right]$$

$$\tau_{r\theta} = \frac{1}{2\sqrt{2\pi r}} \cos\frac{\theta}{2}\left[K_I \sin\theta + K_{II}(3\cos\theta - 1)\right] \qquad (6.1)$$

For $\theta = \theta_m$ the shear stress $\tau_{r\theta} = 0$. In that particular case σ_θ is the principal stress. The angle θ_m follows from equating the second Equation (6.1) to zero. Obviously, $\cos\frac{\theta_m}{2} = 0$ or $\theta_m = \pi$ is the case for which $\sigma_\theta = 0$. The only other possibility is

$$K_I \sin\theta_m + (3\cos\theta_m - 1) = 0 \qquad (6.2)$$

Equation (6.2) can be solved indirectly by writing

$$\frac{K_{II}}{K_I} = \frac{\sin\theta_m}{1 - 3\cos\theta_m} \qquad (6.3)$$

and by determining the ratio of K_{II}/K_I for various values of θ_m. It can be solved directly by writing

$$2K_I \sin\frac{\theta_m}{2}\cos\frac{\theta_m}{2} + 3K_{II}\left(\cos^2\frac{\theta_m}{2} - \sin^2\frac{\theta_m}{2}\right) - K_{II}\left(\sin^2\frac{\theta_m}{2} + \cos^2\frac{\theta_m}{2}\right) = 0 \qquad (6.4)$$

which yields

$$2K_{II}\tan^2\frac{\theta_m}{2} - K_I \tan\frac{\theta_m}{2} - K_{II} = 0 \quad . \qquad (6.5)$$

So that,

$$\left(\tan \frac{\theta_m}{2}\right)_{1,2} = \tfrac{1}{4} \frac{K_I}{K_{II}} \pm \tfrac{1}{4} \sqrt{\left(\frac{K_I}{K_{II}}\right)^2 + 8} \quad . \tag{6.6}$$

The principal stress $\sigma_1 = \sigma_\theta$ $(\theta = \theta_m)$, hence

$$\sigma_1 = \frac{1}{\sqrt{2\pi r}} \cos \frac{\theta_m}{2} \left[K_I \cos^2 \frac{\theta_m}{2} - \frac{3}{2} K_{II} \sin \theta_m\right] \tag{6.7}$$

or

$$\sigma_1 = \frac{1}{\sqrt{2\pi r}} \cos^2 \frac{\theta_m}{2} \left[K_I \cos \frac{\theta_m}{2} - 3K_{II} \sin \frac{\theta_m}{2}\right] \tag{6.8}$$

It can now be postulated that the rate of growth of the fatigue crack would be the same as in an equivalent pure Mode I case with equal principal stress. For the Mode I case the stresses are given by

$$\left.\begin{aligned} \sigma_y &= \frac{1}{\sqrt{2\pi r}} \cos \frac{\theta}{2} \left(1 + \sin \frac{\theta}{2} \sin \frac{3\theta}{2}\right) \\ \tau_{xy} &= \frac{1}{\sqrt{2\pi r}} \cos \frac{\theta}{2} \sin \frac{\theta}{2} \cos \frac{3\theta}{2} \end{aligned}\right] \tag{6.9}$$

Apparently $\tau_{xy} = 0$ for $\theta = 0$, hence for the case of $\theta = 0$, the stress σ_y is the principal stress:

$$\sigma_1 = \frac{K_I}{\sqrt{2\pi r}} \tag{6.10}$$

Mode I cracks grow along $\theta = 0$, thus Equation (6.10) is also the relevant principal stress.

If the rate of growth in mixed mode can be analyzed as if an equivalent Mode I was operating at K_{Ieq}, the magnitude of K_{Ieq} follows from equating Equations (6.8) and (6.10):

$$K_{Ieq} = K_I \cos^3 \frac{\theta_m}{2} - 3K_{II} \cos^2 \frac{\theta_m}{2} \sin \frac{\theta_m}{2} \tag{6.11}$$

where K_I and K_{II} are the acting stress intensity factors. The rate of crack propagation would be:

$$\frac{da}{dN} = f(\Delta K_{Ieq}) \tag{6.12}$$

where $f(\Delta K_{Ieq})$ is the same as $f(\Delta K)$ for the pure Mode I case. Thus, the mixed mode results, if processed according to Equations (6.6), (6.11) and (6.12), would fall on the same curve as pure Mode I data.

Equation (6.6) was evaluated to give θ_m as a function of K_{II}/K_I. The results are shown in Figure 41. (The dash-dot lines in Figure 41 are for the strain energy density criterion, which will be discussed in the next section.) For the four test cases considered, the following crack extension angles are predicted (Figure 41).

K_I/K_{II}	Predicted Angle	Actual Angle (tests)
0	0	0
0.34	-31.8	-29
0.73	-47.7	-45
$\infty \left(\frac{K_{II}}{K_I} = 0\right)$	-70.5	-56

The predicted angles agree very well with the actual angles observed in the tests (Figure 36), except in the case $K_{II}/K_I = 0$. The discrepancy could be a result of the fact that a slight misalignment of the specimen would introduce a finite K_I, because the crack would be out of the plane of zero bending moment (Figure 11). However, this would imply that the three specimens tested at nominal pure shear were likely to show largely different crack angles. Yet, the three angles were the same within one degree.

Using θ_m and the corresponding ratio K_I/K_{II}, Equation (6.11) can be evaluated. The result is shown in Figure 42. It appears that the equivalent Mode I case would be a K_{Ieq} of 1.5 times the applied K_I for $K_{II}/K_I = 0.73$, and of 1.15 times the applied K_I for $K_{II}/K_I = 0.34$. If this result were applied to the test data in, e.g., Figure 38, the lowest data point for $K_{II}/K_I = 0.73$ would move from $\Delta K = 11$ ksi $\sqrt{in}$ to 16.5 $\sqrt{in}$. This would indeed bring it in line with the baseline data. However, after some crack extension, the K_{II} contribution rapidly decreases to zero (Figure 37), which means that other data points would move much less.

Taking the ratios K_{II}/K_I following from Figure 37, some of the data were replotted on the basis of ΔK_{Ieq} in Figure 43. This confirms the statement made in the previous paragraph that only the lowest data points move far enough to fall in line with baseline data.

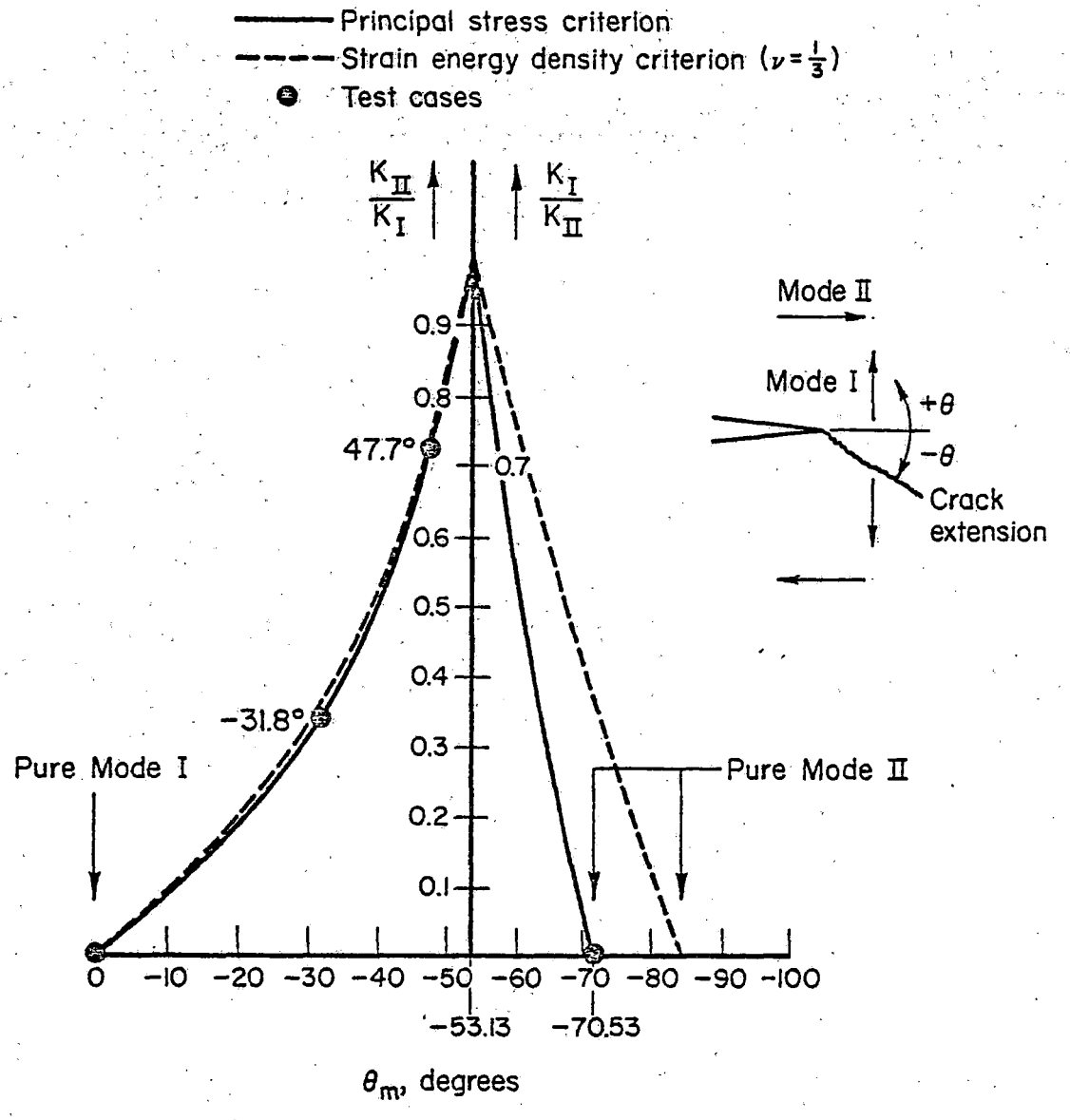

FIGURE 41. CRACK EXTENSION ANGLE FOR MIXED MODE LOADING

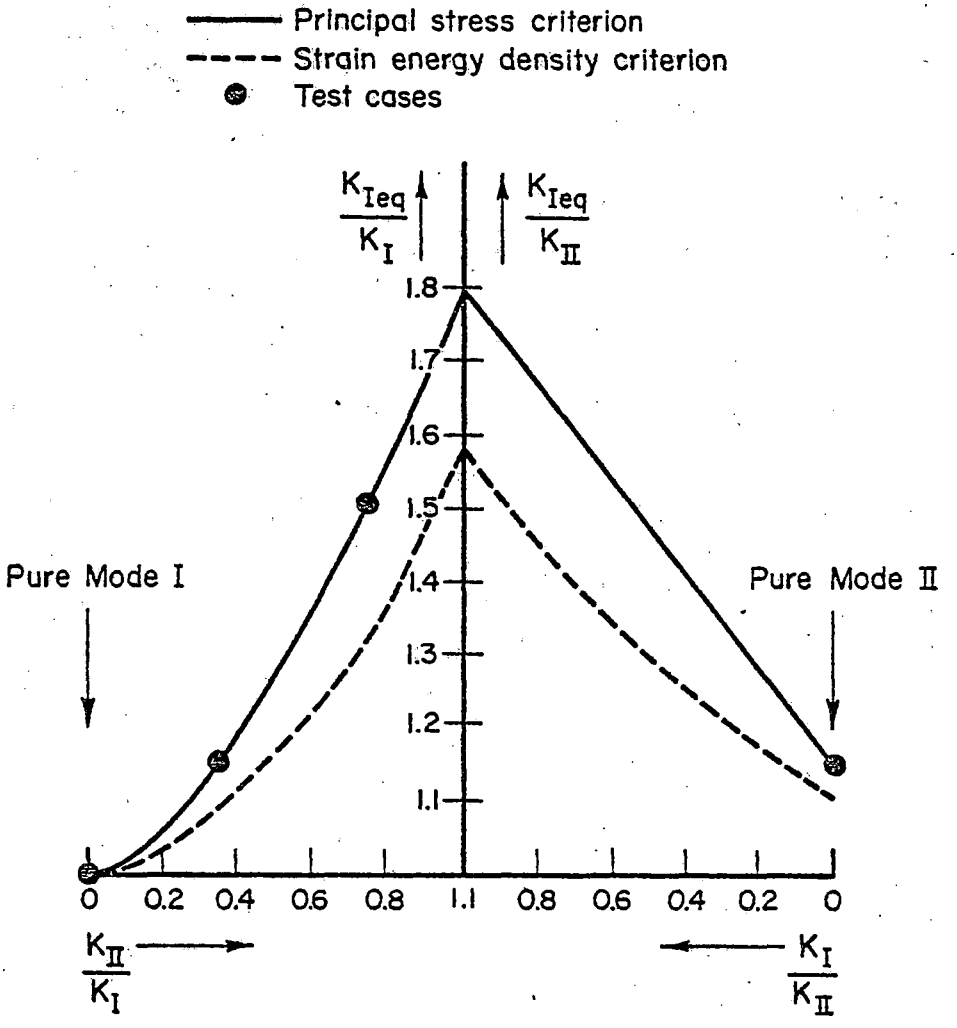

FIGURE 42. EQUIVALENT MODE I STRESS INTENSITY FOR MIXED MODE LOADING

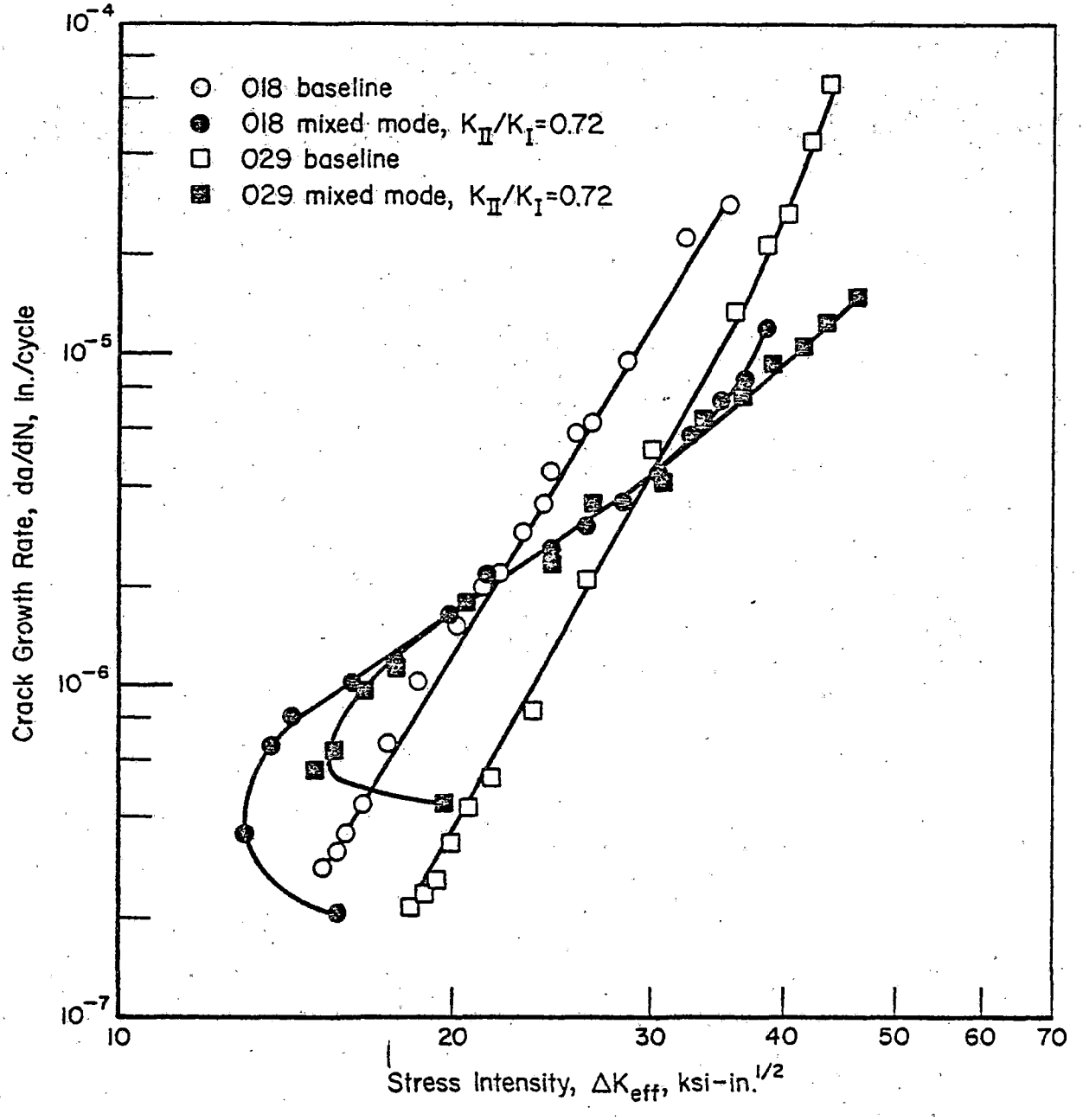

FIGURE 43. MIXED MODE TEST DATA ON THE BASIS OF ΔK_{EFF} FOR THE PRINCIPAL STRESS CRITERION

6.3 Energy Related Criteria

Another mixed mode fracture criterion was proposed by Sih[8], based on elastic strain energy density. The strain energy dW in a unit volume dV is given by

$$dW = \left\{ \frac{1}{2E} \left(\sigma_x^2 + \sigma_y^2 + \sigma_z^2 \right) - \frac{\nu}{E} \left(\sigma_x \sigma_y + \sigma_y \sigma_z + \sigma_z \sigma_x \right) + \frac{1}{2\mu} \left(\tau_{xy}^2 + \tau_{yz}^2 + \tau_{zx}^2 \right) \right\} dV \quad (6.13)$$

where E is Young's modulus and μ is the shear modulus. The strain energy can be determined for the mixed mode stress field at a crack tip, by noting that $\sigma_x = \sigma_{xI} + \sigma_{xII}$, etc., where σ_{xI} and σ_{xII} are the stresses in X-direction due to the Mode I and Mode II loading, respectively.

In accordance with Equation (4.2) all stresses can be expressed as:

$$\sigma_{ij} = \frac{K_I}{\sqrt{2\pi r}} f_{Iij}(\theta) + \frac{K_{II}}{\sqrt{2\pi r}} f_{IIij}(\theta) \quad (6.14)$$

Therefore the strain energy density dW/dV can be evaluated as

$$\frac{dW}{dV} = \frac{S(\theta)}{r} = \frac{1}{r} \left(a_{11} K_I^2 + 2 a_{12} K_I K_{II} + a_{22} K_{II}^2 \right)$$

$$a_{11} = \frac{1}{16\mu} \left[(1 + \cos\theta)(\varkappa - \cos\theta) \right]$$

$$a_{12} = \frac{1}{16\mu} \sin\theta \, (2\cos\theta - \varkappa + 1) \quad (6.15)$$

$$a_{22} = \frac{1}{16\mu} \left[(\varkappa + 1)(1 - \cos\theta) + (1 + \cos\theta)(3\cos\theta - 1) \right]$$

where $\varkappa = (3 - 4\nu)$ for plane strain, and $\varkappa = (3 - \nu)/(1 + \nu)$ for plane stress, ν being Poisson's ratio.

The mixed mode fracture criterion now states that crack propagation will take place in the direction where the strain energy density is minimum, i.e., θ_m follows from

$$\frac{dS}{d\theta} = 0 \; ; \; \frac{d^2S}{d\theta^2} > 0 \quad (6.16)$$

The value of $(S_{min})_{\theta = \theta_m}$ at which the crack starts propagating is considered to be a material property S_{cr}.

The crack propagation angle is a function of the ratio of K_{II}/K_I. Values of θ_m following from Equations (6.15) and (6.16) were given already in Figure 41 for $\nu = 1/3$. Up to $K_{II}/K_I = 1$ the angle is practically the same as for the principal stress criterion. For larger K_{II}/K_I ratios the angle is larger than for the principal stress criterion. Thus, the observed crack angles agree equally well with the strain energy density criterion, although the discrepancy is somewhat larger for the pure Mode II case.

As in the case of the principal stress criterion an equivalent Mode I case can be defined that would cause the same rate of crack growth as the mixed mode loading. For Mode I loading

$$\{S_I(\theta)\}_{min} = S_I(\theta = \theta_m) = a_{11}K_I^2 \quad . \tag{6.17}$$

With θ_m for Mode I loading equal to zero, Equation (6.17) reduces to

$$S_I(\theta = 0) = \frac{2(\varkappa - 1)}{16\mu} K_I^2 \quad . \tag{6.18}$$

Equal crack growth rates would occur if $S_{I,II}(\theta_m) = S_I(\theta = 0)$. Thus, the equivalent Mode I follows from equating Equation (6.18) to the first of Equations (6.15) with $\theta = \theta_m$.

$$K_{Ieq} = \left\{ \frac{16\mu}{2(\varkappa - 1)} \left(a_{11}K_I^2 + 2a_{12}K_IK_{II} + a_{22}K_I^2\right)_{\theta = \theta_m} \right\}^{\frac{1}{2}} \tag{6.19}$$

This equivalent Mode I stress intensity factor was given in Figure 42 as a function of K_{II}/K_I. It appears that K_{eq} is lower for the strain energy density criterion than for the principal stress criterion. For the experimental case of $K_{II}/K_I = 0.73$, the equivalent Mode I stress intensity is only 1.3 times the active K_I, as compared to a factor of 1.5 for the principal stress criterion. As a result the data points in Figure 43 would not move as close to the baseline data as they do when the principal stress criterion applies.

Other energy related criteria have been proposed. The simplest criterion states that the strain energy release rate G for fracture (or for equal crack growth rates) is the same for all modes of loading, including

mixed mode loading. This means that (e.g., Reference 3)

$$G_{Ieq} = G_I + G_{II} \quad . \tag{6.20}$$

Since G_I is proportional to K_I^2/E and G_{II} is proportional to K_{II}^2/E, it follows that

$$K_{eq}^2 = K_I^2 + K_{II}^2 \quad . \tag{6.21}$$

For the experimental case of $K_{II}/K_I = 0.73$, this equation predicts that $K_{eq} = 1.24$ times the active K_I. Obviously, this leads to an even smaller shift of the data points (Figure 43) than with the strain energy density criterion.

The criterion of Equations (6.20) and (6.21) tacitly assumes that crack extension is self-similar, i.e., crack growth takes place in the length direction of the crack. Thus, a value for θ_m is not predicted, since it is assumed to be zero, which is in obvious contradiction with experimental evidence. Also, G_I and G_{II} would be different for a different angle of crack extension.

The more realistic energy release rate criterion is that crack growth occurs in the direction producing the largest energy release rate. It can be shown[9] that this criterion is equivalent to the principal stress criterion. Henceforth, it opens no new avenues.

6.4 Adequacy of Criteria

All criteria are compared in Figure 44, in the type of diagram generally used to display mixed mode criteria. For each criterion the locus is given for all combined mode loading cases that produce equal K_{Ieq}. For example, for the principal stress criterion a K_I of 0.8 ksi $\sqrt{in}$ combined with a K_{II} of 0.35 ksi $\sqrt{in}$ would be equivalent to Mode I loading at 1 ksi $\sqrt{in}$. Obviously, the principal stress criterion is the most severe in that it attributes a larger influence to K_{II} than the other criteria. In the above example a K_I of 0.8 ksi $\sqrt{in}$ can be combined with a K_{II} of 0.5 ksi $\sqrt{in}$ (strain energy density) or with K_{II} of 0.6 ksi $\sqrt{in}$ (self similar energy release) to be equivalent to a Mode I case with 1 ksi $\sqrt{in}$.

Two publications on mixed mode fatigue crack propagation exist. Iida and Kobayashi[10] conducted experiments on tension panels with oblique cracks, but the cracks turned immediately to a Mode I plane as in the present investigation. Roberts and Kibler[11] performed experiments in Mode II with a static Mode I load, but they do not present the Mode I data necessary for comparison.

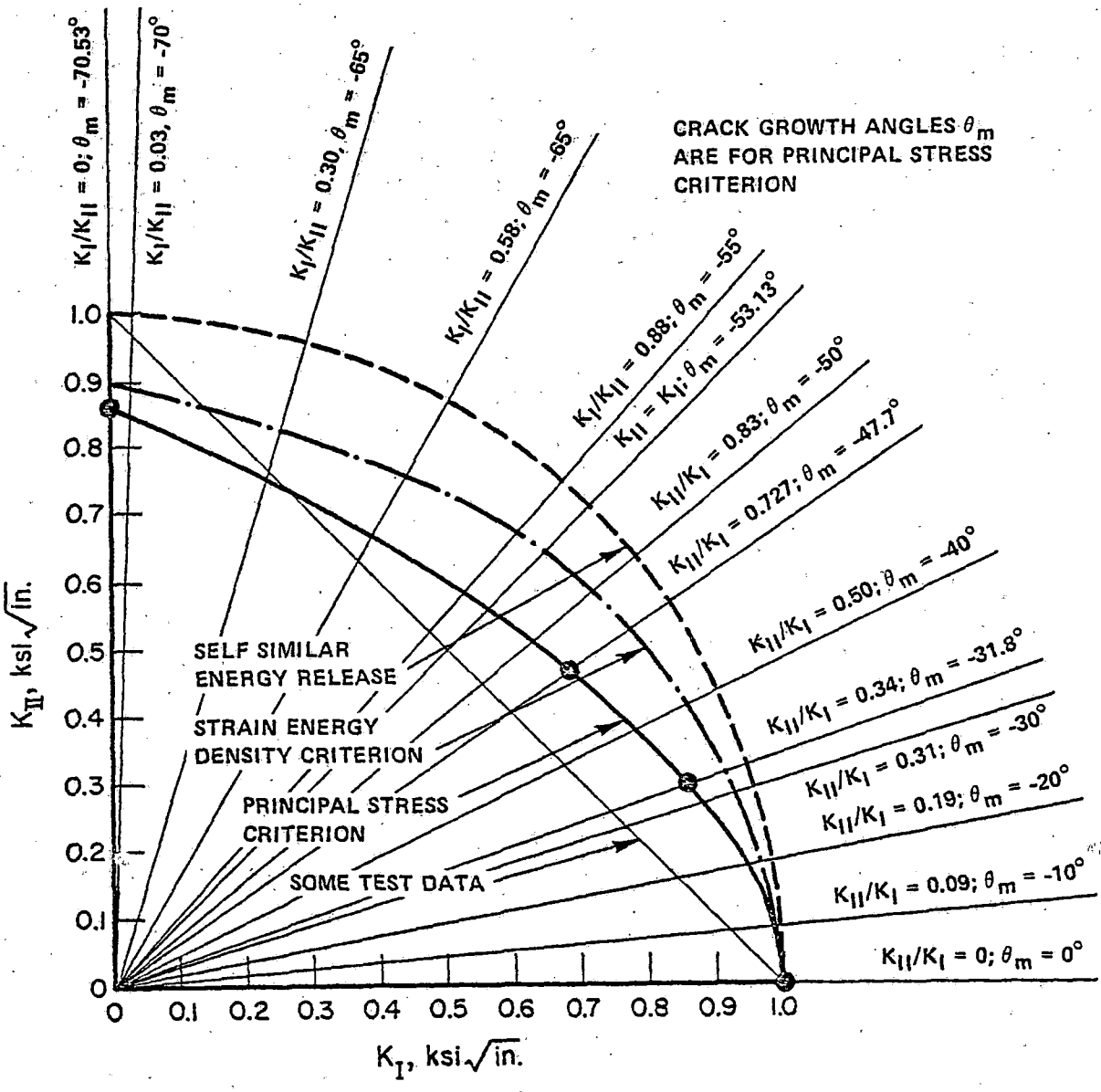

FIGURE 44. LOCUS OF CONSTANT K_{Ieq} FOR MIXED MODE LOADING ACCORDING TO VARIOUS CRITERIA

Several investigators published data of mixed mode residual strength (toughness) tests [7,12,13,14,15]. In most cases the data are presented in a diagram like in Figure 44. The applied K_I is plotted along the abscissa, the applied K_{II} along the ordinate. The data points then fall on a curve that represents $K_{Ieq} = K_{Ic}$, which intersects the abscissa at $K_I = K_{Ic}$. Most of these data fall somewhere in between the curves for the principal stress criterion and the strain energy density criterion. Some data are reported[14,15] that fall on the straight line also shown in Figure 44, representing

$$K_{eq} = K_I + K_{II} \quad \text{or} \quad K_I + K_{II} = K_{Ic} \tag{6.22}$$

and suggesting an even stronger influence of K_{II} than predicted by the principal stress criterion. Liu's[15] test data on shear panels with oblique cracks obey Equation (6.22). Therefore, Liu suggested that mixed mode results are not only dependent upon the magnitudes of K_I and K_{II}, but also on loading conditions.

The present test data indicate that the crack extension angle is best predicted by the principal stress criterion. Also, the initial crack growth rates show the best agreement with the Mode I data if K_{eq} is determined by Equation (6.11) following from the principal stress criterion. Therefore, it is concluded for the time being that the principal stress criterion is the most appropriate for fatigue crack propagation.

The problem of mixed mode cracking can certainly not be dismissed because the experiments show that the cracks turn into a direction with pure Mode I. Roberts and Kibler[11] have shown already that Mode II cracks can grow in a self-similar manner if the loading changes sign in every cycle. This happens also in service but the experiments did not reproduce this condition.

Figure 45 shows various possibilities for mixed mode loading. The top part shows K_I and K_{II} as a function of time. Case a, at the left represents the situation of the present experiments and of those of Iida and Kobayashi[10]. K_I and K_{II} are in phase and K_{II} never reverses sign. The bottom left of Figure 45 shows an oversimplified version of what happens in a rail which is adequate for the present discussion. When a wheel load P travels over the rail the bending moment (at a fixed Point A) changes with time from zero to a maximum and back to zero. The other force, however, changes sign when P passes over A. Thus, K_{II} goes through a cycle of reversed loading when K_I rises from zero to a maximum and decreases to zero, which is shown in the top diagram (Case b) of Figure 45.

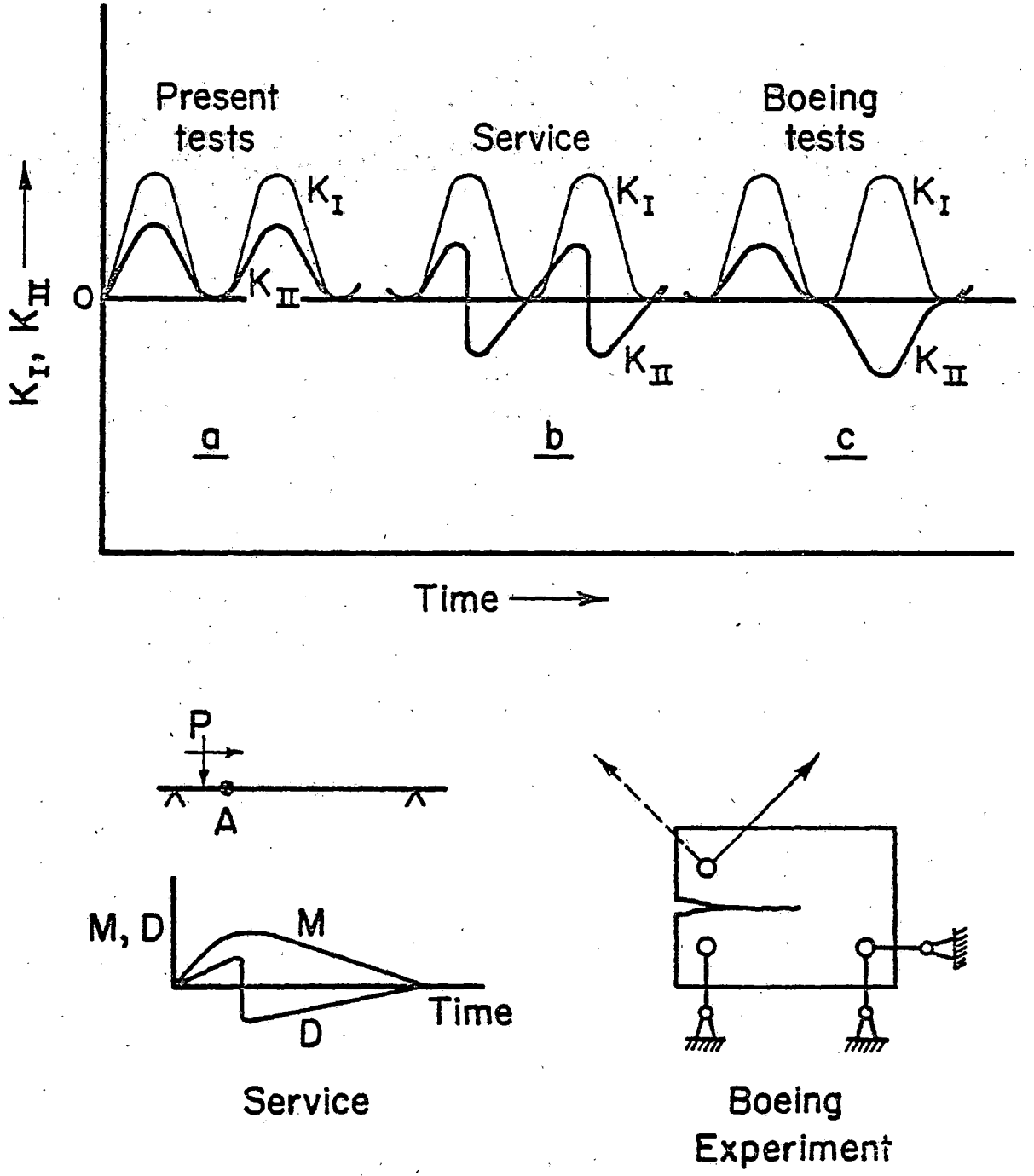

FIGURE 45. MIXED MODE CYCLIC HISTORIES

If the crack wants to turn into a direction of pure Mode I, it will try to turn one way during the positive K_{II} applications, and the other way during the negative K_{II} applications. As a result, the crack will grow in a self-similar manner, so that the K_{II} contribution is not eliminated.

It can easily be seen that Case b loading can be reproduced in an experiment only if two directions of loading are available. This will be accomplished in the present program under a subcontract to the Boeing Airplane Company. Experiments in this subcontract will be of the type shown at the bottom right of Figure 45. Compact tension specimens will be loaded in two directions, and the load will change direction after every application. This results in the loading shown at the top right of Figure 45 (Case c). Since K_{II} will be changing sign, the cracks are expected to grow straight.

7. THE CRACK GROWTH EQUATION

As was discussed already in Section 4.1, fatigue crack propagation data from laboratory specimens are not directly applicable for crack growth predictions, unless they can be expressed in a unique way, independent of crack size and geometry. It was shown that the data can be described uniquely on the basis of the stress intensity factor. Thus, a crack in a rail subjected to the same stress intensity as a crack in a specimen, will exhibit the same rate of growth.

Unfortunately, the stress intensity range ΔK, is not the only parameter that affects the rate of growth. A different R-ratio (or equivalently a different K_{max}) results in a different relation between da/dN and ΔK. Moreover, the critical stress intensity for failure, K_{Ic} or K_c and the threshold stress intensity, K_{th}, have an overriding effect at high and low ΔK's, respectively. When making crack growth predictions, it is often useful to have a formula for the crack growth rate that accounts for the composite effects of ΔK, R, K_c and K_{th}. A formula, applicable to the rail steels as tested in this investigation will be derived below.

An equation accounting for the effects of R-ratio and K_c is the Forman equation given already in Section 4.

$$\frac{da}{dN} = C \frac{\Delta K^n}{(1 - R)\ K_c - \Delta K} \tag{7.1}$$

When writing this equation as

$$\left\{(1 - R)\ K_c - \Delta K\right\} \frac{da}{dN} = C\ \Delta K^n \tag{7.2}$$

it follows that all data should condense to one straight line of slope n if $\left\{(1 - R)\ K_c - \Delta K\right\} da/dN$ is plotted as a function of ΔK on double-logarithmic paper. This was done for points taken from the trend line data in Figure 15 (LT direction and room temperature). The result is shown in Figure 46. Obviously, the data do not condense to a lingle line, which means that Equation (7.1) does not adequately account for the effect of R (or K_{max}).

By noting that $\Delta K = (1 - R)\ K_{max}$, Equation (7.1) can be rewritten as

$$\frac{da}{dN} = C \frac{K_{max}\ \Delta K^{n-1}}{K_c - K_{max}} \tag{7.3}$$

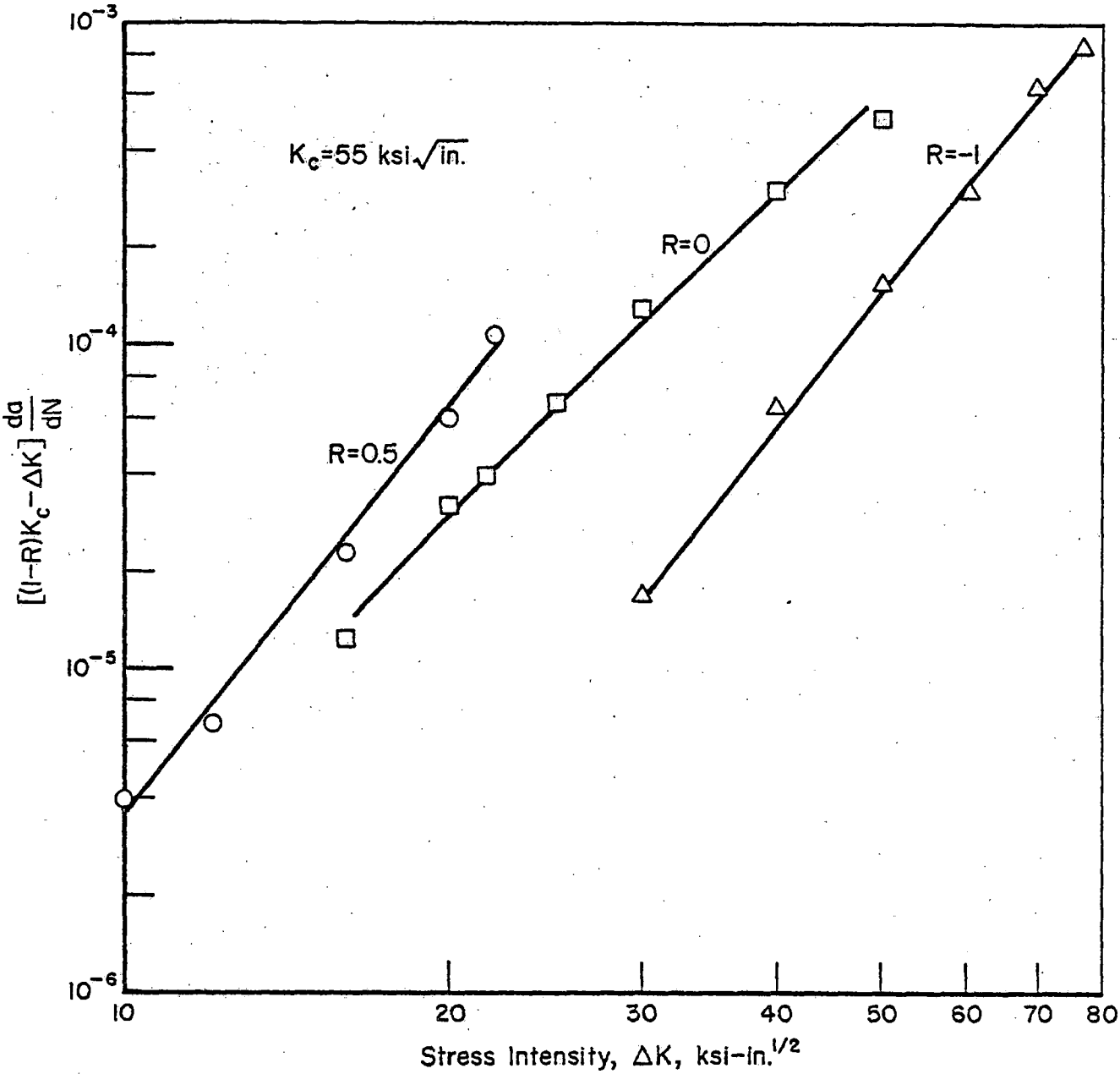

FIGURE 46. INAPPLICABILITY OF FORMAN EQUATION, ORIENTATION LT, ROOM TEMPERATURE

The effect of R-ratio stems from having both K_{max} and ΔK in the above equation. A stronger R-ratio effect would be obtained by modifying Equation (7.3) to

$$\frac{da}{dN} = C \frac{K_{max}^{n} \Delta K^2}{K_c - K_{max}} \tag{7.4}$$

which can be written in terms of K_{max} and R as

$$\frac{da}{dN} = C(1 - R)^2 \frac{K_{max}^{n+2}}{K_c - K_{max}} \tag{7.5}$$

Equation (7.5) implies that all data should condense to one straight line on double-logarithmic paper if $\{(K_c - K_{max})/(1 - R)^2\}$ da/dN is plotted versus K_{max}. Results for the same data as in Figure 46 are plotted in Figure 47. One straight line is now obtained reasonably well, which means that Equation (7.5) adequately accounts for the R-ratio effect.

Not included in Figure 46 are the data for R = -1. It can readily be seen in Figure 15 that the data for R = -1 are displaced by a factor of 2 along the ΔK axis with respect to the data at R = 0. This means that only the positive part of the cycle is active, i.e., the data should be treated as if R = 0 with $\Delta K_{eff} = \frac{1}{2}\Delta K = K_{max}$. This was pointed out in more detail in Section 5.

Equation (7.5) does not yet account for threshold behavior. This can be accomplished by introducing a factor $(K_{max}^2 - K_{th}^2)$ to give

$$\frac{da}{dN} = C(1 - R)^2 (K_{max}^2 - K_{th}^2) \frac{K_{max}^{m-1}}{K_c - K_{max}} \tag{7.6}$$

If R < 0 it should be taken as zero. The threshold values were only slightly dependent upon R, if based on K_{max}. For example in Figure 15, the ΔK_{th} is 7 ksi $\sqrt{in}$ for R = 0.5, 13.5 ksi $\sqrt{in}$ for R = 0 and 28 ksi $\sqrt{in}$ for R = -1. Thus, the values for $K_{max\,th}$ were 14, 13.5 and 14 ksi $\sqrt{in}$, respectively. Therefore, Equation (7.6) will be based on a single threshold value, namely the one found at R = 0.

The above equation can be written as

$$\frac{\frac{K_c}{K_{max}} - 1}{(1 - R)^2 \left\{1 - \left(\frac{K_{th}}{K_{max}}\right)^2\right\}} \frac{da}{dN} = C K_{max}^{m} \tag{7.7}$$

When plotting the left side of the equation versus the right side on double

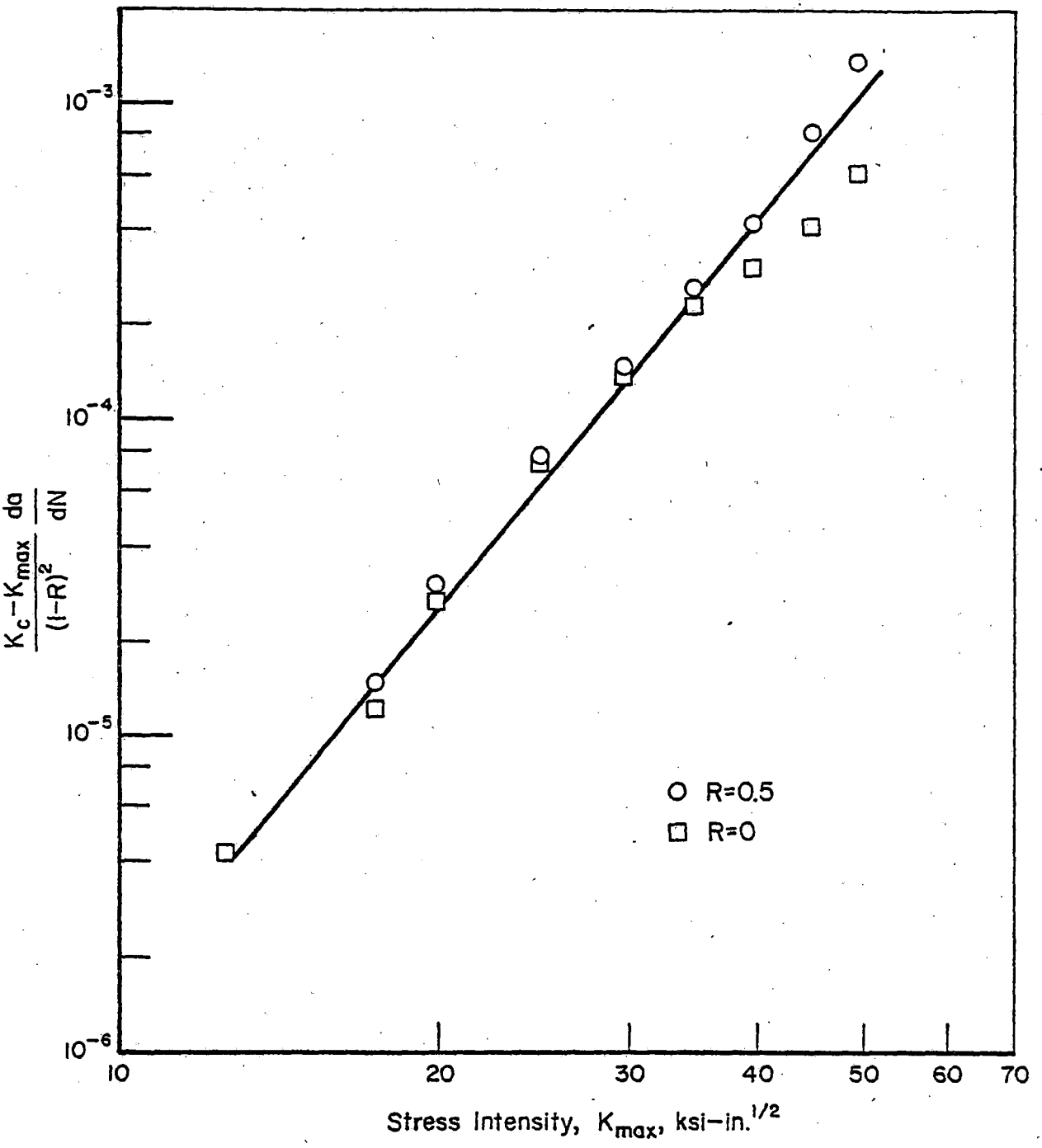

FIGURE 47. CRACK GROWTH EQUATION NOT ACCOUNTING FOR THRESHOLD, ORIENTATION LT, ROOM TEMPERATURE

logarithmic paper a single straight line should result. Of course, now the data in the threshold region should be included (they were not in Figures 46 and 47). This plot is shown in Figure 48. It appears that Equation (7.7) is reasonably satisfied.

In order to show the adequacy of Equation (7.7) it was rewritten in terms of ΔK to give

$$\frac{da}{dN} = C(1 - \bar{R})^{2-m} \left\{\Delta K^2 - (1 - R)^2 K_{th}^2\right\} \frac{\Delta K^{m-1}}{(1 - R)K_c - \Delta K} \qquad (7.8)$$

It should be noted now that $\bar{R} = R$ for $R > 0$, and $\bar{R} = 0$ for $R \leq 0$. The trend lines for the LT orientation and room temperature are replotted in Figure 49. Also plotted are points predicted by Equation (7.8). Obviously, the effects of R, K_c and K_{th} are adequately accounted for. The generality of Equation (7.8) is shown by similar plots for different cases in Figures 50 through 53.

Apparently, Equation (7.8) can be used generally to describe the crack growth behavior of the rail steels used in the present experiments. Since Equations (7.6) and (7.8) are equivalent, Equation (7.6) is recommended for use. Not only is Equation (7.6) much simpler, it also is more appropriate for service cracks in rails, since it is expressed in K_{max}. The maximum stress intensity in rails is likely to be determined by the residual stress level. Cyclic stresses are mostly from the (tension) residual stress level down. Thus, all stress cycles at a given size of crack would have a common K_{max}. Therefore, it is more useful to have a crack growth equation expressed in K_{max}.

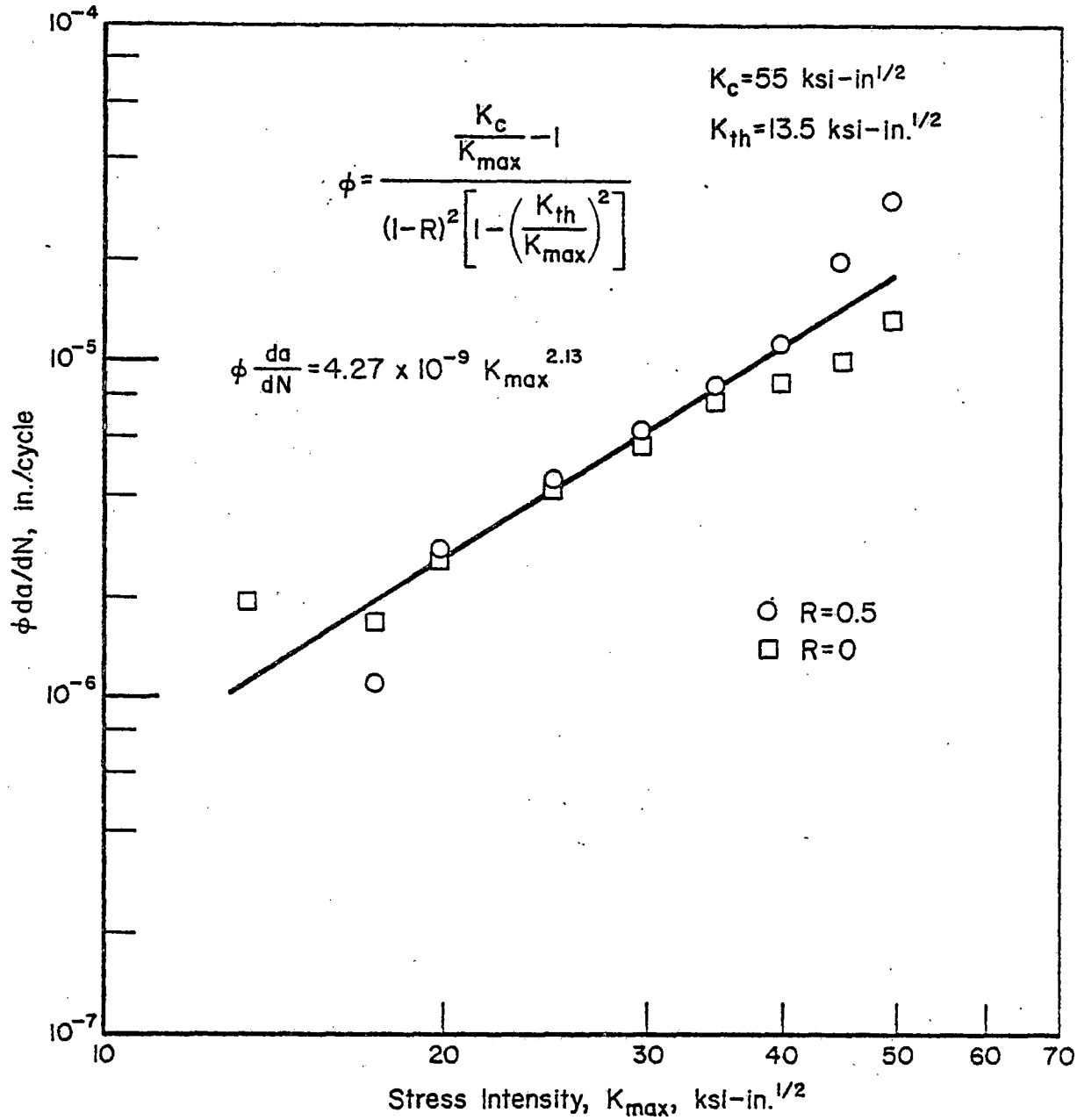

FIGURE 48. CRACK GROWTH EQUATION ACCOUNTING FOR THRESHOLD, ORIENTATION LT, ROOM TEMPERATURE

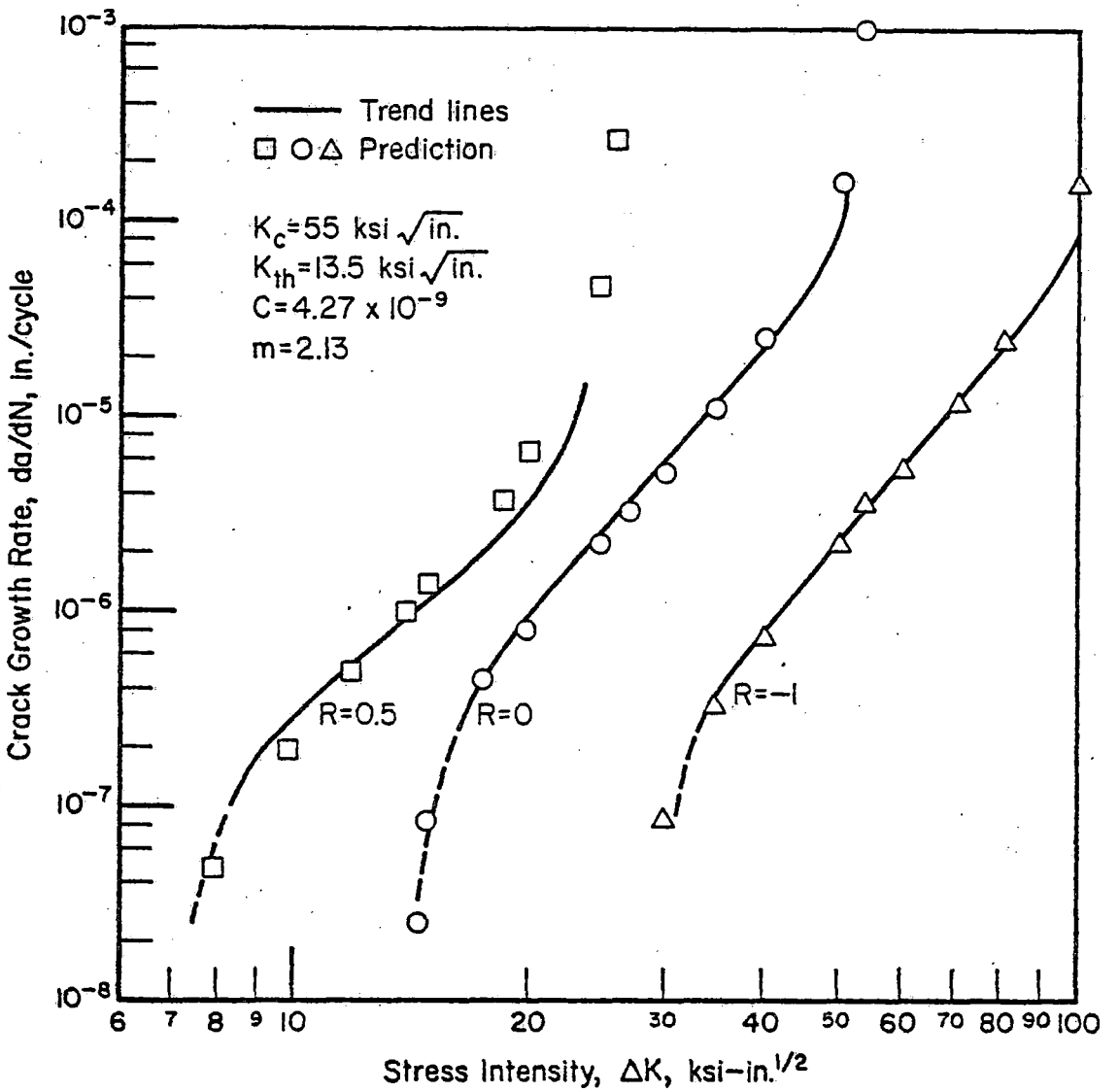

FIGURE 49. APPLICABILITY OF CRACK GROWTH EQUATIONS, ORIENTATION LT, ROOM TEMPERATURE

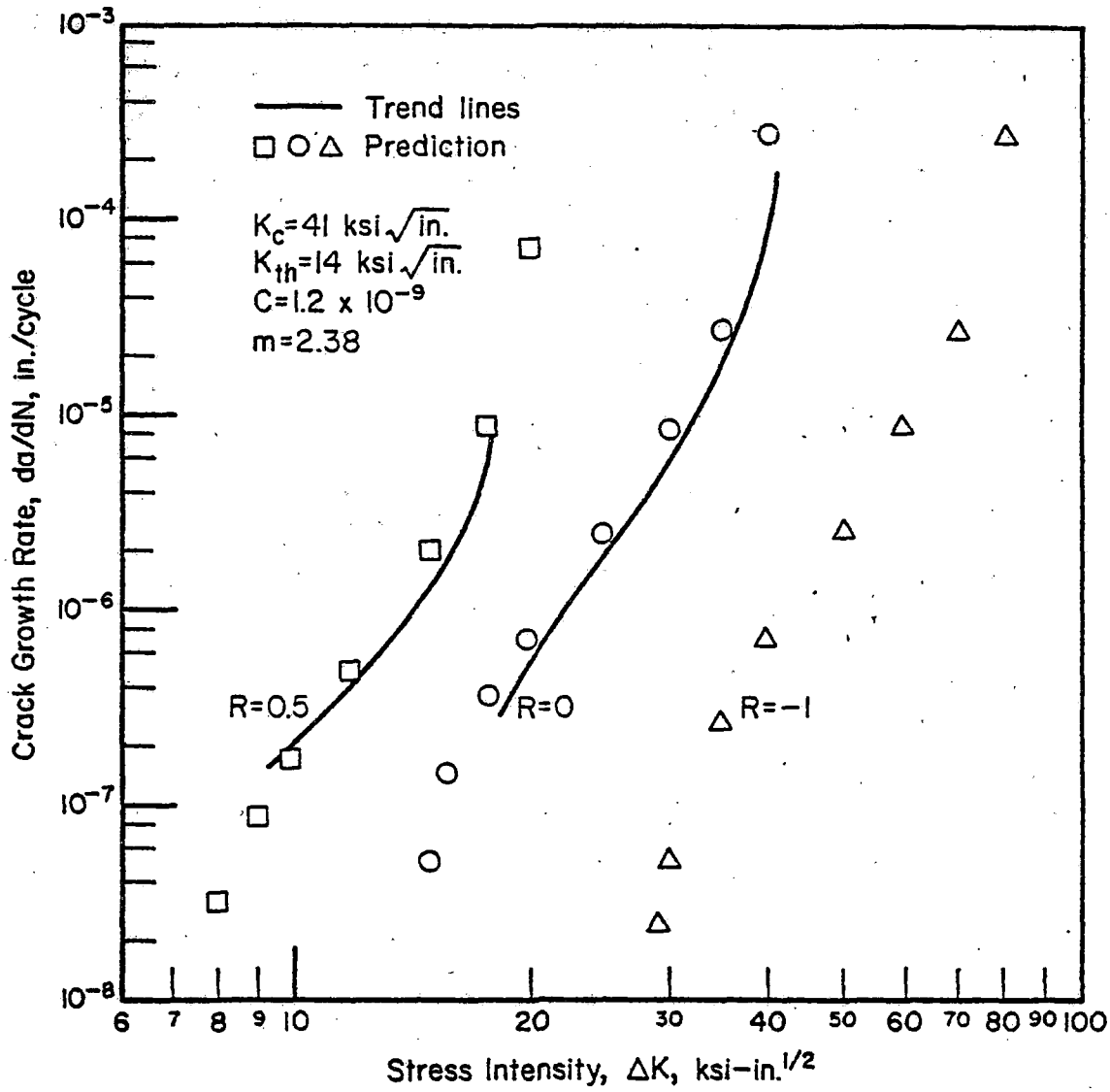

FIGURE 50. APPLICABILITY OF CRACK GROWTH EQUATION, ORIENTATION LT, -40 F

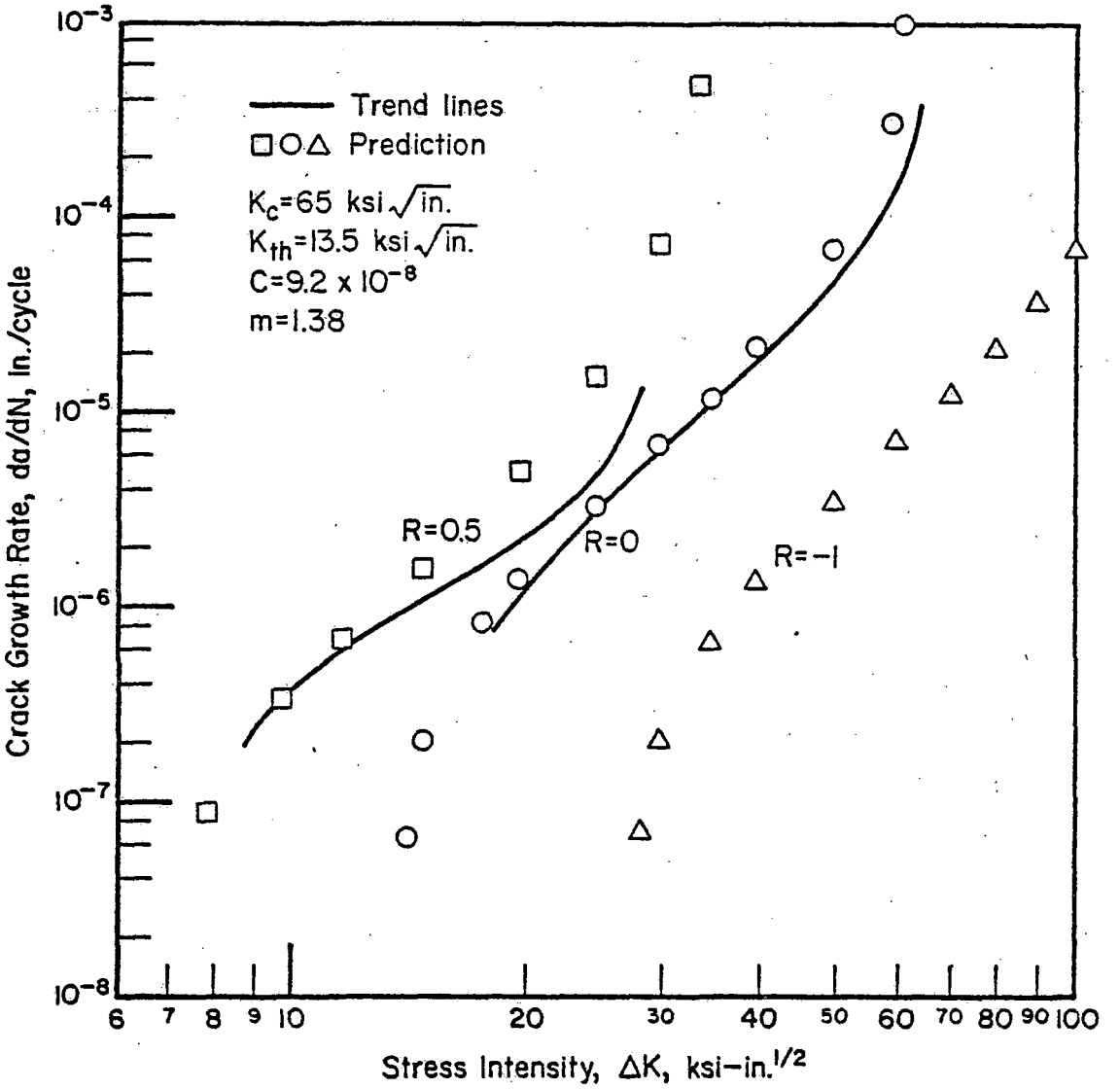

FIGURE 51. APPLICABILITY OF CRACK GROWTH EQUATION, ORIENTATION LT, +140 F

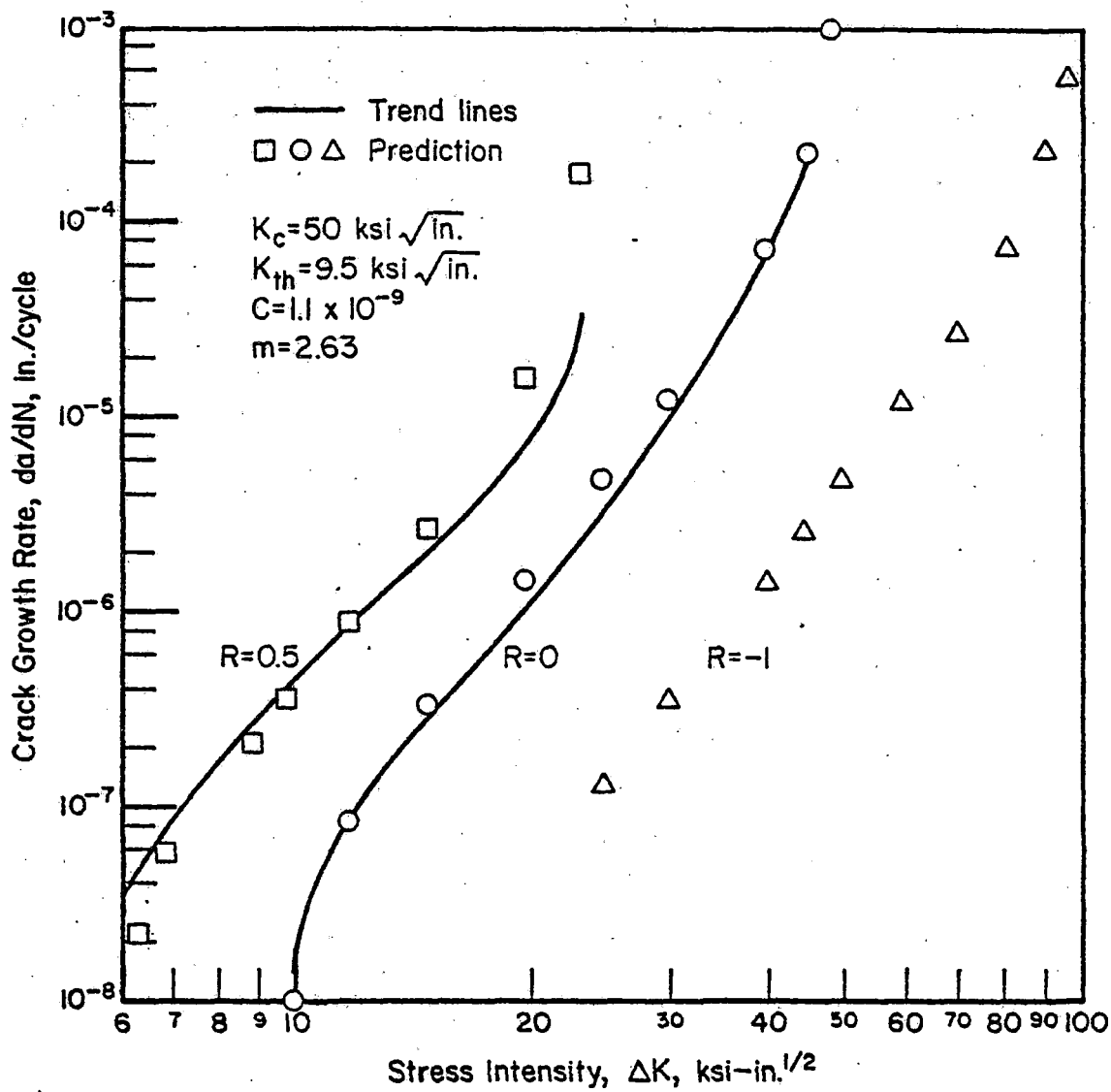

FIGURE 52. APPLICABILITY OF CRACK GROWTH EQUATION, ORIENTATION TL, ROOM TEMPERATURE

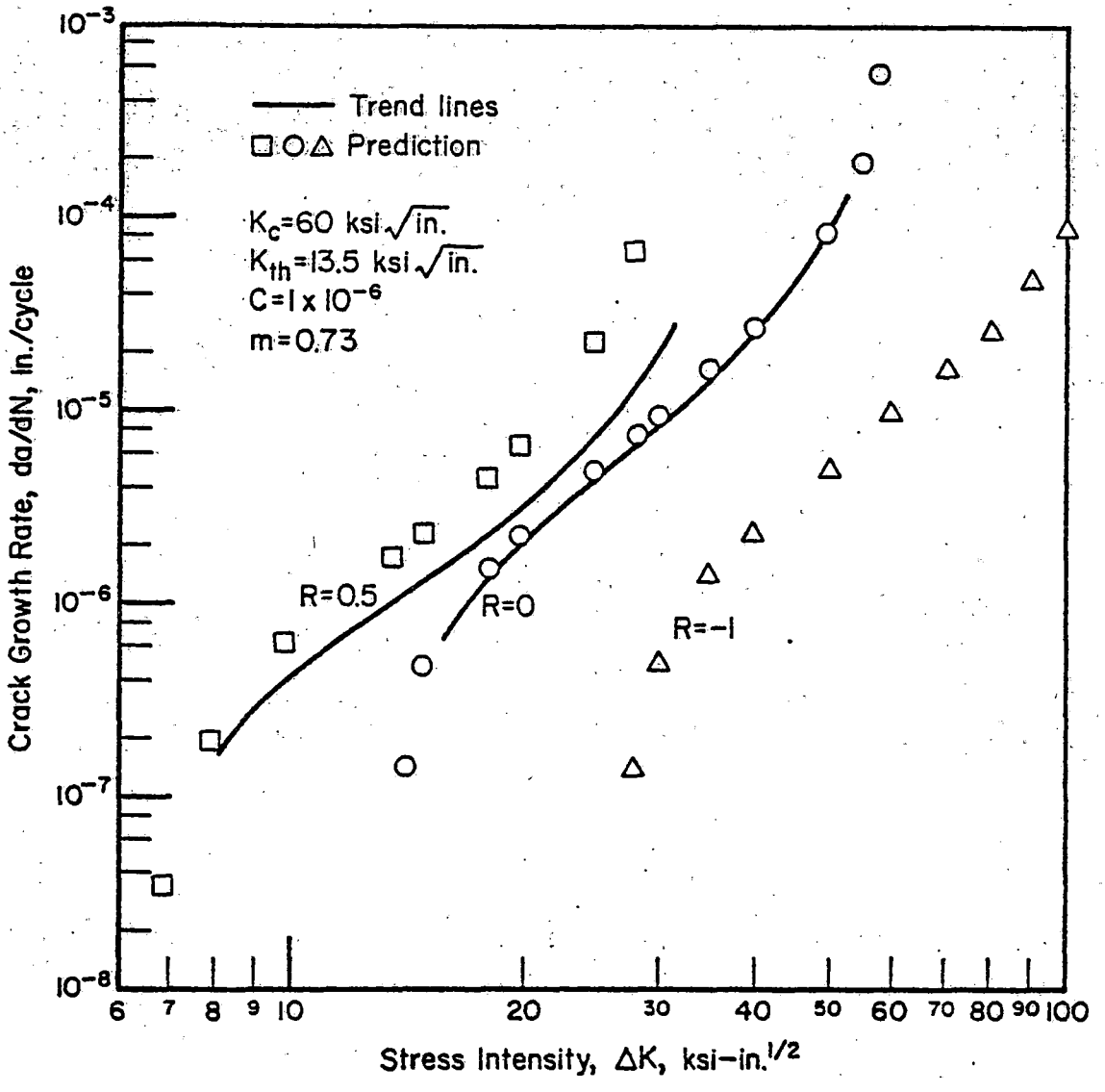

FIGURE 53. APPLICABILITY OF CRACK GROWTH EQUATION, ORIENTATION TL, +140 F

8. VARIABILITY IN CRACK-GROWTH BEHAVIOR

8.1 Basis for Statistical Analysis

Early in this experimental program it became apparent that the crack-growth behavior of the investigated rail steels was subject to substantial variability and that it would not be possible to exactly define the cracking characteristics of even a single rail heat.

This observation was not really surprising though, since all material properties are subject to some degree of uncertainty and even the simplest physical characteristics of a material (e.g., hardness, tensile strength, and elastic modulus) display variability.

Because of this uncertainty or variability, a material property can often be best described by performing repetitive experiments and determining the mean property value along with a measure of the observed variability in property values. Many physical properties of materials display a statistical variability which is nearly normal or logarithmically normal. In these cases a single parameter - the standard deviation - can be computed to quantify the variability in a collection of material property test results.

This approach was taken to evaluate the variability in crack-growth behavior of the various subgroups of rail tests. Before these data could be statistically analyzed, however, it was necessary to translate the overall crack-growth rate curves into single-valued quantities that would reflect the material's resistance to fatigue-cracking under constant amplitude cyclic load conditions. This was done by a numerical integration of the da/dN-ΔK curve for each specimen from a stress-intensity level of 20 ksi $\sqrt{in}$ to the apparent fracture toughness level for the material. The integration was performed on a ficticious compact-tension type specimen (W = 3.00 inches) so that crack lengths ranged from an initial value of about 1.00 inch to around 2.00 inches at specimen failure. The result of this integration was an analytical prediction of the number of cycles required to grow a crack in a CT type specimen (like the one used in this program) from a length of 1.00 inch to failure. By evaluating the various crack-growth curves in this manner, it was possible to quantitatively compare crack-growth resistance of all the different specimen geometries tested under a variety of loading conditions.

8.2 Baseline Crack-Growth Data

In Phase 1 of this program, one constant amplitude FCP test was completed on each of the 66 heats of rail material. It was obvious at the time the testing was underway that the cracking behavior from one specimen to the next was rather variable, in fact it was observed that the actual number of cycles to grow a crack from 1.00 inch to failure ranged from 150,000 to more than 2,000,000 cycles for the various material heats. It was presumed initially that the rail samples displaying the lowest fatigue lives were inherently inferior in crack propagation resistance to the other material heats. This point had not been verified, however, so it was decided that a statistical review of the data would be helpful.

Employing the procedures described earlier, each da/dN versus ΔK curve was numerically integrated from a stress intensity of 20 ksi $\sqrt{in}$ to the apparent fracture toughness, K_c, and the resultant cycles to failure were recorded. These computed fatigue lives were then statistically analyzed to attempt to identify superior and inferior crack-growth material groupings.

The first observation was that the analytically determined and actual experimental crack propagation lives were quite similar. This was as expected since the same specimen geometries were assumed and the same initial stress intensity levels were chosen. The second observation was substantially more significant. A statistical check (Chi-Squared test) on the total collection of 66 data points indicated that the entire collection of data could be described by a single normal distribution, which in turn, implied that the low test results from the baseline experiments merely represented the low side of the variability band in crack-growth resistance for the rail steels investigated. Figure 54 displays the ranking of fatigue lives versus the predicted failure percentages for a log-normal distribution. If the data corresponded exactly with log-normality they would all fall upon the straight line drawn through the data. Some minor variations from log-normality are evident but the general trend of the data is toward log-normality.

From the ranking of fatigue lives presented in Figure 54 it is evident that the average logarithmetic fatigue life was 5.68 (50 percent failures). This translates to an average number of cycles to failure of 478,630. The standard deviation of this collection of logarithmic fatigue lives was found to be 0.30. According to the statistics of normal distributions, the mean value

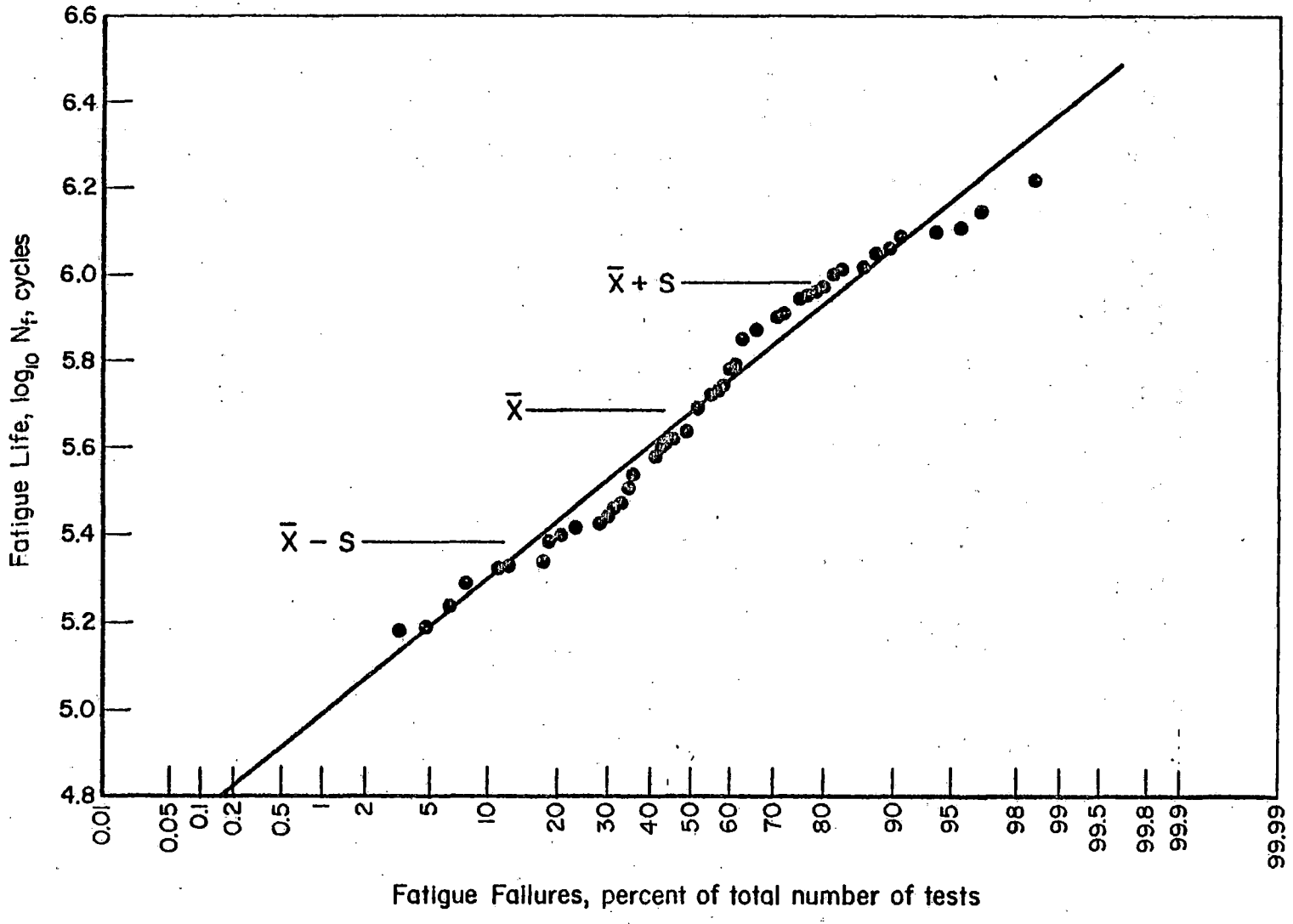

FIGURE 54. DISTRIBUTION OF BASELINE FCP LIVES FOR 64 RAIL SAMPLES

of a data population plus or minus 1 standard deviation, should contain approximately 58 percent of the total data population. In this case there were 66 total test results, which meant that 58 percent of 66 data points (≈ 38) should lie between the logarithmic fatigue lives of 5.38 and 5.98 (239,880 and 954,990 cycles, respectively). In actuality 40 specimens out of 66 failed within those cycle limits, which represents 61 percent of the total population. The comparison between the theoretical statistics and actual statistics is good.

As an additional comment on the variability in crack-propagation lives of the baseline experiments it is interesting to compare the ratio of the logarithmic standard deviation of the 66 data points to the logarithmic mean value of the population. That ratio (0.30/5.68) is a value of about 0.053 (5.3 percent). This is commonly called the coefficient of variation in a collection of data, and the lower the ratio, the lower the data variability. Simple tensile tests commonly display coefficients of variation of 3 percent or greater, while it is not uncommon for high-cycle fatigue data to show coefficients of variation from 5 to 10 percent. The main point to be made is that the scatter in crack-propagation lives evident in the collection of 66 rail heats was not large compared to other similar types of data.

The statistical analysis can be extended to other crack length and loading conditions as well. This is important because it allows prediction of constant amplitude crack-propagation lives for various initial crack sizes. For example, by using a power law relation between da/dN and ΔK, and assuming an initial ΔK level of 10 ksi $\sqrt{in}$ a series of crack propagation lives were calculated for each rail heat. The distribution of computed crack-propagation cycles to failure is shown in Figure 55. It is readily apparent from this figure that the slope of the probability line (coefficient of variation) is nearly identical to that in Figure 54 even though the ranking of individual heat fatigue lives changed in numerous cases (due to crossing of da/dN - ΔK function lines). The computed logarithmic mean fatigue life for all of the rail heats was 6.787 (6,123,500 cycles). A standard deviation of 0.357 was found for the logarithmic fatigue lives. Chi squared check of the data indicated normality with 95 percent confidence. Other curves can easily be generated for other crack sizes, load levels and specimen geometries.

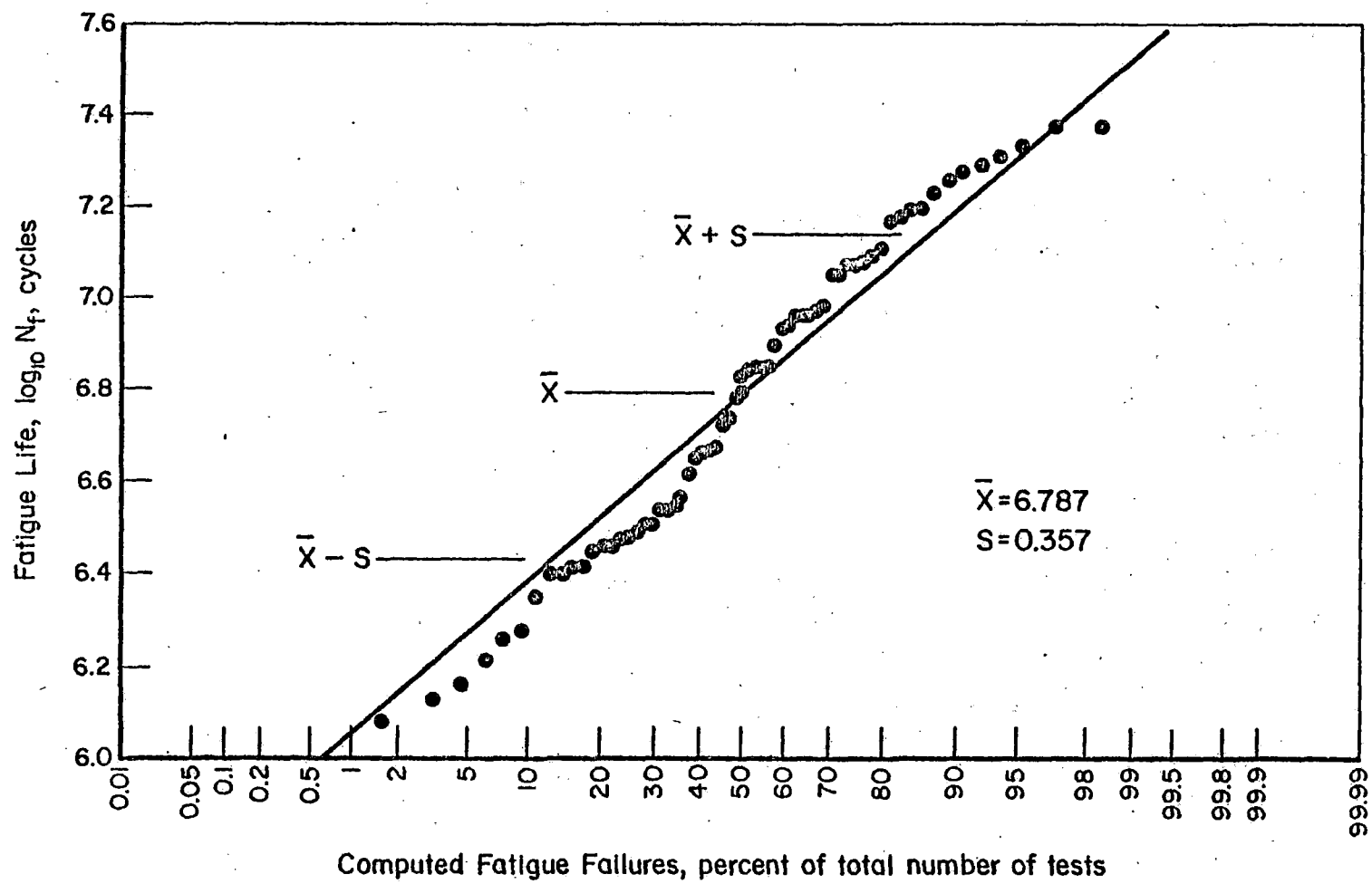

FIGURE 55. DISTRIBUTION OF COMPUTED BASELINE FCP LIVES FOR 64 RAIL SAMPLES ASSUMING EACH TEST WAS STARTED AT A STRESS INTENSITY OF 10 KSI$\sqrt{\text{IN.}}$

8.3 Phase 2 Crack-Growth Data for R = 0

It was a natural extension of the baseline data analysis to do a similar review of the Phase 2 test data generated on other specimen types, cracking orientations, test temperatures, and frequencies.

The computed statistics for all of the R = 0 subsets of FCP data are shown in Table 3. Some of the data collections are small but they do provide reasonable indications of the comparative crack-propagation lives for the different test conditions. As an additional illustrative aid, these same data are presented in Figure 56. The data points denote mean crack-propagation lives and the solid and dashed bounds indicate plus and minus one and two standard deviation limits from the mean.

Standard statistical checks (F and t tests) were made on the various categories of data to determine whether any of the data sets could be combined, i.e., showed no significant differences in either mean value or standard deviation. If 2 groups of data could be combined it meant that, for the test conditions studied in this program, the variable or combination of variables differentiating those groups had an insignificant effect on the crack propagation life.

Through this analysis it was determined that data groups 2, 5, 9 and 10 were statistically similar and could be combined with 95 percent confidence. Groups 3, 7, 6 and 11 could also be combined. These are all LT specimens. One conclusion drawn from this was that the -40 F and room temperature test conditions produced similar crack-growth lives, while the +140 F temperatures produced significantly lower lives. Another conclusion was that the TL and SL orientations of cracking produced significantly lower crack-growth lives than the LT orientation, with the SL orientation displaying the lowest overall crack-growth lives.

The only minor surprise in these findings was that the -40 F and room temperature data displayed no significant differences, even though it was evident from the individual data displays that these test conditions produced da/dN versus ΔK curves with different slopes and different critical toughness asymptotes. Apparently the load levels were such that the 2 differing factors tended to offset each other. This overlap of data for the 2 different temperatures must, therefore, be considered somewhat fortuitous and does not indicate a total absence of low temperature effect on cracking behavior. Specimens tested at lower load levels would probably have shown higher crack-propagation lives at the -40 F temperature than at room temperature and conversely, specimens

TABLE 3. COMPARISON OF R = 0 FCP DATA GENERATED AT VARIOUS TEMPERATURES IN SEVERAL ORIENTATIONS (MAX. INITIAL STRESS INTENSITY = 20 KSI $\sqrt{IN}$)

Data Group	Description	Orientation	Temperature, F	No. of Data	Logarithmic Mean Life, $\bar{X}$	Logarithmic Std. Dev., S
1	Baseline CT Data	LT	68	66	5.68	0.30
2	SEN Data	LT	68	6	5.73	0.28
3	CT Data	TL	68	3	5.59	0.08
4	CT Data	SL	68	3	5.21	0.04
5	Temperature Effect CT	LT	-40	5	5.74	0.24
6	Temperature Effect CT	LT	140	3	5.38	0.17
7	Temperature Effect CT	TL	-40	4	5.58	0.13
8	Temperature Effect CT	TL	140	3	5.34	0.11
9	Frequency Effect CT	LT	-40	3	5.76	0.12
10	Frequency Effect CT	LT	68	3	5.66	0.16
11	Frequency Effect CT	LT	140	3	5.67	0.08
12	Fowler's Data[16]	LS	68	6	4.59	0.04

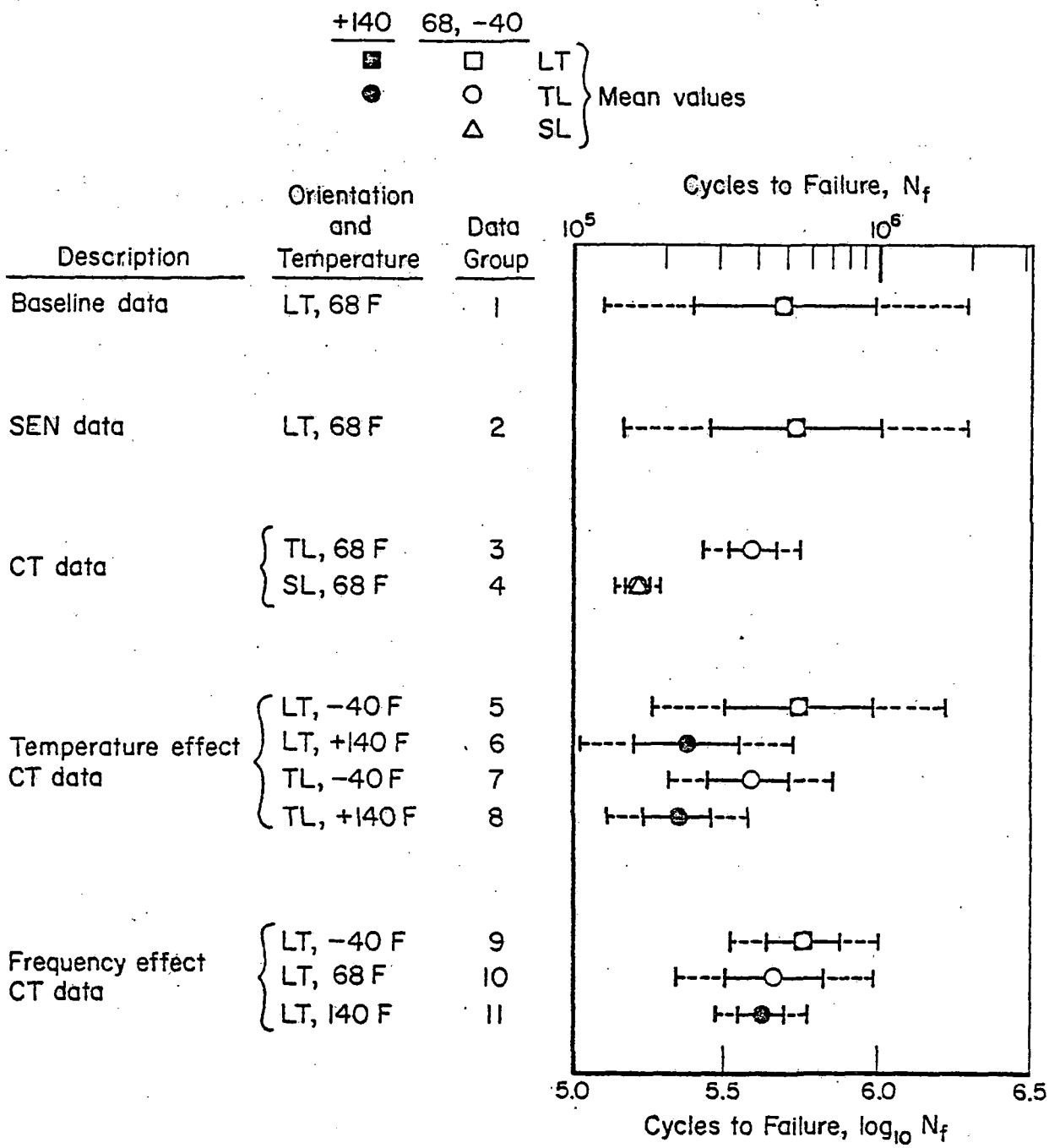

FIGURE 56. COMPARISON OF R = 0.0 FCP DATA GENERATED AT VARIOUS TEMPERATURES IN SEVERAL ORIENTATIONS

tested at higher loads would almost surely have displayed lower crack-propagation lives at the reduced temperature level.

Some limited crack growth data generated by Fowler[16] is included as the last entry in Table 3. The mean log life of these data is substantially smaller than of the data of the present program. The most likely reason for the discrepancy is the different orientation. Fowler's data are for the LS orientation. LS and LT are growing in the same plane but in different directions. It is somewhat surprising though that Fowler's data have a lower mean log life than the present SL data (Table 3). However, indirectly the same results were obtained here with the surface flaw specimens. At the specimen surface, the surface flaws were growing in LS. According to Figure 35a, the growth in that direction was substantially faster than in the SL direction, by a factor of 3 on the average. The mean log life for SL was 5.21 (Table 3). Hence, the LS surface flaw results suggest a mean log life of 5.21 - log 3 = 4.74, which is much closer to Fowler's results.

In accordance with the higher growth rates, Fowler also found lower threshold values ($\Delta K \approx 7 - 8$ ksi $\sqrt{in}$). An extrapolation of the LS surface flaw data in Figure 35a to the threshold regime, suggests a threshold value on the order of 7 ksi $\sqrt{in}$. Thus, the two data sets are in good agreement.

These observations emphasize the anisotropy of rails with regard to crack growth properties. In particular, the results indicate that a transverse fissure in a rail head will have a tendency to develop into an elliptical flaw with the major axis in horizontal direction and the minor axis in the vertical direction. This is in agreement with service experience. Naturally, the stress distribution in the rail head will have a strong influence on the flaw shape also. Therefore, the above conclusion is only of a qualitative nature.

8.4 Phase 2 Crack-Growth Data for R = 0.50

A somewhat more limited collection of data was generated at a stress ratio of 0.50, but there was sufficient data to observe the effects of temperature and orientation on crack-growth resistance. Table 4 provides a tabulation of the statistically analyzed data subgroups generated at R = 0.50. Figure 57 displays those data for each category.

As with the R = 0 data, the -40 F and room temperature data groups could be combined, but the +140 F data fell significantly below the other temperatures. Orientation was again found to be a significant factor on crack-growth life.

TABLE 4. COMPARISON OF R = 0.50 FCP DATA GENERATED AT VARIOUS TEMPERATURES IN SEVERAL ORIENTATIONS (MAX. INITIAL STRESS INTENSITY = 20 KSI $\sqrt{IN}$)

Data Group	Description	Orientation	Temperature, F	No. of Data	Logarithmic Mean Life, $\bar{X}$	Logarithmic Std. Dev., S
1	SEN Data	LT	68	6	6.27	0.09
2	CT Data	TL	68	6	6.04	0.01
3	Temperature Effect CT	LT	-40	3	6.26	0.04
4	Temperature Effect CT	LT	140	3	6.10	0.03
5	Temperature Effect CT	TL	-40	3	6.23	0.10
6	Temperature Effect CT	TL	140	3	6.10	0.04

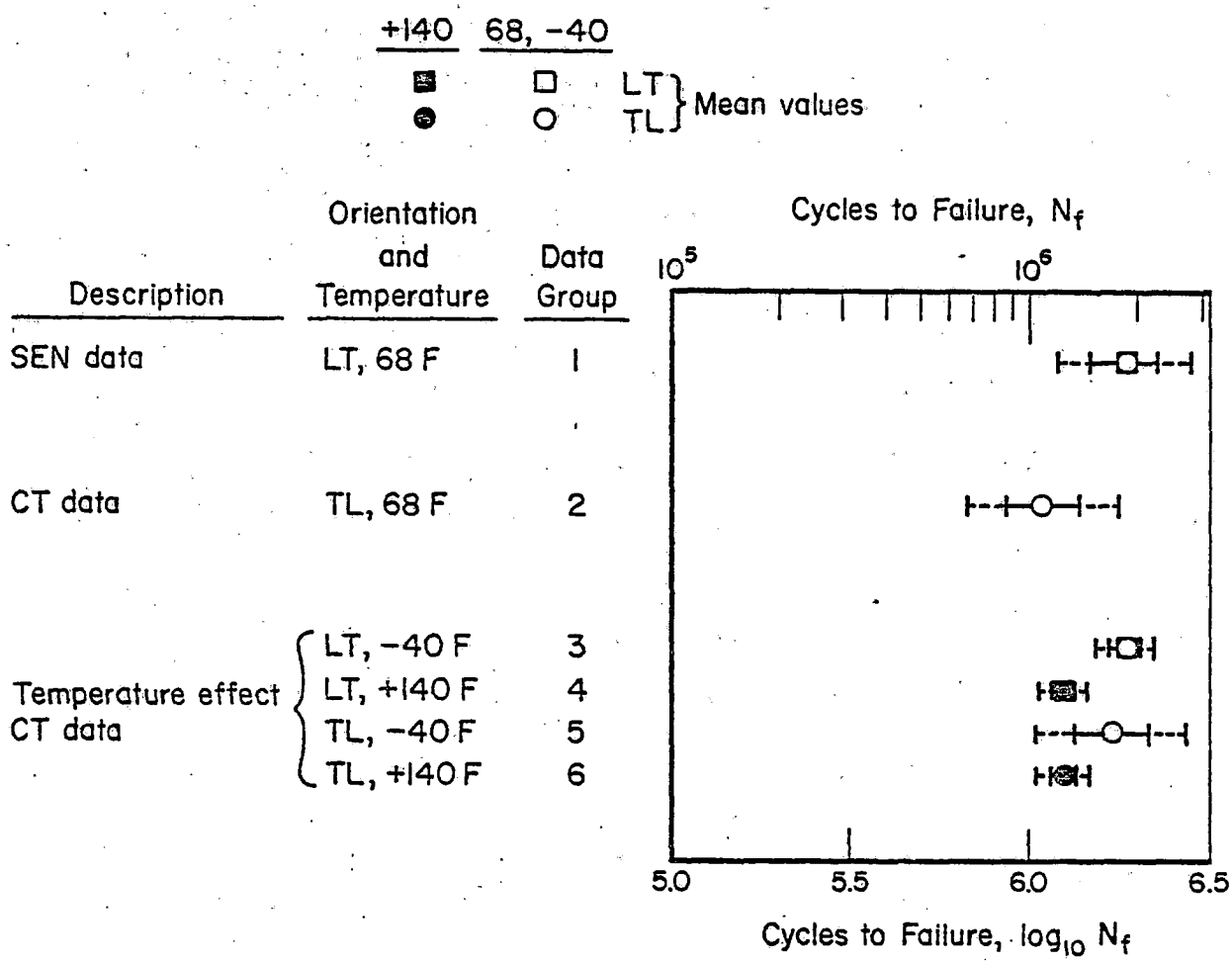

FIGURE 57. COMPARISON OF R = 0.50 FCP DATA GENERATED AT VARIOUS TEMPERATURES IN THREE ORIENTATIONS

On the basis of a statistical combination of the appropriate data subgroups a condensed tabulation of crack-growth resistance data was formed as shown in Table 5. The effects of temperature, orientation, and stress ratio are evident from this data display. It is also interesting to note that the coefficient of variation for these various groups is quite small — in many cases it is less than 3 percent — which indicates excellent repeatability in the test data.

8.5 Correlation with Other Material Properties

In Phase I of this research program an attempt was made[1] to correlate crack growth behavior with other mechanical properties, chemical composition and microstructural parameters. No correlations were found, apart from a weak correlation with hardness. The statistical analysis in the previous subsections indicated that crack growth properties behave more or less as a random variable.

Yet 9 rail samples were selected for additional testing in this phase of the program to further examine the effect of various material parameters on crack growth. These samples were listed in Table 1. The test data are presented in Figure 58 for the LT direction and in Figure 59 for the TL direction. The band of other data (Figure 15) is also shown in these figures.

The crack growth lives for these specimens are compared in Table 6 with the crack growth lives of other specimens from the same rail samples tested in Phase I (LT results only). It turns out that the results of the first and second test on the same sample are very close in some cases, but appreciably different in other cases. Mean log lives and standard deviations are also compared, showing the same statistical sample properties.

The average data of the two specimens of each sample were taken for a comparison with other material parameters in Table 7. The results are listed in the order of increasing life. Chemical composition, mechanical properties and pearlite content are listed and valued by 0, + or —. The parameter is given as zero if it was within one standard deviation of the mean of all 66 samples. If it was more than one standard deviation above the mean, a + is indicated, and if it was more than one standard deviation below the mean, a — is indicated. In the case of pearlite, a zero means 100 percent pearlite and a — means less than 100% pearlite. The mean log life of all 66 samples was 5.68 with a standard deviation of 0.30. Thus, all 9 sample lives were within one standard deviation of the mean (see Table 7).

TABLE 5. OVERALL FCP STATISTICS FOR THE VARIOUS STRESS RATIOS, TEMPERATURES, FREQUENCIES AND SPECIMEN ORIENTATIONS

Orientation	Temperature, F	Stress Ratio	No. of Data	Logarithmic Mean Life, $\bar{X}$	Logarithmic Std. Dev., S
LT	68 and -40	0.00	17	5.73	0.23
		0.50	9	6.27	0.08
		-1.00	6	5.71	0.27
	140	0.00	6	5.50	0.13
		0.50	3	6.10	0.03
TL	68 and -40	0.00	7	5.58	0.12
		0.50	9	6.10	0.10
	140	0.00	3	5.34	0.12
		0.50	3	6.10	0.04
SL	68	0.00	3	5.21	0.04

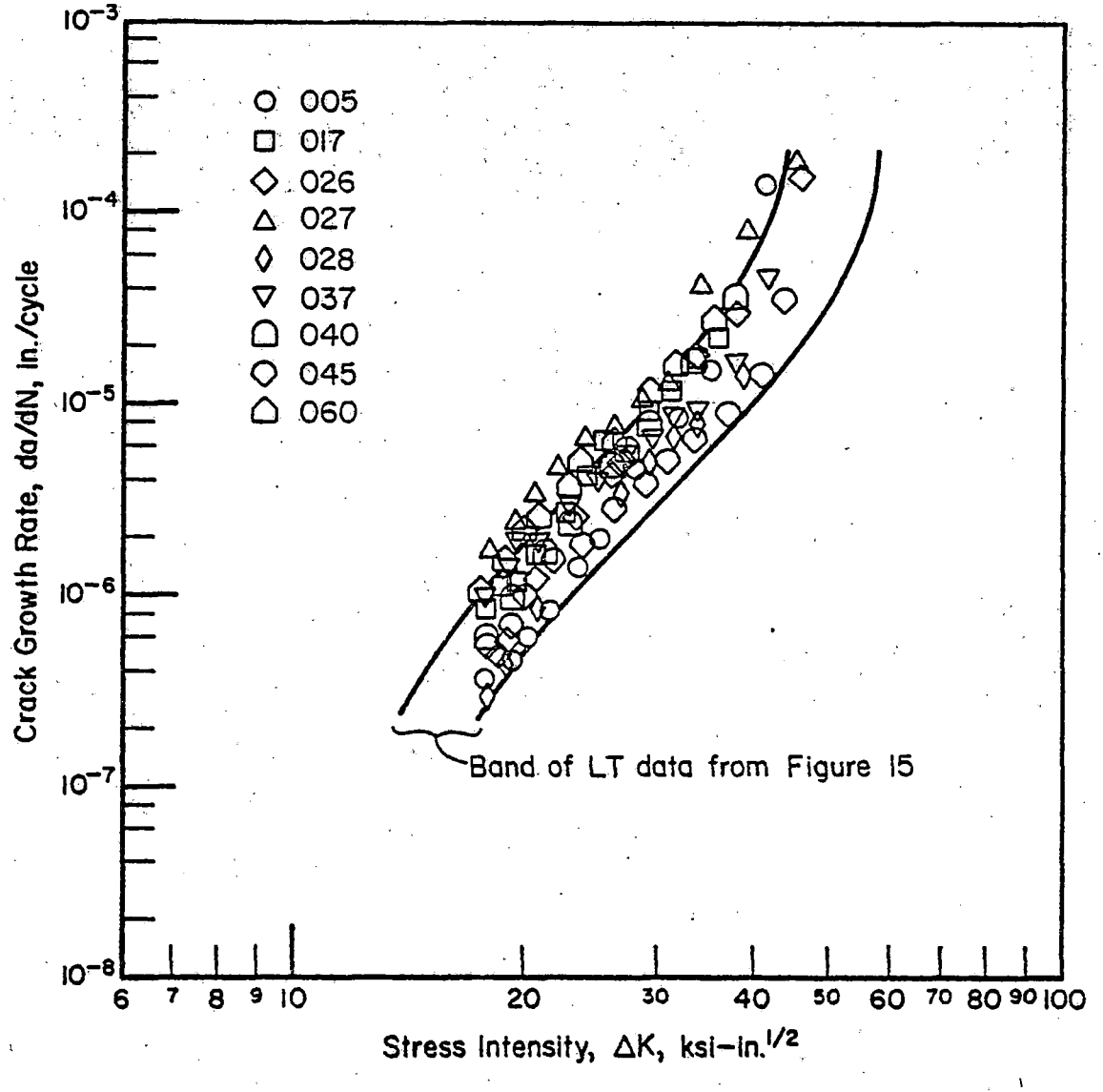

FIGURE 58. ADDITIONAL BASELINE DATA, ROOM TEMPERATURE AT R = 0, CT SPECIMENS IN LT DIRECTION

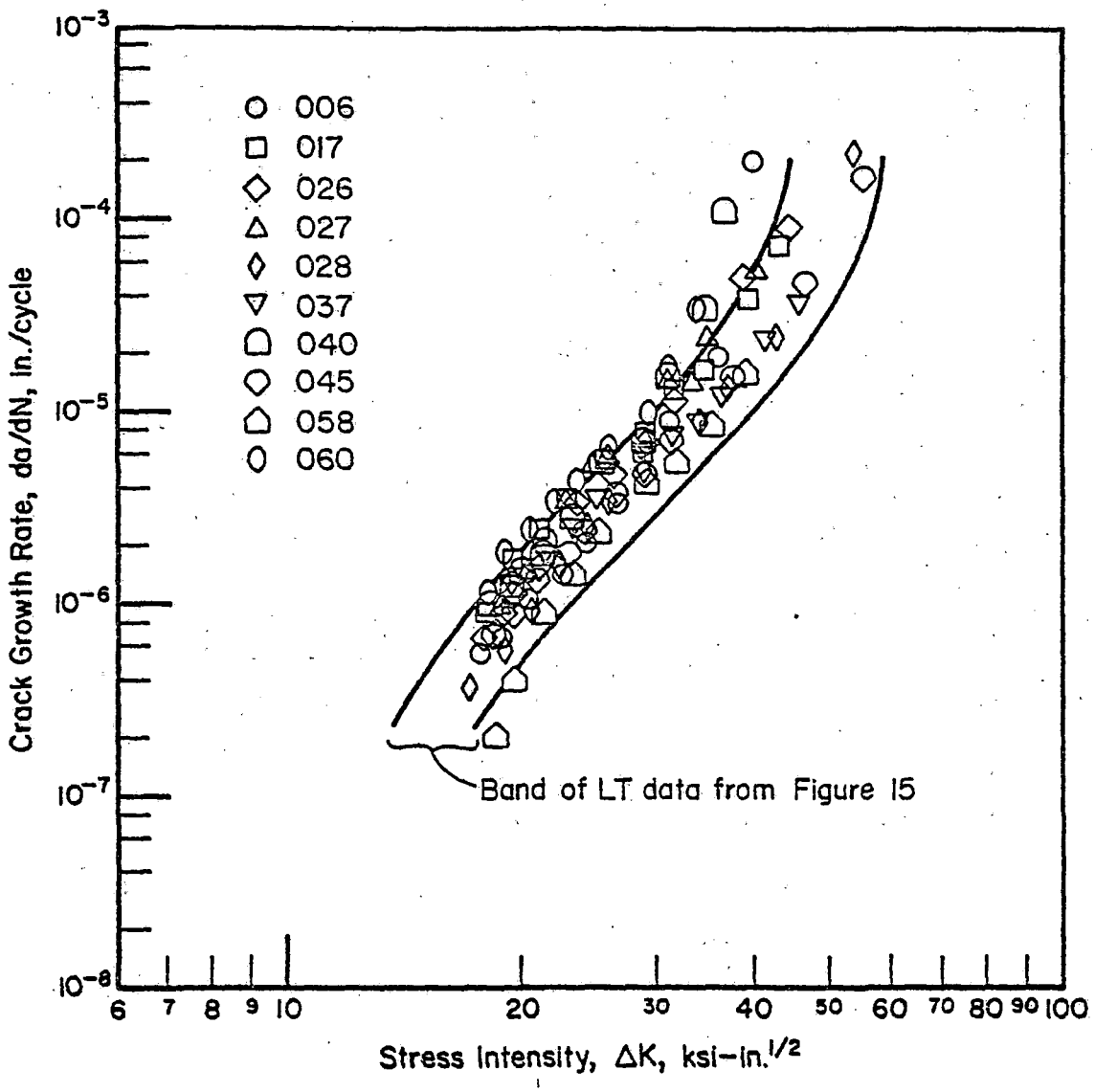

FIGURE 59. ADDITIONAL BASELINE DATA, ROOM TEMPERATURE AT R = 0, CT SPECIMENS IN TL DIRECTION

TABLE 6. ADDITIONAL CRACK GROWTH TEST RESULTS

Heat No.	Orientation	Kilocycles to Failure, N_f	Cycles to a = 1.0 in., N	Cycles from a = 1.0 in. to a_f, ΔN	Baseline Results	Percent Difference in Log Life
017	LT	556	278	278	288	-0.3
	TL	504	267	237	--	--
028	LT	1,291	607	684	536	+1.8
	TL	936	443	493	--	--
060	LT	411	213	198	247	-1.8
	TL	376	181	195	--	--
026	LT	659	260	399	233	+4.2
	TL	626	311	315	--	--
027	LT	311	155	156	890	-12.7
	TL	534	280	254	--	--
037	LT	494	225	269	617	-6.2
	TL	521	225	296	--	--
005	LT	1,091	440	651	271	+7.0
	TL	785	350	435	--	--
040	LT	625	296	329	323	+0.1
	TL	462	219	243	--	--
045	LT	792	338	454	1,019	-5.8
	TL	678	295	383	--	--

	Original 9 Samples	New Tests on 9 Samples	66 Baseline Samples
Average of Logarithmic Crack Growth Lives	5.53	5.63	5.68
Standard Deviation of Logarithmic Crack Growth Lives	.22	.25	.30

TABLE 7. RANKING OF EXPERIMENTAL RESULTS OF ADDITIONAL BASELINE TESTS

Sample Number	Average Life, kilocycles	Chemical Composition				UTS	TYS	Pearlite	Log Life
		C	Mn	S	O				
060	222	0	0	−	0	0	0	0	5.35
017	283	0	0	+	−	0	0	0	5.45
026	316	0	0	+	0	0	0	0	5.50
040	326	−	−	0	+	+	+	−	5.51
037	443	0	0	−	0	−	0	−	5.65
005	461	−	+	0	0	0	0	0	5.66
027	523	0	0	0	0	0	0	0	5.72
028	610	0	0	0	+	0	0	−	5.79
045	736	−	−	0	+		−	−	5.87

For Sample No. 027, all material parameters are zero, while this sample had a life of 523,000 cycles. Samples 040 and 045 have mostly nonzero entrees, and all deviations are to the same side, except the yield stress. Yet Sample No. 040 has a life of 326,000 cycles and Sample No. 045 has a life of 736,000 cycles, which spreads the results to both sides of Sample 027.

The fact that crack growth properties do not show obvious correlations with any other material parameters may not be as surprising as it seems. All parameters listed in Table 7 are bulk properties, i.e., they are an average for a large conglomerate of grains, pearlite colonies, and inclusions. However, fatigue crack propagation is not a bulk property but a very local property. Every cycle the crack propagates over a small distance varying from 10^{-7} to 10^{-4} inches. For every cycle, then, only an extremely small amount of material comes into play. Thus, the variability in crack growth is much more a function of the local variations in structural and chemical composition. Most of the crack propagation life is spent when the crack is still very small. If in that part of life material is encountered where the local properties are poor, the crack will grow quickly through this region, thus causing a drastic reduction in total crack growth life. If in a later stage of crack growth, material is encountered with much better properties, some of the loss is made up for, but since crack growth rates are already high due to the high K, the total life still remains low.

Thus, crack growth is much more dependent upon local variations in the material than other material properties. As a consequence, any correlations with bulk material properties are not observed, obvious, or easily assessible. Another consequence is that variability of crack growth properties within a material can be almost as large as the variability among materials of the same type (i.e., variability within one rail as opposed to variability among rails). Only if the bulk properties show very drastic changes can a general trend in crack growth properties be observed. This is the case if the effect of orientation is considered, where the SL direction has consistently worse properties than the LT direction.

The variability of all parameters for 66 rail samples is given in Table 8. Despite the large variations in chemical composition the bulk properties of tensile strength and yield stress do not vary much. The standard deviation as a percent of the mean for the chemical composition is on the order of 10 percent or more. This number is only a few percent for the mechanical properties, and more important, also for the log life. Apparently, the large variations in chemical and structural parameters are not reflected in the variability of the crack growth life.

TABLE 8. VARIABILITY OF RAIL PROPERTIES

Variable	Low Value	High Value	Mean	Standard Deviation	Standard Deviation in Percent of Mean
% C	.57	.85	.76	.06	8
% Mn	.61	1.48	.88	.17	20
% S	.014	.052	.029	.010	34
Grain Diameter, mm	.066	.120	.087	.021	25
Pearlite Interlamellar Spacing, Å	2,470	4,160	3,211	632	20
TUS, ksi	111	142	133	5.5	4
TYS, ksi	60	82	73	5	7
Crack Growth Life, log cycles	5.18	6.22	5.68	.30	5

9. IMPLICATIONS FOR THE FAILURE MODEL

The present results and those of Phase I[1] are a unique and complete representation of fatigue crack growth properties of rail steels. The effects of R-ratio, orientation and some other parameters were investigated to an extent that parallels can be drawn for all rail materials with a high degree of confidence. In order to predict crack growth under service loading from constant amplitude loading, an adequate description of da/dN data is required. Such a description is now available by means of the crack growth equation derived in section 7.

Therefore, all baseline information for the subsequent development of a rail failure model is available. In the last phase of this program fatigue crack propagation under variable amplitude service loading will be investigated. A rationale will be developed to predict the behavior under service loading on the basis of constant amplitude data. Such a rationale will not predict a particular test result under a particular random sequence of loads, because the variability within one material will not be accounted for, as discussed above. However, the rationale will predict the behavior of the family of rail steels. A reliability analysis, or some sort of statistical analysis will then be required to account for the variability in service.

It is of great interest to know how the variability in crack growth properties will affect reliability analysis. Some appreciation for this can be obtained from Table 9. The first line in this table shows the variability parameters of crack growth. If the entire variability in crack growth was due to a difference in general stress levels, the variability in stress levels would be as in the 3 lower lines of Table 9, assuming a 4th, 5th and 6th power dependence between da/dN and ΔK.

On the average the rail materials showed da/dN to be depending on ΔK to the 5th power. According to Table 9, a standard deviation of 15 percent in stress then gives the same variability in crack growth as observed in the experiments. A 15 percent error in stress seems to be a possible cumulative error, if the following contributors would have a 5 percent error each:

(a) load spectrum,

(b) stress analysis,

(c) stress intensity analysis.

The accuracy of these contributors cannot be expected to be much better than 5 percent. In addition, there will be errors introduced by the assumptions

TABLE 9. VARIABILITY IN STRESS FOR EQUIVALENT VARIABILITY IN CRACK GROWTH LIFE

Variable	Low Value	High Value	Mean	Standard Deviation	Standard Deviation in Percent of Mean
Crack Growth Life, log cycles	5.18	6.22	5.68	.30	5
Equivalent Variability in Stress, ksi (4th Power)	.75	1.36	1	.19	19
Equivalent Variability in Stress, ksi (5th Power)	.79	1.28	1	.15	15
Equivalent Variability in Stress, ksi (6th Power)	.83	1.23	1	.12	12

on flaw location and flaw shape. Therefore, it is concluded that the variability in crack growth properties is of the order of magnitude of the variability (error) of predictions due to accuracy limitations.

REFERENCES

(1) Fedderson, C. E., Buchheit, R. D. and Broek, D., "Fatigue Crack Propagation in Rail Steels", DOT Report DOT-TSC-1076, July, 1976.

(2) Fedderson, C. E. and Broek, D., "Fatigue Crack Propagation in Rail Steels", To be published in an ASTM STP.

(3) Broek, D., "Elementary Engineering Fracture Mechanics", Noordhoff Int. Publ., Leyden, Holland (1974).

(4) Rosenfield, A. R. and McEvily, A. J., "Some Recent Developments in Fatigue and Fracture", AGARD-R-610 (1973), pp. 23-54.

(5) Kobayashi, A. S., "Approximate Stress Intensity Factor for an Embedded Elliptical Crack Near to Parallel Free Surfaces", Int. J. Fracture Mechanics, 1 (1965), pp. 81-95.

(6) Shah, R. C. and Kobayashi, A. S., "Stress Intensity Factors for an Elliptical crack Approaching the Surface of a Semi-Infinite Solid, Int. J. Fracture, 9 (1973), pp. 133-146.

(7) Erdogan, F. and Sih, G. C., "On the Crack Extension in Plates Under Plane Loading and Transverse Shear", J. Basic Engrg., 85 (1963), pp. 519-527.

(8) Sih, G. C., "Strain-Energy-Density Factor Applied to Mixed Mode Crack Problems", Int. of Fracture, 10 (1974), pp. 305-322.

(9) Nuismer, R. J., "An Energy Release Rate Criterion for Mixed Mode Fracture", Int. J. Fracture, 11 (1975), pp. 245-250.

(10) Iida, S. and Kobayashi, A. S., "Crack Propagation Rate in 7075-T6 Plates Under Cyclic Tensile and Transverse Shear Loadings", J. Basic Engrg., 91 (1969), pp. 764-769.

(11) Roberts, R. and Kibler, J. J., "Mode II Fatigue Crack Propagation", J. Basic Engrg., 93 (1971), pp. 671-680.

(12) Pook, L. P., "The Effect of Crack Angle on Fracture Toughness", NEL Report 449 (1970).

(13) Hoskin, B. C., Groff, D. G. and Foden, P. J., "Fracture of Tension Panels With Oblique Cracks", Aer. Res. Lab, Melbourne, Rept. SM 305 (1965).

(14) Shah, R. C., "Fracture Under Combined Modes in 4340 Steel", ASTM STP 560 (1974), pp. 29-52.

(15) Liu, A. F., "Crack Growth and Failure of Aluminum Plate Under In-Plane Shear", AIAA Paper 73-253 (1973).

(16) Fowler, G. J., "Fatigue Crack Initiation and Propagation in Pearlitic Rail Steels", Ph.D. Dissertation, U. of California, Los Angeles.

APPENDIX A

BASIC CRACK LENGTH CYCLES DATA FOR PHASE II CONSTANT AMPLITUDE EXPERIMENTS

The following tabulations present the crack length measurements and associated cycle count for the experiments discussed in this report. The first measurement point in each tabulation represents the precrack length on the specimen surface after crack initiation out of the chevron notch. The final crack length represents the last crack size that could be monitored before fracture.

Specimen coding is in accordance with the text and figures.

TABLE A-1. BASIC CRACK LENGTH-CYCLES DATA FOR FIGURE 12

Specimen 006		Specimen 013		Specimen 019	
CRACK LENGTH, A, INCH	CYCLE COUNT, N, KC	CRACK LENGTH, A, INCH	CYCLE COUNT, N, KC	CRACK LENGTH, A, INCH	CYCLE COUNT, N, KC
.915	502.40	.923	120.00	.913	247.65
.948	600.00	.957	150.00	.972	340.00
.982	690.00	1.045	200.00	1.054	426.00
1.031	785.00	1.094	220.00	1.112	465.00
1.070	843.00	1.156	241.00	1.143	480.00
1.116	903.00	1.224	260.00	1.188	501.00
1.227	985.00	1.279	272.00	1.245	516.80
1.261	1000.00	1.316	280.00	1.321	530.00
1.338	1020.00	1.374	290.00	1.428	539.20
1.438	1036.00	1.444	300.00	1.480	541.00
1.600	1044.78	1.501	307.00	1.500	541.50
		1.550	310.00	1.530	542.10
		1.602	312.50	1.573	542.50
		1.654	313.60	1.592	542.76
		1.695	314.20		
		1.739	315.00		
		1.784	316.00		
		1.816	316.40		

TABLE A-1. (Continued)

Specimen 029		Specimen 020		Specimen 023-1	
CRACK LENGTH, A, INCH	CYCLE COUNT, N, KC	CRACK LENGTH, A, INCH	CYCLE COUNT, N, KC	CRACK LENGTH, A, INCH	CYCLE COUNT, N, KC
.920	334.91	.911	325.00	.986	715.00
.942	390.00	.922	370.00	1.029	850.00
.980	460.00	.947	415.00	1.063	952.00
1.020	523.00	.972	470.00	1.100	1060.00
1.059	570.00	1.006	525.00	1.165	1225.00
1.102	616.00	1.037	565.00	1.228	1335.00
1.143	650.00	1.078	610.00	1.297	1430.00
1.198	685.00	1.135	666.00	1.359	1500.00
1.249	707.00	1.182	697.00	1.417	1540.00
1.300	725.00	1.237	727.00	1.487	1571.00
1.344	735.00	1.260	737.00	1.542	1580.00
1.388	743.00	1.307	752.00	1.585	1584.00
1.418	748.00	1.352	765.00	1.641	1587.00
1.447	752.00	1.396	775.00	1.697	1587.40
1.472	755.00	1.434	782.00	1.780	1588.10
1.501	758.00	1.462	787.00		
1.521	760.00	1.487	791.00		
1.568	763.00	1.529	796.00		
1.611	765.00	1.574	800.00		
1.711	769.25	1.643	805.00		
1.806	770.12	1.768	810.00		
		1.910	811.25		

TABLE A-1. (Concluded)

Specimen LT002-1		Specimen LT035-1		Specimen LT036-1	
CRACK LENGTH, A, INCH	CYCLE COUNT, N, KC	CRACK LENGTH, A, INCH	CYCLE COUNT, N, KC	CRACK LENGTH, A, INCH	CYCLE COUNT, N, KC
.918	340.00	.921	350.00	.940	313.00
.943	384.00	.936	406.20	.963	331.50
1.000	495.00	.973	515.30	1.032	381.50
1.094	554.60	.996	572.30	1.056	421.50
1.150	595.30	1.046	686.00	1.092	480.00
1.210	630.00	1.114	813.15	1.142	536.50
1.251	651.30	1.153	873.40	1.320	649.10
1.313	677.00	1.237	982.10	1.351	661.00
1.370	698.00	1.280	1030.00	1.383	672.00
1.414	709.40	1.341	1108.00	1.421	684.50
1.469	722.70	1.377	1142.00	1.457	695.00
1.521	734.00	1.407	1163.80	1.509	705.00
1.602	746.80	1.452	1187.40	1.541	711.00
1.653	753.00	1.491	1204.50	1.573	715.50
1.694	756.50	1.526	1217.00	1.615	720.50
1.731	760.00	1.572	1230.00	1.659	725.60
1.766	762.30	1.626	1243.00	1.714	729.00
1.832	766.00	1.674	1251.00	1.743	730.50
1.889	768.50	1.719	1257.00	1.793	732.50
1.935	770.00	1.771	1262.00	1.842	733.50
1.994	771.40	1.817	1265.40	1.880	734.00
		1.875	1268.20		
		1.934	1271.00		
		1.998	1272.00		

TABLE A-2. BASIC CRACK LENGTH-CYCLES DATA FOR FIGURE 13

Specimen 009		Specimen 016		Specimen 024	
CRACK LENGTH, A, INCH	CYCLE COUNT, N, KC	CRACK LENGTH, A, INCH	CYCLE COUNT, N, KC	CRACK LENGTH, A, INCH	CYCLE COUNT, N, KC
.909	111.46	.919	150.00	.922	1673.00
.909	113.47	.944	200.00	.936	1733.00
.910	117.47	1.028	300.00	.945	1768.00
.913	127.47	1.051	320.00	.956	1818.00
.918	137.47	1.107	360.00	1.009	1908.50
.922	147.47	1.161	393.00	1.049	1949.00
.956	185.00	1.207	415.00	1.087	1980.00
1.000	225.00	1.256	435.00	1.124	2005.00
1.049	263.00	1.312	452.00	1.242	2046.30
1.098	293.00	1.369	465.00	1.264	2052.00
1.145	318.00	1.421	475.00	1.283	2055.00
1.198	342.00	1.492	485.00	1.311	2058.50
1.243	358.00	1.549	489.00	1.340	2062.00
1.284	368.55	1.611	492.00	1.366	2065.00
1.324	378.00	1.727	494.00	1.393	2067.50
1.368	386.00	1.816	494.47	1.436	2069.50
1.416	393.00			1.478	2071.50
1.478	399.00			1.519	2073.00
1.549	403.00			1.581	2074.50
1.602	405.00			1.620	2075.00
1.668	405.96			1.662	2075.25
				1.742	2075.33

TABLE A-2. (Continued)

Specimen 030		Specimen 031		Specimen 035	
CRACK LENGTH, A, INCH	CYCLE COUNT, N, KC	CRACK LENGTH, A, INCH	CYCLE COUNT, N, KC	CRACK LENGTH, A, INCH	CYCLE COUNT, N, KC
.919	196.80	.922	310.00	.923	120.00
.953	252.00	.964	560.00	.938	150.00
1.036	321.00	.997	670.00	.979	200.00
1.091	350.00	1.042	781.20	1.027	242.00
1.137	370.00	1.086	869.21	1.053	260.80
1.176	383.00	1.130	940.00	1.099	285.00
1.220	394.00	1.164	983.00	1.140	305.00
1.272	405.00	1.200	1024.33	1.201	325.00
1.350	416.00	1.243	1063.35	1.270	347.00
1.394	420.00	1.283	1090.78	1.292	352.00
1.439	425.00	1.349	1120.50	1.331	361.00
1.504	430.00	1.395	1135.00	1.362	366.50
1.575	433.50	1.459	1148.00	1.396	372.00
1.642	435.70	1.531	1156.75	1.443	377.00
1.686	436.30	1.618	1163.00	1.469	380.00
1.745	436.70	1.698	1166.00	1.490	382.00
1.791	436.96	1.856	1168.00	1.520	385.00
1.847	437.13	1.902	1166.22	1.560	388.00
1.903	437.27			1.624	391.00
				1.691	393.00
				1.744	394.00
				1.908	394.81

TABLE A-3. BASIC CRACK LENGTH-CYCLES DATA FOR FIGURE 14

Specimen 007		Specimen 013-2		Specimen 016-1	
CRACK LENGTH, A, INCH	CYCLE COUNT, N, KC	CRACK LENGTH, A, INCH	CYCLE COUNT, N, KC	CRACK LENGTH, A, INCH	CYCLE COUNT, N, KC
1.051	407.40	.910	757.00	1.064	3105.86
1.101	438.40	.937	1017.29	1.114	3168.03
1.151	461.10	.965	1167.29	1.364	3333.02
1.201	477.80	1.006	1317.29	1.414	3349.23
1.251	483.50	1.054	1467.29	1.464	3361.85
1.301	487.00	1.105	1620.00	1.514	3367.80
1.351	490.30	1.157	1756.00	1.564	3371.30
		1.221	1866.00		
		1.282	1966.00		
		1.320	2016.00		
		1.364	2070.00		
		1.413	2120.00		
		1.447	2150.00		
		1.478	2175.00		
		1.510	2200.00		
		1.556	2225.00		
		1.595	2240.00		
		1.633	2255.00		
		1.663	2270.00		
		1.702	2285.00		
		1.758	2300.00		
		1.825	2315.00		
		1.901	2330.00		
		1.959	2338.54		

TABLE A-3. (Continued)

Specimen 020-1		Specimen 022		Specimen 036	
CRACK LENGTH, A, INCH	CYCLE COUNT, N, KC	CRACK LENGTH, A, INCH	CYCLE COUNT, N, KC	CRACK LENGTH, A, INCH	CYCLE COUNT, N, KC
1.049	020.40	1.056	941.80	1.068	1489.60
1.099	075.74	1.106	980.10	1.118	1570.80
1.149	710.07	1.156	1009.80	1.168	1629.70
1.199	741.99	1.206	1035.50	1.218	1680.20
1.249	767.17	1.256	1056.20	1.268	1721.10
1.299	787.56	1.306	1072.90	1.318	1753.50
1.349	804.05	1.356	1086.40	1.368	1778.10
1.399	816.96	1.406	1096.60	1.418	1795.30
1.449	828.22	1.456	1103.80	1.468	1811.50
1.499	835.05	1.506	1109.80	1.518	1825.40
1.549	838.62	1.556	1111.70	1.568	1837.40
1.599	838.25	1.606	1115.20	1.618	1837.60
1.649	840.77	1.656	1115.50	1.668	1840.60
1.699	842.07				

TABLE A-4. BASIC CRACK LENGTH-CYCLES DATA FOR FIGURE 17

Specimen TL007-1		Specimen TL009-1		Specimen TL023-2	
CRACK LENGTH, A, INCH	CYCLE COUNT, N, KC	CRACK LENGTH, A, INCH	CYCLE COUNT, N, KC	CRACK LENGTH, A, INCH	CYCLE COUNT, N, KC
.915	365.00	.963	180.00	.913	500.00
.954	525.00	1.009	215.00	.965	590.00
1.011	660.00	1.059	261.00	1.022	700.00
1.072	765.00	1.107	305.00	1.073	800.00
1.121	840.00	1.159	349.10	1.141	883.00
1.168	892.70	1.209	385.00	1.195	930.00
1.220	940.00	1.264	413.00	1.272	975.00
1.266	970.00	1.308	435.00	1.322	995.00
1.325	997.00	1.363	457.00	1.365	1010.00
1.368	1013.00	1.410	474.00	1.398	1020.00
1.424	1030.00	1.459	488.00	1.435	1030.00
1.468	1040.00	1.525	500.30	1.484	1040.00
1.515	1049.00	1.571	507.90	1.547	1050.00
1.569	1057.00	1.609	513.40	1.581	1054.00
1.624	1062.00	1.630	515.90	1.622	1058.00
1.672	1066.00	1.715	520.00	1.660	1062.00
1.741	1069.00	1.748	521.50	1.716	1066.00
1.810	1070.50	1.818	523.20	1.771	1068.00
				1.835	1070.00
				1.893	1071.16
				1.973	1071.48

TABLE A-5. BASIC CRACK LENGTH-CYCLES DATA FOR FIGURE 18

Specimen TL001-1		Specimen TL002-1		Specimen TL006-1	
CRACK LENGTH, A, INCH	CYCLE COUNT, N, KC	CRACK LENGTH, A, INCH	CYCLE COUNT, N, KC	CRACK LENGTH, A, INCH	CYCLE COUNT, N, KC
.917	200.00	.951	260.00	.927	130.00
.936	450.00	1.002	310.00	.980	300.00
.972	860.00	1.034	500.00	1.016	410.00
1.010	1060.00	1.080	620.00	1.068	550.00
1.085	1360.00	1.123	720.00	1.110	670.00
1.143	1800.00	1.163	810.00	1.145	750.00
1.197	1940.00	1.214	910.00	1.191	850.00
1.251	2050.00	1.269	1000.00	1.251	960.00
1.294	2120.00	1.326	1090.00	1.297	1040.00
1.336	2185.00	1.388	1170.00	1.354	1130.00
1.378	2250.00	1.454	1240.00	1.402	1180.00
1.440	2320.00	1.501	1280.00	1.457	1230.00
1.481	2370.00	1.569	1330.00	1.501	1265.00
1.526	2425.00	1.622	1360.00	1.556	1305.00
1.585	2475.00	1.684	1390.00	1.599	1330.00
1.698	2530.00	1.738	1410.00	1.646	1350.00
1.748	2540.00	1.772	1420.00	1.685	1365.00
1.788	2544.00	1.807	1430.00	1.729	1380.00
1.817	2550.00	1.847	1440.00	1.785	1392.50
1.845	2552.00	1.901	1450.00	1.813	1400.00
1.936	2552.58	1.932	1455.00	1.836	1405.00
		1.961	1460.00	1.857	1410.00
		2.002	1462.70	1.902	1412.50
		2.082	1464.63	1.933	1415.00
				1.980	1420.61

TABLE A-5. (Continued)

Specimen TL007-2		Specimen TL009-2		Specimen TL023-1	
CRACK LENGTH, A, INCH	CYCLE COUNT, N, KC	CRACK LENGTH, A, INCH	CYCLE COUNT, N, KC	CRACK LENGTH, A, INCH	CYCLE COUNT, N, KC
.918	300.00	.960	286.50	1.014	280.00
.970	400.00	1.019	480.00	1.059	410.00
1.013	480.00	1.081	650.00	1.111	550.00
1.047	550.00	1.148	810.00	1.152	650.00
1.099	640.00	1.207	920.00	1.209	771.00
1.150	720.00	1.251	1010.00	1.260	870.00
1.208	810.00	1.286	1080.00	1.315	950.00
1.277	910.00	1.331	1150.00	1.365	1020.00
1.328	965.00	1.372	1200.00	1.434	1100.00
1.373	1015.00	1.408	1250.00	1.489	1150.00
1.412	1055.00	1.454	1300.00	1.545	1190.00
1.464	1101.00	1.503	1340.50	1.589	1220.00
1.520	1140.20	1.555	1380.00	1.625	1240.00
1.638	1200.00	1.587	1400.00	1.661	1260.00
1.663	1210.00	1.624	1420.00	1.719	1280.00
1.690	1220.00	1.644	1430.00	1.742	1290.00
1.725	1230.00	1.662	1440.00	1.775	1300.00
1.760	1235.00	1.684	1450.00	1.810	1305.00
1.821	1245.00	1.729	1460.00	1.842	1310.00
1.868	1248.00	1.801	1470.00	1.883	1315.00
1.902	1248.85	1.845	1472.00	1.907	1320.00
		1.860	1472.02	1.951	1325.00
				1.969	1327.11

TABLE A-6. BASIC CRACK LENGTH-CYCLES DATA FOR FIGURE 19

Specimen SL016		Specimen SL022		Specimen SL029	
CRACK LENGTH, A, INCH	CYCLE COUNT, N, KC	CRACK LENGTH, A, INCH	CYCLE COUNT, N, KC	CRACK LENGTH, A, INCH	CYCLE COUNT, N, KC
.766	180.00	.760	180.00	.775	201.00
.827	245.00	.795	230.00	.830	270.00
.888	300.00	.842	275.00	.876	320.00
.929	335.00	.894	330.00	.924	361.00
.974	360.00	.966	380.00	1.017	415.00
1.036	390.00	1.002	400.00	1.075	440.00
1.078	401.00	1.052	421.00	1.167	460.00
1.107	410.00	1.092	435.00	1.194	465.00
1.145	420.00	1.162	450.00	1.215	468.00
1.191	430.00	1.196	455.00	1.238	471.00
1.221	435.00	1.229	460.00	1.272	474.00
1.274	440.00	1.275	465.00	1.316	477.00
1.302	442.00	1.310	467.50	1.349	479.00
1.330	444.00	1.344	470.00	1.374	480.00
1.386	446.00	1.395	472.00	1.400	481.00
1.449	446.58	1.436	473.50	1.438	482.00
		1.493	474.50	1.525	482.67
		1.501	474.56		

TABLE A-7. BASIC CRACK LENGTH-CYCLES DATA FOR FIGURE 21

Specimen LT001-1		Specimen LT006-1		Specimen LT013-1	
CRACK LENGTH, A, INCH	CYCLE COUNT, N, KC	CRACK LENGTH, A, INCH	CYCLE COUNT, N, KC	CRACK LENGTH, A, INCH	CYCLE COUNT, N, KC
.919	240.00	.952	183.00	1.022	322.00
.991	265.10	1.040	238.80	1.087	341.60
1.041	293.10	1.090	258.90	1.137	361.20
1.091	318.40	1.140	276.80	1.227	392.00
1.141	346.50	1.190	293.30	1.237	396.30
1.191	372.90	1.240	307.70	1.287	412.80
1.241	400.60	1.290	320.70	1.337	426.50
1.291	423.40	1.340	331.90	1.387	438.10
1.341	447.30	1.390	342.40	1.437	449.30
1.391	468.50	1.440	350.60	1.487	458.90
1.441	487.50	1.490	358.00	1.537	467.50
1.491	505.70	1.540	364.10	1.587	474.80
1.541	521.00	1.590	369.20	1.637	481.30
1.590	534.50	1.640	373.80	1.687	486.90
1.641	543.40	1.690	377.30	1.737	491.50
1.691	553.40	1.740	380.80	1.787	495.60
1.741	560.90	1.790	383.40	1.837	499.20
1.791	566.20	1.840	385.50	1.887	502.40
1.841	570.50	1.890	387.70	1.000	505.20
1.891	573.50	1.940	389.10	1.987	507.30
1.941	575.00	1.990	390.70	2.037	509.60
2.020	578.60	2.150	392.40	2.380	515.10

TABLE A-7. (Continued)

Specimen LT029-1		Specimen LT030-1		Specimen LT031-2	
CRACK LENGTH, A, INCH	CYCLE COUNT, N, KC	CRACK LENGTH, A, INCH	CYCLE COUNT, N, KC	CRACK LENGTH, A, INCH	CYCLE COUNT, N, KC
.921	403.00	.924	675.00	.908	485.00
1.261	683.90	1.076	934.93	1.055	761.80
1.361	701.30	1.125	999.38	1.155	873.40
1.461	730.90	1.175	1049.92	1.254	954.40
1.511	742.80	1.226	1096.29	1.355	1006.90
1.561	752.40	1.276	1134.34	1.454	1041.30
1.611	760.50	1.326	1163.76	1.504	1054.20
1.661	767.10	1.375	1191.32	1.555	1064.40
1.711	772.10	1.425	1212.53	1.605	1072.40
1.761	776.40	1.476	1229.19	1.655	1078.70
1.811	780.00	1.526	1243.84	1.704	1083.30
1.861	782.90	1.576	1254.55	1.754	1087.60
1.911	785.10	1.625	1264.79	1.805	1090.90
1.961	786.60	1.675	1273.10	1.855	1093.30
2.011	787.50	1.726	1279.09	1.905	1095.20
2.068	787.80	1.776	1284.39	1.954	1096.50
2.118	788.10	1.826	1288.41	2.004	1097.30
2.168	788.30	1.875	1291.60	2.068	1097.70
		1.925	1294.11	2.117	1097.80
		1.976	1295.88	2.168	1097.90
		2.025	1296.61		
		2.080	1297.06		

TABLE A-8. BASIC CRACK LENGTH-CYCLES DATA FOR FIGURE 22

Specimen LT020-1		Specimen LT022-2		Specimen LT023-3	
CRACK LENGTH, A, INCH	CYCLE COUNT, N, KC	CRACK LENGTH, A, INCH	CYCLE COUNT, N, KC	CRACK LENGTH, A, INCH	CYCLE COUNT, N, KC
.940	1200.00	1.045	81.00	1.035	637.90
1.055	1539.40	1.095	101.52	1.085	707.50
1.155	1622.10	1.145	118.41	1.135	830.90
1.355	2218.10	1.195	131.83	1.185	959.30
1.455	2364.30	1.245	142.52	1.235	1074.30
1.505	2418.60	1.295	152.22	1.285	1163.80
1.555	2465.80	1.345	160.82	1.335	1244.90
1.605	2508.40	1.395	167.83	1.385	1324.80
1.655	2543.40	1.445	174.58	1.435	1390.30
1.705	2578.50	1.495	180.23	1.485	1449.60
1.755	2604.40	1.545	185.06	1.535	1502.60
1.805	2625.00	1.595	189.77	1.585	1546.40
1.855	2640.60	1.645	193.46	1.635	1587.70
1.905	2655.20	1.695	196.54	1.685	1622.40
1.955	2668.30	1.745	199.44	1.735	1654.90
2.005	2678.00	1.795	201.82	1.785	1680.10
2.063	2682.90	1.845	204.11	1.835	1703.10
2.113	2690.80	1.895	206.14	1.885	1725.20
2.163	2698.10	1.945	2079.20	1.935	1739.00
2.213	2705.00	1.995	209.71	1.985	1756.30
				2.135	1794.70

TABLE A-9. BASIC CRACK LENGTH-CYCLES DATA FOR FIGURE 23

Specimen LT001-2		Specimen LT006-2		Specimen LT007-2	
CRACK LENGTH, A, INCH	CYCLE COUNT, N, KC	CRACK LENGTH, A, INCH	CYCLE COUNT, N, KC	CRACK LENGTH, A, INCH	CYCLE COUNT, N, KC
.970	270.00	.991	347.00	1.054	83.85
1.000	361.62	1.050	423.75	1.104	99.74
1.062	470.00	1.108	460.92	1.154	111.18
1.090	520.00	1.150	561.61	1.204	118.70
1.137	570.00	1.200	620.20	1.254	124.43
1.150	620.00	1.250	655.41	1.304	129.35
1.190	670.00	1.300	674.07	1.354	133.33
1.220	720.00	1.450	710.07	1.404	136.42
1.261	770.00			1.454	139.00
1.290	820.00			1.504	140.74
1.344	880.00			1.554	142.95
1.391	940.00			1.604	143.53
1.442	1000.00			1.654	143.75
1.499	1060.00			1.704	143.76
1.589	1120.00			1.754	143.79
1.610	1140.00			1.804	143.83
1.750	1170.00			1.854	1438.30

TABLE A-9. (Continued)

Specimen LT013-2		Specimen LT030-2		Specimen LT002-2	
CRACK LENGTH, A, INCH	CYCLE COUNT, N, KC	CRACK LENGTH, A, INCH	CYCLE COUNT, N, KC	CRACK LENGTH, A, INCH	CYCLE COUNT, N, KC
.925	163.00	1.033	56.39	1.003	215.40
1.053	277.72	1.083	67.08	1.103	273.70
1.102	317.49	1.133	76.72	1.203	292.40
1.152	355.36	1.183	83.15	1.253	363.40
1.203	391.18	1.233	86.91	1.303	426.10
1.253	454.61	1.283	95.15	1.403	480.20
1.303	482.15	1.333	101.93	1.453	525.80
1.352	502.05	1.383	105.98	1.503	564.70
1.402	521.16	1.433	109.04	1.553	597.00
1.453	526.06	1.483	111.35	1.603	624.20
1.503	544.36	1.533	113.41	1.653	647.60
1.553	557.99	1.583	115.28	1.703	665.90
1.602	566.65	1.633	116.98	1.753	682.40
1.652	574.33	1.683	118.84	1.803	696.20
1.703	576.66	1.733	119.17	1.853	705.80
1.753	583.63	1.783	119.67	1.903	711.60
		1.833	120.37	1.953	714.00
		1.883	120.57	2.103	714.90
		1.933	120.62		

TABLE A-9. (Concluded)

Specimen LT029-2		Specimen LT031-1	
CRACK LENGTH, A, INCH	CYCLE COUNT, N, KC	CRACK LENGTH, A, INCH	CYCLE COUNT, N, KC
1.014	104.60	1.044	279.90
1.064	171.50	1.094	355.30
1.114	228.80	1.144	415.50
1.164	276.30	1.194	465.00
1.214	318.60	1.244	504.00
1.264	356.30	1.294	539.00
1.314	399.00	1.344	564.70
1.364	429.50	1.394	586.10
1.414	455.70	1.444	604.60
1.464	475.50	1.494	614.60
1.514	493.60	1.544	623.50
1.564	501.30	1.594	633.70
1.614	509.10	1.644	638.50
1.664	514.60	1.694	640.80
1.714	518.90	1.744	643.40
1.764	520.00	1.894	643.40
1.814	520.10	1.944	643.40
1.864	520.50		

TABLE A-10. BASIC CRACK LENGTH-CYCLES DATA FOR FIGURE 24

Specimen LT009-2		Specimen LT019-1		Specimen LT023-2	
CRACK LENGTH, A, INCH	CYCLE COUNT, N, KC	CRACK LENGTH, A, INCH	CYCLE COUNT, N, KC	CRACK LENGTH, A, INCH	CYCLE COUNT, N, KC
1.038	75.13	1.002	1051.23	1.040	1450.90
1.088	95.04	1.112	1750.96	1.090	1641.70
1.138	118.26	1.162	1949.04	1.140	1843.30
1.188	142.21	1.212	2120.41	1.190	2017.50
1.238	160.90	1.262	2270.00	1.240	2178.10
1.288	175.59	1.312	2389.02	1.290	2308.40
1.338	190.61	1.362	2490.37	1.340	2434.80
1.388	203.77	1.412	2584.00	1.390	2520.70
1.438	215.70	1.462	2641.20	1.440	2592.30
1.488	224.92	1.512	2691.33	1.490	2665.50
1.538	233.37	1.562	2737.09	1.540	2665.60
1.588	238.89	1.612	2748.47	1.590	2820.30
1.638	240.41	1.662	2770.31	1.640	2859.00
1.688	242.07	1.712	2813.77	1.690	2859.00
1.738	243.53	1.762	2812.87	1.740	2926.50
1.788	244.40	1.812	2813.94	1.790	2955.80
1.838	2444.00	1.862	2826.08	1.840	2974.60
				1.890	2990.90
				1.940	2995.80

TABLE A-11. BASIC CRACK LENGTH-CYCLES DATA FOR FIGURE 26

Specimen TL013-1		Specimen TL019-1		Specimen TL020-2	
CRACK LENGTH, A, INCH	CYCLE COUNT, N, KC	CRACK LENGTH, A, INCH	CYCLE COUNT, N, KC	CRACK LENGTH, A, INCH	CYCLE COUNT, N, KC
.912	180.00	.911	230.00	.986	416.50
1.078	248.60	1.063	335.40	1.036	447.50
1.128	267.70	1.114	362.00	1.086	474.70
1.178	284.10	1.164	385.40	1.136	504.90
1.227	298.90	1.214	405.90	1.186	531.10
1.277	313.00	1.263	423.60	1.236	557.60
1.328	324.50	1.313	439.90	1.286	580.80
1.378	336.10	1.364	453.20	1.336	601.40
1.428	346.50	1.414	465.40	1.386	618.20
1.477	354.60	1.464	475.30	1.436	633.70
1.527	361.50	1.513	482.90	1.486	645.90
1.578	367.70	1.563	489.70	1.536	656.30
1.628	372.90	1.614	495.60	1.586	665.30
1.678	377.50	1.664	499.70	1.636	672.70
1.727	381.70	1.714	502.70	1.686	678.60
1.777	384.90	1.763	505.30	1.736	683.40
1.828	387.70	1.813	507.40	1.786	687.40
1.878	390.10	1.864	509.10	1.836	690.20
1.928	392.00	1.914	510.60	1.886	693.00
1.977	393.40	1.964	511.00	1.936	694.90
2.028	394.50	2.014	511.20	2.250	700.50
2.278	396.90	2.100	511.30		

TABLE A-12. BASIC CRACK LENGTH-CYCLES DATA FOR FIGURE 27

Specimen TL002-2		Specimen TL022-1		Specimen TL024-1	
CRACK LENGTH, A, INCH	CYCLE COUNT, N, KC	CRACK LENGTH, A, INCH	CYCLE COUNT, N, KC	CRACK LENGTH, A, INCH	CYCLE COUNT, N, KC
.931	280.00	.929	480.00	.910	300.00
1.054	679.40	1.059	869.80	1.041	908.20
1.154	942.30	1.109	1003.10	1.091	1065.00
1.254	1147.70	1.159	1125.60	1.191	1341.40
1.354	1317.00	1.209	1232.30	1.291	1546.10
1.454	1446.20	1.259	1324.50	1.391	1686.10
1.504	1496.10	1.309	1413.60	1.441	1755.10
1.554	1540.90	1.359	1486.70	1.491	1805.40
1.604	1579.90	1.409	1550.00	1.541	1852.80
1.654	1614.00	1.459	1608.60	1.591	1892.40
1.704	1644.20	1.509	1655.70	1.641	1925.90
1.754	1669.10	1.559	1696.50	1.691	1951.90
1.804	1690.70	1.609	1734.70	1.741	1976.00
1.854	1709.10	1.659	1767.60	1.791	1996.20
1.904	1724.40	1.709	1795.70	1.841	2017.80
1.954	1737.00	1.759	1818.70	1.891	2031.30
2.004	1747.30	1.809	1837.30	1.941	2040.00
2.061	1757.20	1.859	1853.10	1.991	2048.10
2.111	1762.90	1.909	1868.40	2.050	2050.70
2.161	1767.10	1.959	1873.80	2.060	2050.90
2.211	1768.80	2.009	1880.50		
2.250	1768.90	2.066	1884.80		
		2.116	1887.50		
		2.166	1889.30		

TABLE A-13. BASIC CRACK LENGTH-CYCLES DATA FOR FIGURE 28

Specimen TL016-1		Specimen TL019-2		Specimen TL024-3	
CRACK LENGTH, A, INCH	CYCLE COUNT, N, KC	CRACK LENGTH, A, INCH	CYCLE COUNT, N, KC	CRACK LENGTH, A, INCH	CYCLE COUNT, N, KC
1.033	108.00	.933	350.00	1.040	245.00
1.083	181.90	.998	473.40	1.103	331.00
1.133	251.60	1.052	542.01	1.152	371.00
1.183	309.00	1.102	595.28	1.200	397.00
1.233	355.40	1.202	677.09	1.266	423.00
1.283	406.70	1.253	712.30	1.297	436.00
1.333	444.80	1.302	737.07	1.370	465.03
1.383	474.90	1.352	758.34		
1.433	503.50	1.402	776.08		
1.483	521.10	1.452	784.86		
1.533	526.10	1.502	794.06		
1.583	533.60	1.552	796.93		
1.633	540.00	1.602	800.05		
1.683	543.50				
1.733	544.70				
1.783	545.00				

TABLE A-13. (Continued)

Specimen TL029-2

CRACK LENGTH, A, INCH	CYCLE COUNT, N, KC
1.046	96.20
1.096	152.70
1.146	200.30
1.196	237.50
1.246	270.00
1.296	295.10
1.346	318.30
1.396	339.70
1.446	361.70
1.496	376.50
1.546	385.10
1.596	392.00
1.646	397.30
1.696	402.20
1.746	403.70
1.796	403.70

TABLE A-14. BASIC CRACK LENGTH-CYCLES DATA FOR FIGURE 29

Specimen TL016-2		Specimen TL022-2		Specimen TL024-2	
CRACK LENGTH, A, INCH	CYCLE COUNT, N, KC	CRACK LENGTH, A, INCH	CYCLE COUNT, N, KC	CRACK LENGTH, A, INCH	CYCLE COUNT, N, KC
1.072	30.60	1.033	1042.34	1.180	387.30
				1.000	- 94.00
1.122	242.60	1.083	1044.21	1.230	521.00
1.172	428.50	1.133	1046.24	1.280	659.90
1.222	597.70	1.183	1048.04	1.330	748.80
1.272	756.60	1.233	2004.96	1.380	822.20
1.322	894.30	1.283	2153.94	1.430	912.10
1.372	1024.40	1.333	2292.65	1.480	963.80
1.422	1149.30	1.383	2400.07	1.530	993.80
1.472	1260.60	1.433	2080.24	1.580	1038.20
1.522	1371.70	1.483	2011.49	1.630	1077.20
1.572	1477.80	1.533	2085.91	1.680	1077.20
1.622	1530.00	1.583	2140.00	1.730	1077.70
1.672	1565.30	1.633	2177.70	1.780	1077.70
1.722	1606.50	1.683	2081.02	1.830	1078.10
1.772	1612.00	1.733	2040.72		
1.822	1634.80	1.783	2070.77		
		1.833	2094.57		
		1.883	2095.11		
		1.933	2095.12		

APPENDIX B

Rail history, chemical composition, experimental details and summary of results of Phase I baseline crack-growth data are presented in this appendix.

A complete description of the Phase I effort was presented in an Interim Report, Reference 1 of this report.

At the outset of this program, an effort was made to assemble a representative sampling of rail materials which are presently, and will continue to be, in service on U. S. railroads. Variations of rail size, rail producer, and year of production were the primary selection criteria. Eleven of the major railroad organizations were contacted for contributions of rail samples. Directly or indirectly samples were received from the following organizations:

- Association of American Railroads
- Boston and Maine Railroad Company
- Chessie System
- Denver and Rio Grande Western Railroad Company
- Penn Central Railroad Company
- Southern Pacific Transportation Company
- Transportation Systems Center
- Union Pacific Railroad Company.

A total of 66 material samples were received representing sizes from 85 lb/yd to 140 lb/yd, produced over a period from 1911 to 1975 in both U. S. and Japanese mills. The samples were given identification numbers from 001 to 066. Basic information on the samples is presented in Table 1.

Chemical analyses of each of the 66 rail samples were made for total carbon, manganese, silicon, and sulfur in percent by weight, and for hydrogen and oxygen in parts per million (ppm). The results of the analyses are presented in Table 2. Duplicate and, in some instances, triplicate analyses were made for hydrogen and oxygen and these are shown individually in the table.

Specifications for the chemical composition of rail steels vary slightly with the rail size (expressed as the weight per yard of rail). The ASTM Standard Specification for Carbon-Steel Rails, ASTM Designation: A1-68a, states the following chemical requirements:

Element, percent	Nominal Weight, lb/yd			
	61-80	81-90	91-120	121 and Over
Carbon	0.55-0.68	0.64-0.77	0.67-0.80	0.69-0.82
Manganese	0.60-0.90	0.60-0.90	0.70-1.00	0.70-1.00
Phosphorus, max	0.04	0.04	0.04	0.04
Silicon	0.10-0.23	0.10-0.23	0.10-0.23	0.10-0.23.

TABLE B-1

RAIL MATERIALS INVENTORY

BCL Sequence Number	Receipt Date	Source	Source Number	Size (lb/yd) Section Number	Type	Controlled Cool	Mill Brand	Year Rolled	Month Rolled	Sample Length, Inches	Remarks
001	10/10/75	TSC	418	130			BSCO	1929	11	34-7/8	Steelton Open Hearth Med. Mang. Ht. 83530 AREA
002			521	85				1911		34	Maryland ASCE
003			399	130				1929	11	37-1/8	Steelton Open Hearth Med. Mang. Ht. 81366 AREA
004			100	85			BSCO	1920		36	Steelton Open Hearth ASCE
005			398	130				1929	9	35-3/8	Steelton Open Hearth Med. Mang. Ht. 81692 AREA
006			VD-1	115	RE			1974		33-1/2	Vacuum Degassed, Sydney VT Rail, New 115 lb A&M
007			VD-2	115	RE			1974		36-1/8	Vacuum Degassed, Sydney VT Rail, New 115 lb A&M
008			535	85				1924		35-5/8	Lackawanna Open Hearth ASCE
009			442	130				1929		36-1/8	Steelton Open Hearth Med. Mang. Ht. 83549
010			539	85				1919		36-1/4	Lackawanna Ht. 850 ASCE
011	10/14/75	AAR	UP-3-4	1330	RE	Yes	CF&I	1965	11	63-1/2	
012			UP-1-1	1330	RE		CF&I	1955	12	47-1/2	
013			PC-1-1	127DM			Illinois	1954	1	60-1/2	
014			UP-1-14	1330	RE	Yes	CF&I	1955	11	48	
015			UP-1-20	1330	RE	Yes	CF&I	1949	2	47-1/2	
016			UP-2A-9	133		Yes	CF&I	1957	5	50-1/2	
017			UP-2A-8	133			CF&I	1957	1	48	
018			UP-2A-2	1330	RE	Yes	CF&I	1953	4	40	
019			UP-3-5	1330	RE	Yes	CF&I	1965	11	40-3/4	
020			SP-2-3	119			CF&I	1957	11	47	
021			UP-1-27	1330	RE	Yes	CF&I	1955	11	42-1/4	
022			UP-2A-21	1330	RE	Yes	CF&I	1956	3	51-1/2	
023			UP-2A-17	133		Yes	CF&I	1957	1	52	
024			UP-2A-22	1330	RE	Yes	CF&I	1956	1	51-1/2	
025			UP-3-1	1330	RE	Yes	USS	1966	7	46-3/4	
026			UP-2A-15	1330	RE	Yes	CF&I	1957	1	49-3/4	
027			UP-1-6	133			CF&I	1956	12	46	
028			UP-2A-18	1330	RE	Yes	CF&I	1953	31	50	
029			SP-2-2	119		Yes	CF&I	1958	11	39-3/4	
030			SP-2-6	119			CF&I	1958	11	48-1/4	
031			UP-1-7	133			CF&I	1956	12	36-3/4	
032			UP-2A-20	13331	RE	Yes	USS	1953	3	47-3/4	
033			UP-1-12	133			CF&I	1955	11	46-1/2	
034			SP-2-5	1190		Yes		1957	1	46-3/4	
035	12/4/75	Denver & Rio Grande	165	1150	RE	Yes	CF&I	1955	5	35-3/4	Heat CH 9332 D3 Defect IDO 5, Defect No. 165
036			143	112	RE		CF&I	1939	2	34-3/4	Heat 10053 F20CH Defect RHJ 2, Defect No. 143
037			401	1155		Yes	CF&I	1943	12	40-1/4	Heat CC 2060 E5 Defect TDDS, Defect No. 401
038			158	1121			CF&I	1930	9	37-3/4	Heat 16422 E 6 IM Defect TDDS, Defect No. 158
039			215	90			CF&I	1924	4	36-1/4	Heat 2521 C, Defect TDDS, Defect No. 215
040			499	100			CF&I	1928	3	36	Heat 2996 B 19, Defect VSH 4 inch (sub for BH) Defect No. 499
041			155	1150	RE	Yes	CF&I	1953	3	36-1/4	Heat 15198 F3 Defect HSH, Defect No. 155
042			496	100			CF&I	1928	3	36	Heat 3004 B1 Defect TDDS, Defect No. 496
043			179	90			CF&I	1921	3	36	Heat 1368, Defect BAJ2, Defect No. 179
044			24	110	RE		CF&I	1936	3	36-1/4	Heat 13116 A10 Defect TDDS, Defect No. 24
045			199	110	RE		CF&I	1930	2	35-1/2	Heat 11121 Defect HSH 5 inch (sub for BH) Defect No. 199
046				133	RE	Yes	CF&I	1966	2	36	Linde Flame Hardened Rail (End Hardened)
047	2/9/76	Chessie		130	RE		Beth.			36	
048				122	CB	Yes	Beth.	1965		36	
049				115	RE	Yes	USS	1950		36	
050				132	RE	Yes	USS	1958		36	
051				130	RE		Inland	1931		36	
052				100	ARAB		USS	1916		36	
053				140	RE	Yes	USS	1956		36	
054				131	RE		USS	1935		36	
055				131	RE		Beth.	1947	9	36	Heat 86462 F-11
056				132	RE		Beth.	1949	5	36	Heat CH 81294 F-11
057				140	RE		Beth.	1953	1	36	Heat CH 83673 C-5
058				140	RE		Beth.	1974		36	Fully Heat Treated, Heat 68674 2-19
059	3/1/76	Chessie		133			USS	1967		36	Sperry detected Defect Heat 95-P-134 827 (Curvemaster)
060				124			Beth.	1975	11	36	Heat 162724-A-21
061				124			Beth.	1975	11	36	Heat 162729-A-12
062				124			Beth.	1975	12	36	Heat 181006-A-32
063				124			Beth.	1975	12	36	Heat 175105-A-6
064				124			Nippon	1975	7	36	Heat A-39262 D-2
065				124			Nippon	1975	7	36	Heat A-39280-D-5
066				124			Nippon	1975	7	36	Heat A-39376 C-7

TABLE B-II

RESULTS OF CHEMICAL ANALYSES OF RAIL SAMPLES 001 THROUGH 066

Rail Sample	Size, lb/yd	Content, weight percent C	Mn	Si	S	Hydrogen Content, ppm	Oxygen Content, ppm
001	130	0.63	1.48	0.21	0.022	0.8, 1.0	100, 96
002	85	0.74	0.61	0.07	0.154[a]	0.8, 0.9	46, 48
003	130	0.77	0.76	0.20	0.036	0.4, 0.5	71, 69
004	85	0.67	0.62	0.30	0.052	0.7, 0.5	519, 435, 659
005	130	0.63	1.36	0.21	0.033	0.6, 0.8	52, 54
006	115	0.72	0.97	0.10	0.028	0.4, 0.4	23, 25
007	115	0.73	0.93	0.18	0.037	0.4, 0.3	24, 26
008	85	0.66	0.94	0.20	0.029	0.8, 0.8	57, 61
009	130	0.61	1.46	0.29	0.039	0.7, 0.7	56, 59
010	85	0.63	0.74	0.14	0.028	1.1, 0.9	132, 138
011	133	0.73	0.81	0.19	0.028	0.4, 0.4	57, 51, 56
012	133	0.79	0.84	0.18	0.029	0.8, 0.7	54, 58
013	127	0.74	0.89	0.24	0.028	0.8, 1.0	51, 47
014	133	0.78	0.74	0.17	0.014	0.8, 0.8	86, 84
015	133	0.76	0.82	0.19	0.033	0.6, 0.6	54, 54
016	133	0.81	0.93	0.17	0.044	0.6, 0.8	39, 43
017	133	0.79	0.85	0.26	0.048	0.9, 1.0	44, 43
018	133	0.75	0.89	0.17	0.046	0.7, 0.6	45, 43
019	133	0.74	0.88	0.21	0.038	0.4, 0.4	38, 36
020	119	0.75	0.83	0.15	0.033	0.8, 0.7	34, 32
021	133	0.79	0.90	0.21	0.024	0.7, 0.6	41, 45
022	133	0.78	0.87	0.20	0.028	0.4, 0.5	46, 47
023	133	0.79	0.92	0.21	0.040	0.6, 0.7	39, 35, 46
024	133	0.81	0.83	0.12	0.030	1.0, 0.7	26, 28
025	133	0.80	0.91	0.23	0.016	0.7, 0.7	29, 27
026	133	0.78	0.94	0.17	0.050	0.5, 0.5	47, 46
027	133	0.78	0.87	0.23	0.022	0.7, 0.6	45, 45
028	133	0.71	0.90	0.17	0.022	0.7, 1.0	79, 53, 69
029	119	0.72	0.89	0.19	0.046	0.5, 0.6	45, 43
030	119	0.80	0.90	0.16	0.028	0.5, 0.7	52, 54
031	133	0.79	0.76	0.15	0.022	0.5, 0.4	53, 49
032	133	0.80	0.94	0.18	0.035	0.5, 0.5	63, 61
033	133	0.78	0.92	0.23	0.025	0.6, 0.5	37, 35
034	119	0.77	1.04	0.17	0.023	0.5, 0.7	38, 38
035	115	0.76	0.80	0.23	0.028	0.5, 0.4	27, 27

TABLE B-II(Continued)

Rail Sample	Size, lb/yd	Content, weight percent C	Mn	Si	S	Hydrogen Content, ppm	Oxygen Content, ppm
036	112	0.75	0.81	0.18	0.016	0.4, 0.5	57, 54
037	115	0.72	0.93	0.25	0.017	0.4, 0.5	86, 67, 61
038	112	0.57	1.48	0.16	0.029	0.3, 0.3	78, 82
039	90	0.71	0.81	0.17	0.028	0.3, 0.3	81, 107, 168
040	100	0.58	0.64	0.08	0.030	0.4, 0.4	39, 34
041	115	0.77	0.81	0.21	0.043	0.4, 0.3	91, 93
042	100	0.63	0.71	0.08	0.026	0.3, 0.4	49, 36, 64
043	90	0.75	0.81	0.15	0.032	0.6, 0.4	84, 85
044	110	0.78	0.88	0.20	0.016	0.3, 0.3	84, 86
045	110	0.65	0.65	0.21	0.027	0.6, 0.5	342, 286, 372
046	133	0.78	0.90	0.20	0.027	0.2, 0.3	49, 48
047	130	0.76	0.46	0.11	0.044	1.1, 0.7	43, 41
048	122	0.79	0.95	0.17	0.022	0.7, 0.6	58, 61
049	115	0.80	0.89	0.11	0.040	0.9, 1.1	48, 50
050	133	0.75	0.91	0.20	0.036	0.5, 0.6	56, 56
051	130	0.84	0.72	0.19	0.016	0.6, 0.5	47, 51
052	100	0.72	0.90	0.19	0.021	0.4, 0.4	52, 54
053	140	0.85	0.91	0.18	0.032	6.1, 6.5	44, 44
054	131	0.78	0.76	0.20	0.021	1.0, 0.6	36, 32
055	131	0.78	0.90	0.17	0.028	0.8, 0.8	33, 35
056	132	0.80	0.90	0.19	0.039	0.7, 0.7	44, 46
057	140	0.77	0.94	0.16	0.028	0.7, 0.9	58, 46, 50
058	140	0.83	0.84	0.18	0.048	0.4, 0.5	47, 44
059	133	0.83	0.98	0.14	0.024	0.4, 0.3	22, 25
060	124	0.80	0.90	0.12	0.013	0.5, 0.4	56, 36, 47
061	124	0.80	0.91	0.12	0.015	0.4, 0.7	46, 46
062	124	0.79	0.84	0.08	0.017	0.3, 0.6	45, 51, 48
063	124	0.79	0.86	0.12	0.033	0.3, 0.3	49, 59, 64
064	124	0.76	0.85	0.18	0.018	0.6, 0.6	43, 49, 54
065	124	0.82	0.90	0.17	0.016	0.3, 0.3	41, 42
066	124	0.75	0.90	0.18	0.019	0.4, 0.7	37, 36

(a) Check analyses of this rail sample for sulfur were 0.127 percent by weight obtained from a 1/2-gram sampling and 0.145 percent by weight obtained from a 1-gram sampling. The average of the three determinations of the sulfur content is 0.142 weight percent.

EXPERIMENTAL DETAILS

Specimens

One tensile specimen and one fatigue-crack-growth specimen were machined from each rail sample. The orientation of the specimens is shown in Figure B-1. Charpy V specimens were taken from six rail samples — 023 and 030 which exhibited a high rate of fatigue-crack growth, 019 and 031 with medium crack-growth rates, and 001 and 036 with low growth rates. Forty-five Charpy specimens were made, 15 from each of the three growth-rate categories. From each category, five specimens were taken in each of the three directions shown in Figure B-1. The specimens were taken from the center of the rail head.

The tensile specimens were standard ASTM 0.25-inch-diameter specimens. Charpy specimens were also of standard dimensions; i.e., 2.165-inch long, 0.394-inch thick with a square cross section.

Fatigue-crack-growth specimens were of the compact tension (CT) type. Their dimensions are shown in Figure B-2. The specimens were provided with a 1.650-inch deep chevron notch (0.900 inch from the load line). Details of the notch can best be observed in Figure 17 which shows two specimens, one before and one after testing.

Testing Procedures

Tensile and Charpy tests were performed in accordance with standard procedures.

To expedite the crack-growth tests, speciments were precracked in a Krause fatigue machine. Crack-growth experiments were conducted in a 25-kip-capacity electrohydraulic servocontrolled fatigue machine.

The tests were performed at constant amplitude, the load cycling between 0 and 2500 pounds, resulting in a stress ratio of R = 0. Cycling frequency was 40 Hz, but was reduced to 4 Hz toward the end of a test to enable more accurate recording of the crack size giving final failure. The laboratory air was kept at 68 F and 50 percent relative humidity.

Crack growth was measured visually, using a 30 power traveling microscope. The cracks were allowed to grow in increments of 0.050 inch, after which the test was stopped for an accurate crack size measurements. Crack size was recorded as a function of the number of load cycles.

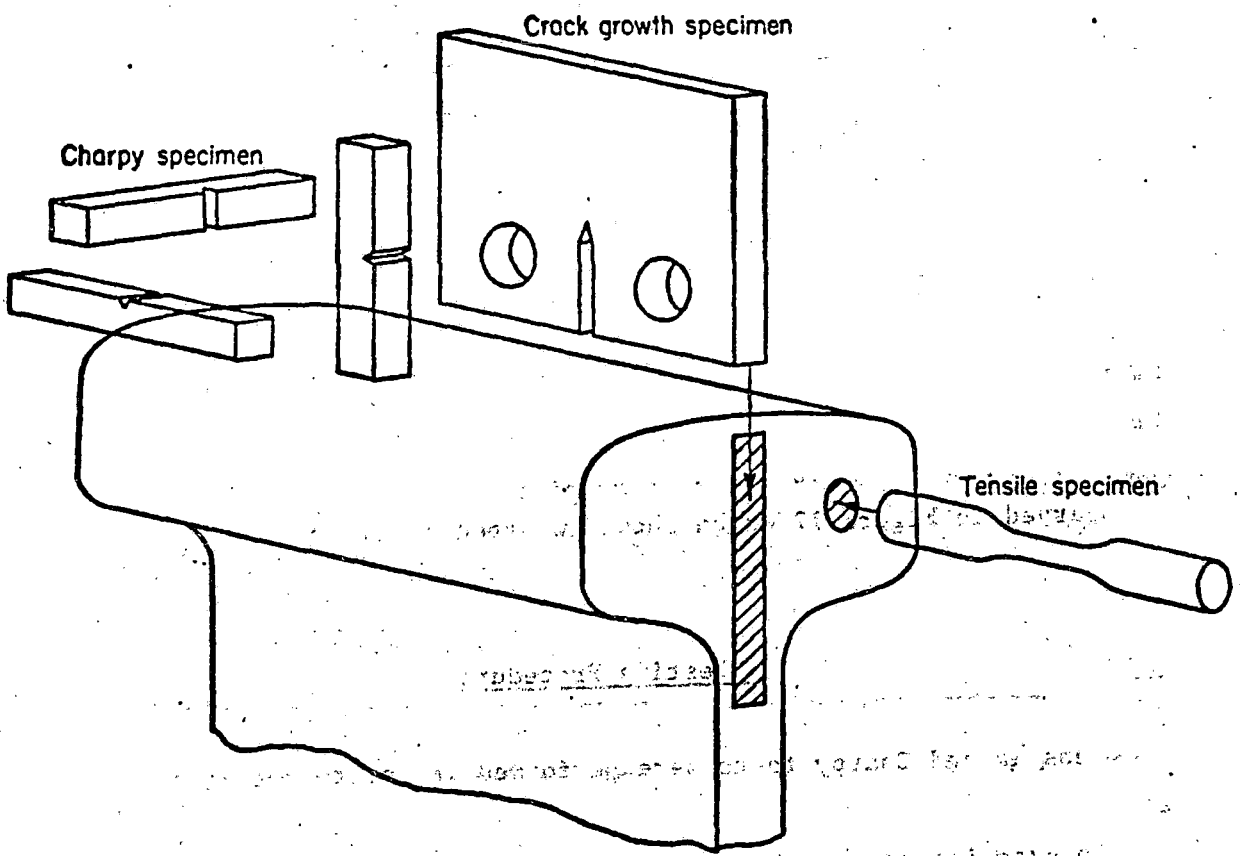

ORIENTATION OF SPECIMENS

FIGURE B-1

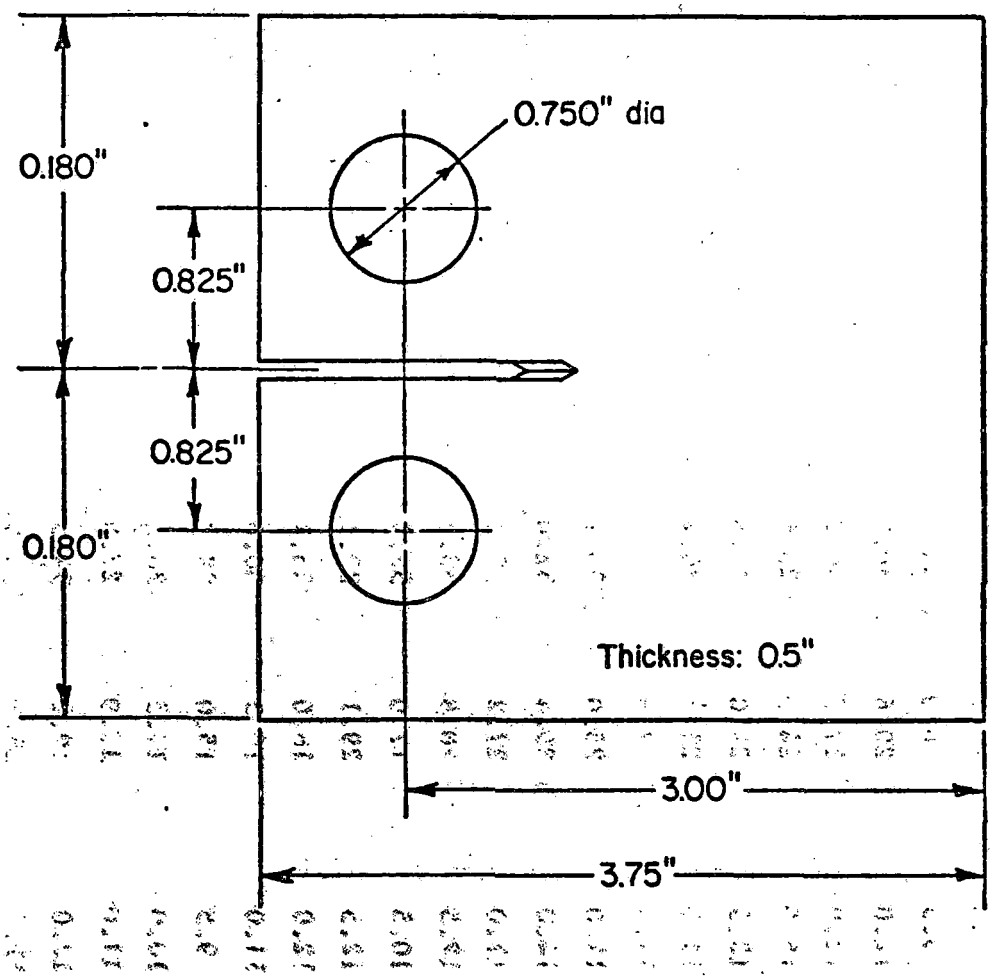

COMPACT TENSION FATIGUE CRACK GROWTH SPECIMEN

FIGURE B-2

TABLE B-III

TENSION TEST RESULTS FOR 66 RAIL SAMPLES

Rail Number	TUS, ksi	TYS, ksi	Elongation in 1 Inch, percent	Reduction in Area, percent	E, 10^3 ksi	True Fracture Stress, ksi	True Fracture Strain, ϵ_t	Ramberg-Osgood Exponent, n	Work Hardening Exponent, 1/n
001	136.4	76.5	13.5	28.0	34.0	171.2	.1266	7.8	.128
002	134.4	74.7	12.0	20.6	30.8	159.4	.1133	7.7	.130
003	137.4	73.6	12.0	17.7	30.3	160.1	.1133	13.1	.076
004	116.0	59.9	15.0	24.0	28.6	144.6	.1397	10.4	.096
005	134.8	76.4	13.5	26.0	31.8	154.9	.1266	11.5	.081
006	135.0	71.2	11.0	21.2	30.2	161.9	.1043	11.5	.087
007	135.8	70.0	12.0	17.6	30.3	156.9	.1133	12.5	.080
008	125.1	67.0	14.0	25.0	30.1	155.9	.1310	10.8	.093
009	139.8	81.8	14.0	29.4	32.0	180.0	.1310	12.0	.083
010	111.5	58.7	17.0	27.2	29.3	143.1	.1570	9.8	.102
011	126.9	73.2	12.5	20.8	33.8	144.3	.1177	10.3	.097
012	134.7	78.3	10.5	17.0	32.4	153.1	.0998	8.4	.119
013	129.3	72.8	12.5	29.1	29.1	160.8	.1177	7.9	.126
014	135.4	75.9	12.0	18.0	33.1	158.7	.1133	7.5	.133
015	131.6	71.5	11.0	16.5	30.6	150.0	.1043	6.0	.167
016	138.6	75.6	9.5	15.0	28.8	154.4	.0907	6.3	.159
017	137.1	74.4	10.0	19.5	28.2	163.6	.0953	6.4	.156
018	133.2	70.6	11.0	19.9	27.5		.1043		
019	131.2	73.4	12.0	19.2	34.5	152.8	.1133	8.5	.118
020	131.4	72.0	11.0	18.4	30.4	152.6	.1043	6.5	.154
021	132.3	77.2	12.0	18.4	32.6	153.9	.1133	9.8	.102
022	130.7	76.0	13.0	22.7	31.7	157.9	.1222	8.2	.122
023	135.1	77.3	10.5	17.9	32.2	155.7	.0998	7.7	.130

TABLE B-III - (Continued)

Rail Number	TUS, ksi	TYS, ksi	Elongation in 1 Inch, percent	Reduction in Area, percent	E, 10^3 ksi	True Fracture Stress, ksi	True Fracture Strain, ϵ_t	Ramberg-Osgood Exponent, n	Work Hardening Exponent, 1/n
024	136.7	74.6	10.0	16.2	32.4	158.7	.0953	6.3	.159
025	141.1	75.7	9.5	18.8	26.5	164.9	.0907	6.3	.159
026	135.0	74.4	11.0	17.5	29.9	153.1	.1043	8.2	.122
027	136.4	69.4	10.0	13.6	29.0	150.1	.0953	6.2	.161
028	129.1	70.5	11.5	18.9	31.8	119.8	.1088	7.5	.133
029	125.5	61.7	12.0	19.9	29.4	146.6	.1133	6.8	.147
030	110.0[a]	76.8	--	--	28.2	--	--	7.1	.140
031	133.4	75.6	11.0	17.6	31.6	149.4	.1043	8.6	.116
032	139.5	80.0	12.0	19.5	34.8	165.3	.1133	8.0	.125
033	135.0	73.3	10.0	13.9	28.6	--	.0953		
034	137.3	77.3	10.5	20.7	30.2	164.3	.0998	6.0	.167
035	128.1	69.3	12.5	19.6	33.6	154.1	.1177	7.2	.139
036	132.1	74.6	12.0	21.4	31.1	155.3	.1133	10.0	.100
037	127.7	68.6	16.0	25.9	32.6	156.8	.1484	9.4	.106
038	124.2	74.9	17.0	42.3	33.7	185.3	.1570	11.5	.087
039	130.7	75.0	14.5	21.6	30.9	155.9	.1354	7.5	.133
040	138.8	83.3	9.5	15.0	26.9	156.5	.0907	7.7	.130
041	132.0	73.6	11.5	22.0	28.6	156.1	.1088	7.7	.130
042	133.0	74.7	10.5	15.9	29.6	151.1	.0998	6.8	.147
043	133.2	75.6	13.0	20.5	32.8	156.9	.1222	6.9	.145
044	139.7	80.0	10.0	15.3	29.3	158.7	.0953	11.5	.087
045	96.8[a]	66.0	8.0	16.3	33.8	98.0	.0769	10.2	.098
046	130.6	75.9	14.5	20.6	28.9	160.5	.1354	25.0	.040

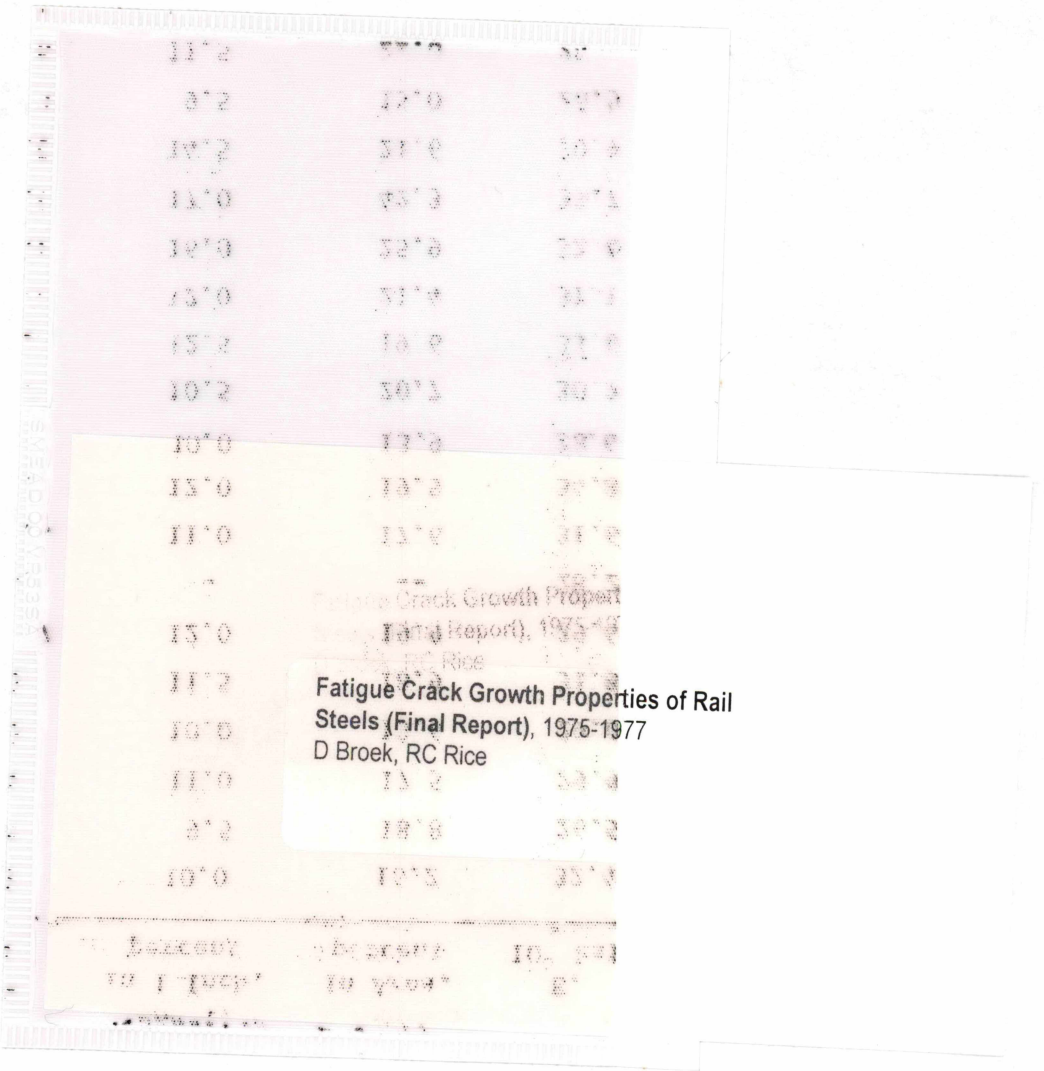

Fatigue Crack Growth Properties of Rail Steels (Final Report), 1975-1977
D Broek, RC Rice